POLITECNICO DI TORINO

Collegio di Ingegneria Chimica e dei Materiali

Corso di Laurea Magistrale

in Ingegneria Chimica e dei Processi Sostenibili

Tesi di Laurea Magistrale

Design of tailor-made curcumin Pickering particles for the stabilization of water-in-oil emulsions

Relatrici

Prof.ssa Elena Simone

Giulia Del Duca

Candidata

Rachele Sgambetterra

s310420

Dicembre 2024

Summary in Italian

Il presente studio si concentra sulla progettazione di particelle di curcumina per la stabilizzazione di emulsioni acqua-in-olio. Le emulsioni sono miscele eterogenee e instabili, in cui un liquido è disperso in un altro liquido immiscibile. La stabilità di questi sistemi può essere ottenuta tramite l'utilizzo di tensioattivi o polimeri anfifilici, che riducono la tensione interfacciale e la repulsione elettrostatica tra le fasi. Negli ultimi anni, l'interesse scientifico si è rivolto verso gli studi riguardanti le emulsioni di Pickering, ovvero emulsioni stabilizzate da particelle solide o colloidali che, adsorbendosi all'interfaccia tra fasi, aumentano la stabilità del sistema. In particolare, l'attenzione si è rivolta verso particelle stabilizzanti di origine naturale, per la loro bassa tossicità e biodegradabilità. Questo lavoro mette in evidenza l'importanza delle proprietà delle particelle solide, come dimensione, forma, polimorfismo e bagnabilità, nella stabilizzazione delle emulsioni di Pickering.

In questo contesto, lo studio ha esplorato l'uso della curcumina, una sostanza estratta dal rizoma della *Curcuma longa*, per le sue interessanti proprietà superficiali che la rendono un potenziale stabilizzante in emulsione. La curcumina è nota per la sua elevata biocompatibilità e sicurezza, anche a dosi elevate; tuttavia, la sua efficacia clinica risulta limitata dalla scarsa solubilità in acqua e dalla bassa biodisponibilità. La ricerca si è quindi focalizzata sulla produzione e caratterizzazione di due polimorfi della curcumina, la forma I (stabile) e la forma III (metastabile) utilizzando un approccio di ingegneria dei cristalli. Per ottenere i due polimorfi in modo riproducibile, sono state selezionate due tecniche di cristallizzazione: la tecnica del cooling per la forma I e la tecnica dell'antisolvente per la forma III. È stata definita la solubilità della curcumina per dimensionare gli esperimenti di cristallizzazione. I test iniziali sono stati eseguiti utilizzando il sistema Crystal 16, con soluzioni di curcumina in miscele di acqua ed etanolo a concentrazioni variabili (da 0.13 a 0.95 mg/g in soluzione), riscaldate fino a 75°C e successivamente raffreddate a 1°C. Sono stati condotti ulteriori test di solubilità mediante cromatografia liquida ad alte prestazioni (HPLC), utilizzando nove rapporti in peso di acqua/etanolo (compresi tra 1:2.5 e 1:20) ed eseguendo un'analisi cromatografica per ciascun rapporto. Infine, sono stati condotti test sulla solubilità della curcumina in soluzioni a pH diversi (acido, basico e neutro), per simulare il comportamento in differenti ambienti fisiologici. La cristallizzazione della forma I è stata realizzata tramite riscaldamento seguito da un raffreddamento controllato. Per la forma III è stata invece utilizzata la tecnica dell'antisolvente, in cui la cristallizzazione avviene tramite l'aggiunta di un antisolvente che riduce la solubilità del soluto nella soluzione. In entrambi i processi è stata valutata l'influenza di due polimeri (carbossimetilcellulosa e k-carragenina) aggiunti a diverse concentrazioni (0.05% e 0.1% in peso) durante la cristallizzazione al fine di studiarne l'effetto sulle proprietà superficiali dei cristalli di curcumina. Le particelle Pickering ottenute sono state caratterizzate in base a forma, dimensione, bagnabilità e concentrazione. Sono state impiegate le seguenti tecniche: spettroscopia Raman e diffrazione a raggi X da polveri (PXRD) per l'identificazione della forma polimorfica; calorimetria differenziale a scansione per lo studio degli effetti termici; microscopia ottica e microscopia elettronica a scansione per l'analisi di forma e dimensione dei cristalli; distribuzione granulometrica e misura dell'angolo di contatto per la valutazione della bagnabilità. Successivamente, sono state preparate emulsioni acqua-in-olio con diverse concentrazioni di acqua (5-20% in peso) e con un quantitativo fisso di curcumina (20 mg) per ciascuna delle forme polimorfiche. Queste emulsioni sono state sottoposte ad analisi della

distribuzione dimensionale delle gocce per valutarne la stabilità e l'efficacia dei polimorfi della curcumina come stabilizzanti Pickering, correlando le dimensioni delle particelle con quelle delle gocce.

I risultati delle prove di solubilità hanno confermato la preferenza della curcumina per ambienti alcalini rispetto a quelli acidi e una solubilità aumentata a temperature prossime a quella corporea. La spettroscopia Raman e le analisi PXRD hanno confermato l'efficacia delle tecniche di cristallizzazione scelte per ottenere i polimorfi desiderati e la diretta dipendenza dalle condizioni di processo. I cristalli ottenuti, di entrambi i polimorfi, presentano una forma allungata e una distribuzione dimensionale uniforme, seppur con evidenti differenze dimensionali, infatti, il valore medio del diametro di Feret per la forma I è di circa 60 μm mentre per la forma III è di circa 2 μm. La misura dell'angolo di contatto, che è risultato sempre maggiore di 90°, ha infine confermato la natura idrofobica della curcumina. La presenza di polimeri non ha determinato variazioni evidenti nella dimensione, forma o polimorfismo dei cristalli. Tuttavia, ha provocato un aumento dell'angolo di contatto, accentuando la natura idrofobica della curcumina e favorendo il posizionamento delle particelle all'interfaccia tra le fasi e migliorando la stabilità del sistema.

L'osservazione al microscopio ottico ed elettronico dei campioni di emulsioni ha evidenziato che i cristalli di forma I tendono a formare una barriera interfacciale meno compatta, formando agglomerati di cristalli che vanno quindi ad alterare la distribuzione dimensionale delle gocce della fase dispersa e quindi rendono il sistema meno stabile. La forma III invece, avendo dimensioni simili a quelle delle gocce tendono a posizionarsi all'interfaccia olio-acqua, aumentando la stabilità del sistema, sebbene quest'ultima non sia mantenuta in modo permanente nel tempo. In conclusione, questo studio conferma che i cristalli di curcumina possono rappresentare una valida alternativa ai tensioattivi tradizionali per la stabilizzazione delle emulsioni Pickering, con applicazioni potenzialmente eco-sostenibili e sicure. È stato evidenziato come la stabilità e l'efficacia delle emulsioni dipendano strettamente dalle proprietà delle particelle di curcumina e come la scelta del polimorfo, della dimensione e della forma delle particelle consenta di modulare le caratteristiche del sistema in base alle applicazioni specifiche. Sviluppi futuri potrebbero concentrarsi sulla modifica delle condizioni di cristallizzazione per ottenere cristalli di dimensioni e forma comparabili per entrambi i polimorfi. Inoltre, si potrebbe indagare l'uso di altri polimeri, variandone la concentrazione in soluzione, e condurre nuovi esperimenti sulla produzione e caratterizzazione di ulteriori polimorfi e co-cristalli della curcumina.

Abstract

Emulsions stabilized by solid particles are a specific type of emulsion in which solid or colloidal particles are used as emulsifiers; these particles adsorb, at oil-water interfaces more strongly than traditional surfactants. These emulsions are known as Pickering emulsions and represent a valid alternative to traditional ones due to their improved stability, biological compatibility, low toxicity, and environmental friendliness. The properties of the solid particles, such as size, shape, polymorphism and wettability, have an important role in stabilising Pickering emulsions. Curcumin was chosen in this work for its interesting interfacial properties, which enable curcumin particles to act as a stabilizer in emulsions. The present research focused on the production and characterization of two curcumin polymorphs, form I and form III. The aim was to produce different curcumin polymorphs of comparable sizes and shape distribution in a reproducible manner, using a crystal engineering approach, and test the two different forms as Pickering stabilizers. Two distinct crystallization techniques were employed to obtain the target polymorphs: form I was generated via cooling, meanwhile form III was obtained through antisolvent addition. The potential influence of polymers (carboxymethyl cellulose and k-carrageenan) on the crystallization process was also investigated to determine if these molecules had any effect on the interfacial properties of the crystals. Initial tests were performed with the Crystal 16 system and High-Performance Liquid Chromatography measurements to determine curcumin solubility in ethanol/water mixtures; additionally, the curcumin solubility was evaluated in aqueous solutions at different pH. The obtained particles underwent a comprehensive characterization: Raman spectroscopy and Powder X-ray Diffraction (PXRD) were used to identify the actual polymorphic form; Differential Scanning Calorimetry (DSC) to assess the effects of temperature; Optical Microscopy and Scanning Electron Microscopy (SEM) to examine particle shape and size distribution (PSD) of the crystals and finally contact angle measurements were conducted to evaluate the wettability of the produced powder. After that, water-in-oil (W/O) emulsions were prepared with different batches of the powders previously obtained with varying water content (range 5 – 20wt%). These emulsions were characterised by Droplet Size Distribution, and their stability was assessed. This study confirms the relationship between the properties of curcumin particles and their effectiveness as Pickering stabilizers. It has been shown that particle size should be an order of magnitude different to the droplets in the dispersed phase to ensure system stability and that crystal shape determines the particle's disposition at the interface.

The two chosen crystallization techniques successfully led to obtaining the two polymorphic forms, demonstrating that crystal engineering can be used to achieve the desired crystalline structures. It also revealed the impact of polymers on particle size.

Alla mia amata nonna, la stella più luminosa.

Ti porto nel cuore, e il mio successo è anche il tuo.

Table of content

List of abbreviations

API: Active Pharmaceutical Ingredients

CMC: Carboxymethylcellulose

CSD: Cambridge Structural Database

CUR: Curcumin

CUR CONC: curcumin concentration

CUR/CMC: crystals of curcumin realized in a jacketed reactor with CMC in solution

CUR/KCAR: crystals of curcumin realized in a jacketed reactor with k-carrageenan in solution

DSC: Differential Scanning Calorimetry

DSD: Droplet Size Distribution

EtOH: ethanol

Exo: exothermic axis

KCAR: k-carrageenan

MCT: Medium-chain triglycerides

MSZW: metastable zone width

O/W: oil-.in-water emulsion

PSD: Particle Size Distribution

PXRD: Powder X-Ray Diffraction

SD: Standard Deviation

SEM: Scanning Electron Microscopy

SOLV/ANTIS: ratio solvent - antisolvent

TNF: Tumour Necrosis Factor

W/O: water-in-oil emulsion

Index of figures

Index of tables

1. Introduction

Emulsions are heterogeneous mixtures in which one liquid is dispersed in another immiscible liquid. The stabilisation of droplets can be achieved by using surfactants or amphiphilic polymers, which reduce interfacial tension and electrostatic repulsion between the phases, resulting in a stable dynamic system. [1] Generally, emulsions are classified as unstable systems. Pickering emulsions, that are emulsions stabilised by solid or colloidal particles rather than by surfactants or chemical emulsifiers have drawn increasing research attention in recent years. [2] The solid particles are located at the interface between two immiscible phases (usually an aqueous phase and an oily one) and offer a physical barrier that prevent the coalescence of the droplets. Pickering emulsions are important for their high stability and their potential to control drug release such as the possibility of promoting transdermal absorption of the drug. [3] They are characterised by the properties of particles used, which play an important role in their stability and performance. The use of molecular surfactants to stabilise emulsions presents many disadvantages for the environment and human health, such as water pollution, non-degradability and enzymatic inhibition. [3] Natural particles such as starch, silica, cellulose nanoparticles, and natural clays are gaining significant success as Pickering stabilisers, as their use reduces environmental impact and enhances the biocompatibility and biodegradability of products.

Curcumin, a hydrophobic substance extracted from the rhizome of the *Curcuma longa* plant, [4] has been selected for its interesting interfacial properties, which enable it to act as a stabiliser in emulsions. [5] It is a GRAS (generally regarded as safe) substance even at high daily doses (8-12 g) but its clinical efficacy is limited by its low solubility in the aqueous phase (7.8 mg/L) and low bioavailability (usually 30-45 minutes). [6]

Firstly, solubility studies of raw curcumin in ethanol-water mixtures were conducted to design the crystallization processes to control curcumin interfacial properties. Furthermore, the solubility of curcumin in solutions of varying pH has been tested to evaluate this aspect in the context of its potential use as a modified-release vehicle. The pH varies in the oropharyngeal tract from values close to 6.5-7.5 in saliva to values between 1.5 and 3.5 in the stomach. [8] In the intestinal tract, the environment is alkaline. All these pH changes can affect the efficacy and stability of curcumin within a pharmaceutical or food product.

Oral administration involves taking the drug by mouth, allowing it to be absorbed in the gastrointestinal tract and then delivered through the bloodstream to the target tissues for its pharmacological effect. Oral drugs often need a protective coating or structural barrier to prevent the active ingredient from being degraded by oral enzymes or the stomach's acidic environment. [9] Studying the interaction of solid particles with various bodily environments can help designing Pickering emulsions that release the active ingredient at the intended site within the digestive system. It is known that external stimuli such as temperature, light, pH changes and electrical and magnetic stimuli can influence the physicochemical properties of the particles and thus cause a destabilization of the emulsion (Figure 1.1). [9]

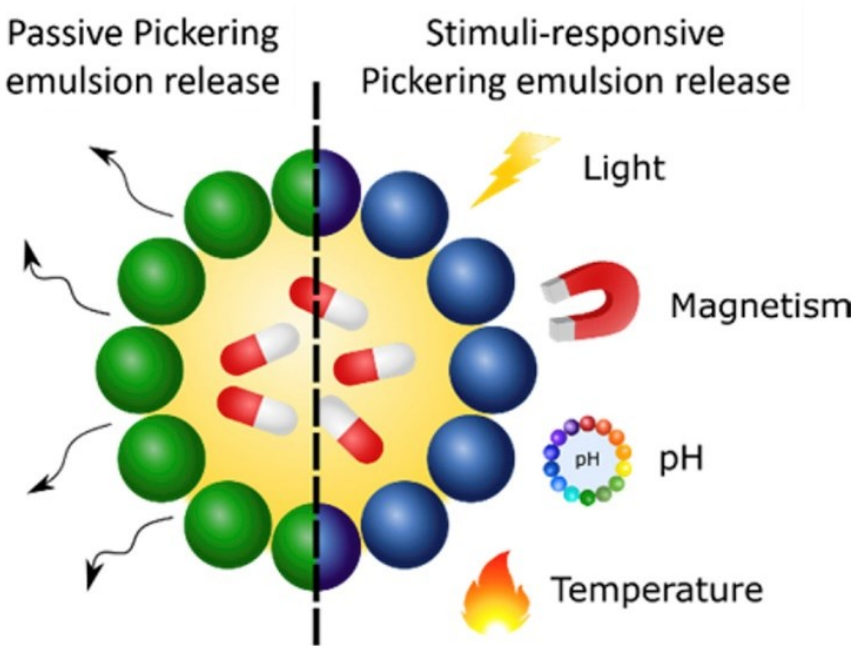

Figure 1.1: External stimuli action on Pickering emulsions [9]

The sensitivity to pH is a widely recognised mechanism employed in drug delivery systems, allowing for the utilisation of the acidic or basic characteristics of target tissues (with a pH of 2-3 in the stomach, pH 7.5 in the intestines, and weakly acidic environments near cancer cells) to initiate the release of the active ingredient. [10]

There are several polymorphic forms of curcumin, which can be classified into stable and metastable forms. Polymorphism is the phenomenon whereby a crystalline material can exist in different crystal structures. [7] The polymorphic form in which a material crystallises directly depends on the conditions of nucleation and growth, which in turn are influenced by external factors such as temperature, pressure, growth rate, presence of impurities. Different polymorphs

have the same chemical composition, but their spatial arrangement and/or conformation varies, which in turn leads to different interfacial properties.

Form I is the most thermodynamically stable polymorph of curcumin and was produced using the cooling crystallization, which is a process through which the solute is precipitated using a temperature variation that generate a supersaturated solution. A temperature ramp is set first increasing and then decreasing the temperature to completely solubilize the solute in solution and then nucleate and grow curcumin particles. Form III is a metastable curcumin polymorph and was obtained using antisolvent crystallization which guarantees a good control over crystal size and shape. [11] Supersaturation can be attained by lowering the solute's solubility with the addition of an antisolvent, that is a solvent where the compound presents a lower solubility. An advantage of this technique is that the process can be carried out at a temperature near the ambient. Also, the process would demand low energy and the change in the solvent composition may favour one crystalline structure instead of others. [12]

1.1 Aim and structure of the thesis

The aim of this thesis was the production and characterization of tailor-made curcumin crystals to use as stabilizers in water-in-oil (W/O) emulsions. Two polymorphs of curcumin were chosen to evaluate their stabilization properties: form I and form III. Experiments were then carried out with polymers in solution to define their effect on the surface properties of the curcumin crystals obtained. Different characterization tests were conducted on the powders obtained: Raman spectroscopy and Powder X-ray Diffraction (PXRD) to identify the polymorphic form; Differential Scanning Calorimetry (DSC) to assess the effects of temperature; Optical Microscopy and Scanning Electron Microscopy (SEM) to examine particle shape and size distribution (PSD) of the crystals and then contact angle measurements to evaluate the wettability of the powder.

All these particle properties affect the stability of the Pickering emulsion so they must be known to allow effective formulation. Water-in-oil (W/O) emulsions were then prepared using curcumin crystals obtained from the previous experiments. For each emulsion, the droplet size distribution was measured, and an evaluation of stability was conducted.

This thesis work is composed of five chapters. The content is shown below:

- Chapter 2: is dedicated to a bibliographic study of emulsions, particularly Pickering emulsions. The types of Pickering particles, their properties and the crystallization process are presented. This is followed by a description of the characterization techniques carried out during this project.
- Chapter 3: describes the materials, equipment used, and techniques performed.
- Chapter 4: concerns the results obtained from this study
- Chapter 5: presents conclusions and possible future developments
- Appendix A shows additional graphs and histograms describing the crystals obtained with the various techniques and operating conditions.

2. Background

2.1 Emulsions

Emulsions are a type of dispersed system consisting of two non-miscible liquids, oil and water. They belong to a category of colloids, which are systems consisting of two distinct phases. While the terms "colloid" and "emulsion" are sometimes used interchangeably, "emulsion" specifically refers to systems where both the dispersed and continuous phases are liquid. In contrast, a colloid can consist of a solid, liquid, or gas mixed with a liquid. The key distinction between the two is that colloids can form with any state of matter, while emulsions are characterised by two liquid components that are initially immiscible. [7]

One of the two liquids called the dispersed phase, occurs in the form of small droplets, with a diameter that usually varies between 100 nm and 100 μm, suspended in the other liquid that constitutes the continuous phase. Depending on the nature of the phases, a distinction can be made between oil-in-water (O/W) emulsions, in which the oil represents the dispersed phase, and water-in-oil (W/O) emulsions, where the dispersed phase is water. [13] The process of forming an emulsion from two separate immiscible steps is called emulsification. The most common methods involve the use of mechanical devices capable of generating intense shear stress capable of deforming the droplets of the dispersed phase until they break. The most widely used equipment for this purpose includes high-pressure homogenizers, sonicators, rotor-stator mixers, and colloidal mills. [9]

As liquids, emulsions do not possess a fixed internal structure. They are generally unstable from a thermodynamic point of view.

Droplets have properties of metastable colloids: Brownian motion is significant for droplets smaller than 1 μm, reversible phase transition resulting from droplet interactions, and irreversible transitions that determine their destruction. [15]

The change in free energy associated with the creation of the dispersed system can be described, according to the second law of thermodynamics, [16] as follows:

$$\Delta G = \gamma_{ow}\Delta A - T\Delta S \qquad (2.1)$$

- ΔG is change in Gibbs free energy
- $\gamma_{ow}\Delta A$ is always a positive term because it indicates the increase in surface area (ΔA) linked to interfacial free energy (e.g., γ_{ow} for oil-water)
- $T\Delta S$ represents the configurational entropy that increases in the system due to the formation of droplets from a segregated system (negligible term). T is the absolute temperature of the system and ΔS is change in entropy

The instability of an emulsion leads to the separation of the two phases, generally due to phenomena such as coalescence or Ostwald ripening. Coalescence is an irreversible process in which droplets come together, progressively increasing in size. Ostwald ripening, on the other hand, occurs when the smaller droplets, being unstable from a thermodynamic point of view, dissolve in the continuous phase and settle on the larger droplets, causing them to grow.

There are also other forms of instability in which the dispersed phase aggregates but is still divided into droplets. In the case of creaming or sedimentation, separation occurs under the effect of gravity, while in flocculation the aggregates are held together by weak attractive forces, such as Van der Waals forces. The latter phenomena are reversible, since there is no complete separation of the phases, allowing the original emulsion to be re-established with a slight mixing. [56]

Despite thermodynamic instability, kinetically stable emulsions can be obtained, in which the droplets remain uniformly dispersed for a significant period thanks to the use of emulsifiers. These substances, such as surfactants (amphiphilic molecules), adsorb on the surface of the droplets and reduce the interfacial tension between the two phases, thus preventing their aggregation. Typically, the surfactant's affinity is highest in the continuous phase. Consequently, hydrophilic surfactants tend to stabilise oil-in-water (O/W) emulsions, while lipophilic surfactants are more effective for water-in-oil (W/O) emulsions. [17]

Emulsifiers can be natural, such as lecithin, proteins, and gum arabic, or synthetic, such as polysorbates and mono-diglycerides. They have applicability in various fields, including cosmetics, food, and pharmaceuticals.

2.2 Pickering emulsions

A Pickering emulsion is a specific type of emulsion that employs solid or colloidal particles as emulsifiers, which adhere to the oil-water interface (Figure 2.1). In 1907, British chemist Percival Spencer Umfreville Pickering claimed that the presence of a layer of solid particles or nanoparticles increased the lifespan of oil droplets and air bubbles in a continuous aqueous phase. [18] The steric barrier of solid particles formed at the liquid-liquid interface ensures stability to Pickering emulsions.

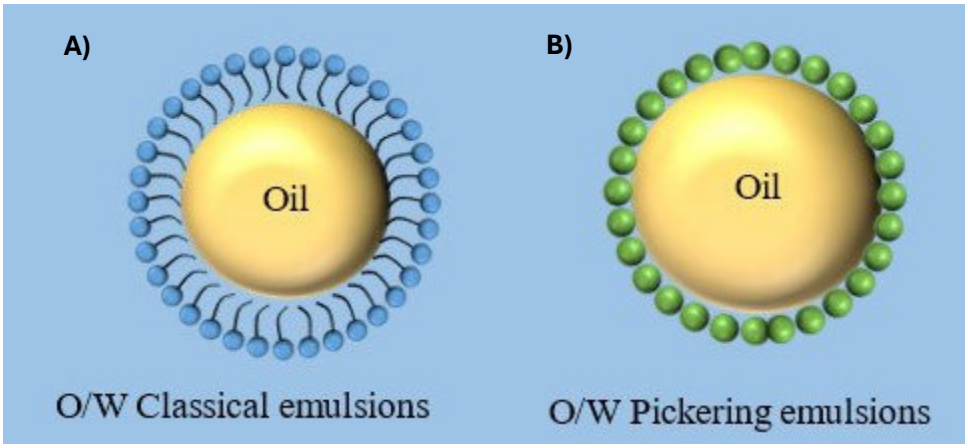

Figure 2.1: A) Molecular surfactants distribution at the interface in classical emulsions (O/W) B) Solid particle distribution in Pickering emulsions (O/W) [19]

The emulsifier must be biocompatible, non-toxic, and capable of being excreted by the body. Long-term stability is also relevant as it must be compatible with the storage time of the product. For these reasons, Pickering emulsions are interesting systems in the field of functional food systems and drug delivery. [3]

The stabilization mechanism offered by solid particles is different from that of surfactants, as it does not result in a reduction in interfacial tension. Conversely, the particles prevent droplet coalescence by creating a steric obstacle and limiting mass transport processes, thus reducing the contact area between the two immiscible phases. The particles adsorbed at the interface can take various configurations, as illustrated in Figure 2.2.

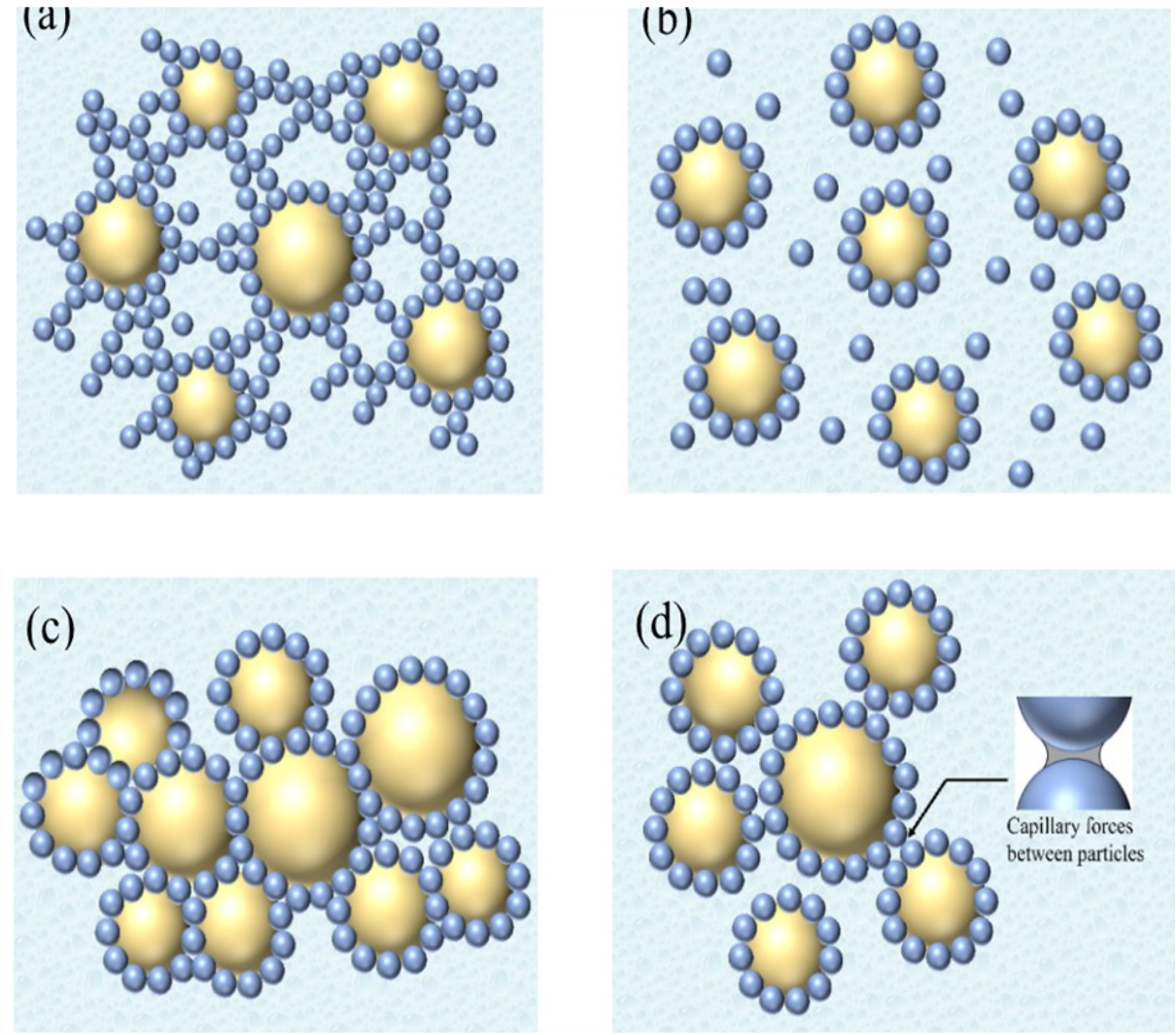

Figure 2.2: Different configuration of particle adsorbed: (a) a three-dimensional lattice that keeps the droplets separate, when solid particles are particularly abundant; (b) barrier to the interface with scattered domains; (c) bridging phenomenon; (d) capillary mechanism at the interface. [3]

The steric barrier prevents liquid droplets from clumping, providing stability to the emulsion. High stability, low toxicity and low cost are the reasons why they find applicability in various fields such as pharmaceuticals, cosmetics, food and oil extraction. [2] In the food industry, complex particles of protein-polysaccharides, gliadins and flavonoids are used as emulsifiers for Pickering emulsions that can transport nutrients, replace animal fats and be used as food packaging and cleaning agents. [20] In cosmetics, these emulsions enhance the penetration of active ingredients into the skin, minimize irritation, and improve product stability. Some Pickering emulsions are used as oil displacement, modification and fracturing fluid agents to increase crude oil recovery efficiency. [3] In pharmaceuticals, specifically in vaccine development, it is possible to use Pickering emulsions as an adjuvant in the formulation of the

vaccine itself. In addition, the application of Pickering emulsions encapsulating and administrating bioactive ingredients is being explored. [18] Additionally, the thick layer of solid particles surrounding the dispersed phase of an emulsion can impede the diffusion of drug molecules, enabling Pickering emulsions to act as efficient systems for encapsulation and controlled drug release. [21]

Using tailor-made stabilizing particles or thickening the layer of particles around the droplets can lead to the development of controlled release formulations designed to sustain the desired drug concentration in the bloodstream or tissues over a longer duration compared to traditional formulations. [22]

Although Pickering emulsions are promising materials, several aspects still need to be improved. [18] For example, the choice of solid particles and the complete understanding of their behaviour under different environmental conditions such as varying pH, temperature and electrical and magnetic stimuli. [9]

2.3 Types of Pickering particles

Type of particles at the interface between phases in an emulsion (oil-in-water or water-in-oil) has a strong effect on its stability, microstructure and physical properties.

Numerous studies have shown that both inorganic particles such as silica, clay, and hydroxyapatite (Hap), as well as organic particles, can act as Pickering emulsifiers. [23] Hydroxyapatite is a major mineral in the human body, as it is found in bones and teeth. Due to its excellent adsorbability, it is widely used as a stabiliser in emulsions when ester groups are present on nanoparticles surface. However, in the absence of these groups, Hap nanoparticles cannot function as Pickering particles. [24] Other studies have focused on the use of silica, as it is easily obtainable; however, its application is limited by its hydrophilic nature. This has led researchers to explore modified silica to achieve different properties for greater versatility. [23] [25] Clay, finally, is one of the most well-known stabilisers because it is inexpensive and readily available; however, it also has a hydrophilic nature, so it must be modified to remain anchored at the water-oil interface.

On the other hand, biological and food-grade particles, such as curcumin, have gained significant attention as Pickering stabilisers due to their high biocompatibility, biodegradability, and potential applications in drug and food delivery. [23]

Curcumin is a naturally derived polyphenol extracted from the *Curcuma longa* plant. It is highly insoluble in an acidic or neutral environment, while it is unstable and decomposes. His hydrophobic nature determines a poor absorption through the intestinal epithelium, it is rapidly metabolized in the liver and intestine, rapidly eliminated through bile and urine, and rapidly degraded as chemically unstable at alkaline pH. However, curcumin has beneficial effects for its anti-inflammatory, antioxidant, antiproliferative and angiogenic activities. [26] Moreover, it may have preventative action against various diseases such as Alzheimer's disease, malaria, cancer, HIV and proliferative diseases. [6] In 1815 Vogel and Pierre Joseph Pelletier were the first to isolate curcumin from the rhizome of turmeric and only in 1910 Lampe and Milobedeska were able to characterize it through analytical techniques.

There are two forms of curcumin, due to tautomerism, i.e. the transfer reaction of a proton between groups of the same molecule: beta-diketone and keto-enol (Figure 2.3). [6] In solution, there is a balance between the forms, but changes in pH may favour one or the other form. In an acidic aqueous environment, the diketone form prevails, while the enol form prevails at a pH greater than eight. Under ambient conditions, curcumin has a structure with a density of 1.3 g/cm^3.

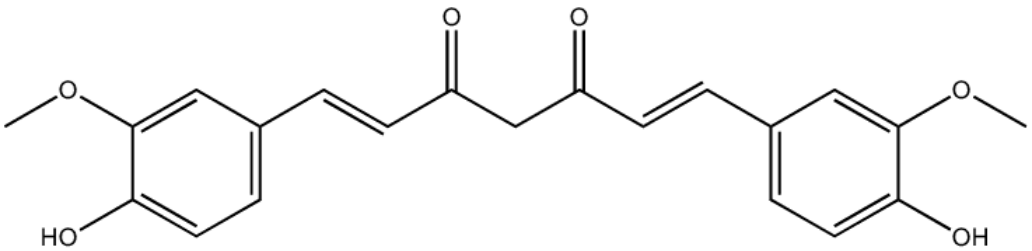

CURCUMIN
Diferuloylmethane

Chemical Formula: $C_{21}H_{20}O_6$
Molecular Weight: 368.4
Elemental Analysis: C, 68.47; H, 5.47; O, 26.06

Figure 2.3: Curcumin chemical structure [30]

The chelating abilities of curcumin with different metal ions and their biochemical activities have been demonstrated. Time-dependent UV spectroscopy has shown that curcumin can

significantly slow degradation within micellar nanocavities due to its interaction with polymer micelles. [33] It has an antioxidant effect as it can activate different antioxidant proteins and has a dual function: it prevents the formation of free radicals and neutralizes existing ones. Curcumin is also renowned for its anti-inflammatory properties as it can block the transcription factor NF-kB and therefore the production of proinflammatory cytokines such as TNF (Tumour Necrosis Factor) and several leucine. Recent studies have shown that the oral intake of curcumin involves a transformation of the same by the intestinal flora and therefore a neuroprotective and regulatory action of the intestinal microbiota. Curcumin is also effective in the treatment of cardiovascular disease, type II diabetes and rheumatoid arthritis. Curcumin is also studied in oncology as it can regulate several transcription factors as NF-kB whose dysfunctions are linked to cancer. [27]

Despite all the benefits listed, curcumin has poor bioavailability, and this reduces its use in the medical and pharmaceutical fields. Over the years, however, techniques have been studied to increase the bioavailability and stability of curcumin such as the addition of adjuvants and complexation with cyclodextrins. Furthermore, attempts have been made to encapsulate curcumin as an API (Active Pharmaceutical Ingredients) dissolved within the dispersed phase. [26]

Due to its lipophilic nature, it can permeate the cell membrane emulating the apoptosis process that induces a partial and reversible loss of membrane integrity which will then be recovered in a short time. This ability of curcumin can be exploited to attack cancer cells as it blocks the angiogenesis processes (formation of new blood vessels) on which they depend strongly. [28] Lou et al. were the first to show that W/O emulsions can be stabilized by natural polyphenols. [5] The efficacy of the action of different polyphenols as stabilizers in Pickering O/W emulsions has been evaluated by the log(P), where P represents the partition coefficient between n-octanol and water. This parameter describes the hydrophobicity of the polyphenolic molecule to which it refers. In the case of curcumin, the log P varies between 2.3 and 3.2 thus defining a marked hydrophobicity at room temperature and neutral pH. [29] However, this parameter is not sufficient to evaluate the stabilizing power of a particle in Pickering emulsions. In fact, it is appropriate to consider the balance between hydrophilic and hydrophobic components of the particle under study using the three-phase contact angle. [5]

In addition, it is appropriate to investigate the molecular structure and crystallographic properties as curcumin is present in the solid state and this can affect the exposure of hydrophilic and hydrophobic groups on the different crystal faces.

2.3.1 Polymorphism

Crystalline materials can be characterised by their structural arrangement, which represents the way atoms and molecules are arranged in an orderly manner. Sometimes, a single chemical substance can exist in multiple crystalline forms, a phenomenon known as polymorphism.

The specific crystalline form that a material can adopt depends on the conditions of nucleation and growth, which are influenced by factors such as temperature, pressure, solvent type, and the presence of impurities in the solution. Polymorphs are crystalline phases made up of the same molecules or ions but arranged or conformed differently in the solid state. Although the chemical composition remains unchanged across the different polymorphs, physicochemical properties such as density, melting point, heat capacity, and thermal conductivity can vary. Moreover, a change in crystal structure can affect the morphology of the crystal, a key parameter in industrial crystallisation processes. [31]

There are several polymorphic forms of curcumin. Specifically, the curcumin available on the market corresponds to the monoclinic form (form I). [6] From II and III are orthorhombic. The monoclinic one has a curved and slightly twisted conformation, whereas the orthorhombic has a linear and planar conformation. During the purification of curcumin, the pressure applied for evaporation of organic solvent determines the polymorphic outcome. [32] Generally, form I is obtained at pressure from 300 to 400 mbar whereas form III is obtained by antisolvent precipitation. It was observed that form III is not stable during time and irreversibly convert to form I upon heating or when in organic solutions at temperatures ranging from 0°C to 50°C. [32]

This study focused on exploring the use of two different polymorphic forms of curcumin as Pickering stabilizers. Aware of the differing properties of the two forms, crystals synthesis was design to obtained, ideally, particles of comparable size and shape, to then compare their stabilising effect as emulsifiers.

It is essential to have strict control over the operating conditions of crystallization processes to obtain the desired polymorph to prevent the transformation of a more stable form.

There are metastable polymorphic forms (not thermodynamically stable) and stable ones. The former tends to transform into the latter over time in certain conditions. In this study, as representative samples of the two types of polymorphs, form I (stable) and form III (metastable) were selected. [31]

2.4 Properties of Pickering particles

The main properties that determine the stabilising effectiveness of solid particles are their size, morphology, surface properties (e.g. wettability) and their concentration in the system (Figure 2.4).

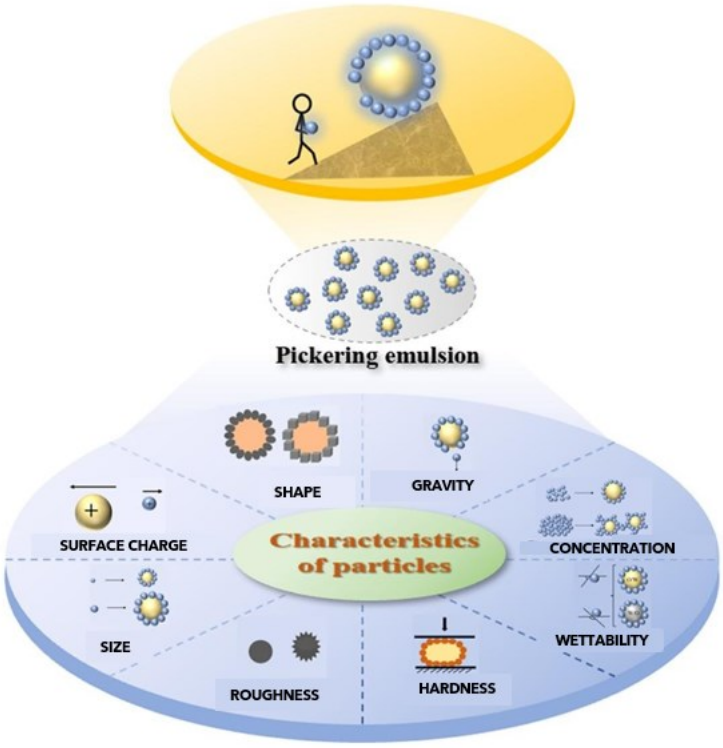

Figure 2.4: Schematic representation of characteristics of Pickering particles. Modified from [3]

To achieve good emulsion stability (e.g., smaller droplet size distribution), the use of particles with a reduced size is desirable. The smaller the particles, the better the packing on the surface of the droplets, providing a more effective barrier against coalescence. [5] The mean droplet diameter in a Pickering emulsion is at least an order of magnitude larger than the mean size of the particles used. In general, they can be between tens of nanometres and micrometres in size.

In addition to size, the shape of the particles is also crucial for emulsion stability. The use of particles with non-spherical geometries, such as cubes, ellipsoids, or needles, can enhance the coverage of the oil-water interface if designed correctly. [34]

The surface charge of solid particles also affects emulsion stability. By modifying parameters such as electrolyte concentration or pH, it is possible to destabilise the emulsion by increasing the electrostatic repulsion between the particles, thereby promoting their detachment from the droplet interface.

The surface roughness of the particles also plays an important role in emulsion stability, influencing the potential at the interface, and the contact angle of the particles, so the wettability of the powder. [23]

Furthermore, it has been observed that the stabilising capacity increases with the concentration of particles dispersed in the liquid phases, which can form a more compact interfacial layer and, in some cases, a three-dimensional network in the continuous phase that restricts the movement of the droplets. [35] Some Pickering particles can self-assemble into ordered structures, contributing to emulsion stabilization and improving the mechanical properties of the continuous phase.

The use of solid particles can improve the thermal and mechanical stability of emulsions, making them less susceptible to temperature changes and mechanical stress, and affect the rheological properties of emulsions, such as viscosity and consistency. This is important for applications where texture is a key factor, such as in food or cosmetic products.

One important aspect to consider is the wettability of the solid with the aqueous phase. The adsorption of particles at the oil-water interface is significantly influenced by the hydrophilic or hydrophobic nature of the surfaces of the solid particles, which relates to the three-phase contact angle of the solid-water-oil system. The particles need to be partially wetted by both phases; however, the continuous phase is typically the liquid that has a greater affinity for the solid. [35]

Depending on whether the particles used are hydrophilic or hydrophobic, we would have a different angle of contact (θ): if the angle formed between the solid and the water phase is less than 90° the powder presents hydrophilic behaviour, hydrophobic if greater than 90° (Figure 2.5).

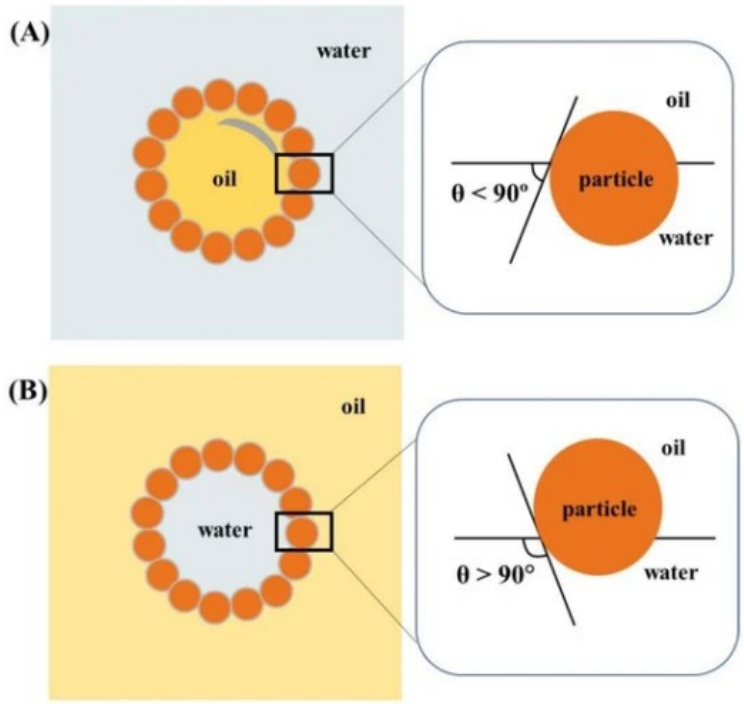

Figure 2.5: (A) Hydrophilic and (B) hydrophobic behaviour of particles at the interface in emulsion [18]

Depending on the hydrophilicity or hydrophobicity of the particles, it is possible to determine whether they can stabilise an oil-in-water (O/W) or water-in-oil (W/O) emulsion, respectively. In the case under consideration in this thesis, the particles are hydrophobic and therefore have the maximum desorption energy at the interface, described by the following equation:

$$E = \pi R^2 \gamma_{ow} (1 + cos\theta)^2 \qquad (2.2)$$

- γ_{ow} is surface tension
- R the radius of the spherical solid particle
- θ contact angle

From the equation a three-phase contact angle value of 90° provides the most favourable conditions for the stabilization of the system so that the particles are adsorbed at the interface and do not remain dispersed in one of the two phases. [36] [18] Binks' research group has investigated the stabilization mechanism of Pickering emulsions using particles with varying degrees of hydrophobicity. [37]

Particle surface properties can be intentionally modified using polymers or surfactants during synthesis processes, which directly affects their effectiveness in stabilizing Pickering emulsions by including variations in their surface properties. Additionally, the use of such polymers can reduce the surface tension and increase the viscosity of the solution, thereby influencing the

kinetics of the crystallisation process. [38] However, an increase in viscosity reduces the frequency of particles collisions and decreases the mass transfer between the solution and the solid-liquid interface, which extends the nucleation time. As a result, a greater number of nuclei are formed; their growth will be hindered, resulting in smaller size distribution of the resulting crystals. Therefore, our interest has moved to the evaluation of the effect of the presence of polymers (carboxymethylcellulose and k-carrageenan) during the crystallization of both curcumin polymorphs.

Carboxymethylcellulose (CMC), identified by the acronym E466, is a polysaccharide, i.e. a sequence of monosaccharides linked by glycosidic bonds. The molecular structure is reported in Figure 2.6. CMC is produced from cellulose, which is reacted with caustic soda and mono-chloroacetic acid. Recent studies have shown that CMC shows stabilising efficacy even at high temperatures. [39] The stabilising capacity is common to polysaccharides because they offer steric encumbrance around droplets and form a viscoelastic layer at the interface when in the presence of hydrophobic groups or protein fractions. CMC differs from cellulose for some carboxymethyl anionic groups as a replacement for hydrogen atoms.

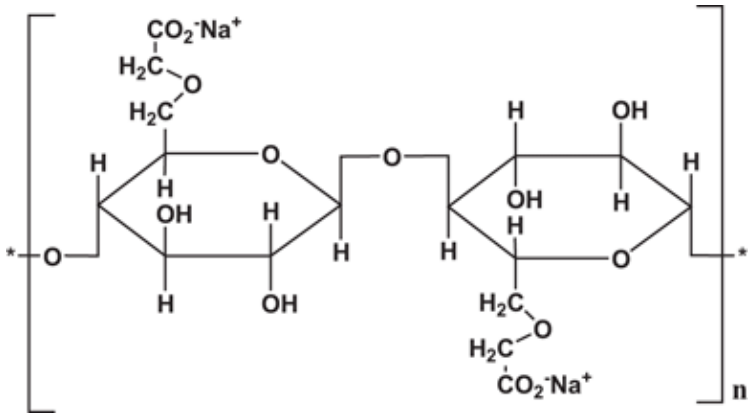

Figure 2.6: Chemical structure of carboxymethylcellulose (CMC) [40]

CMC is easily available and has a low cost, it can be extracted from plants (e.g., sago palm, corn husk, sugarcane bagasse, wastepaper) and has a structure characterized by both crystalline and amorphous regions. [39] In the pharmaceutical field, it is used, as an excipient, for oral formulations for ophthalmic use or injectable preparations. It is possible to modify its morphology via a chemical treatment, due to the presence of reactive hydroxyl groups that affect the surface area of the nanocrystals. [23] CMC is insoluble in water, so it is possible,

following esterification, oxidation, and cationization reactions, to vary the hydrophobicity of the particles and use them as a stabilizer in Pickering emulsions. [18]

K-carrageenan is a polymer with a disaccharide repeating unit derived from galactose. It is an ionic polysaccharide, obtained from red algae and often used as a food additive for its gelling, stabilizing and thickening properties.

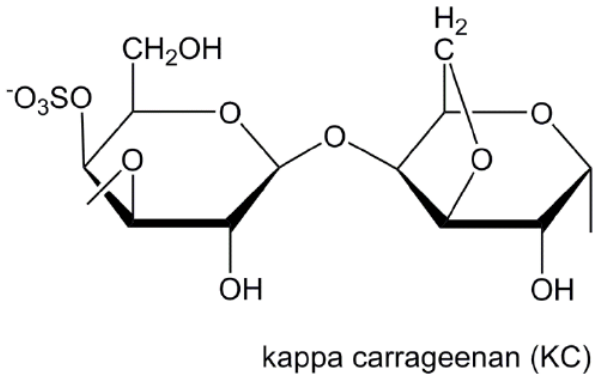

Figure 2.7: Chemical structure of K-carrageenan [41]

K-carrageenan (Figure 2.7), when in solution with curcumin, forms complexes that enhance the solubility of curcumin in aqueous solutions, facilitating its absorption in the body. [42] [43] The increased melting point of curcumin indicates the colour protection provided by carrageenan chains. [42] Furthermore, the hydrogen polymer-curcumin bond causes a change in the solubility of curcumin (from $1\ \mu g/mL$ to $25-37\ \mu g/mL$) at neutral pH. [43] K-carrageenan can stabilize curcumin and slowing its degradation. [42]

2.5 Crystallization

Crystallization techniques are used to produce solid particles and have numerous applications in the chemical and pharmaceutical industries. The crystallization process involves a phase transition from the molecular state to the solid state, where the molecules are arranged in an orderly structure. [31] This process is triggered by supersaturation, which is the condition in which the maximum limit of solute that can dissolve in the solvent is exceeded. [31]

Supersaturation can be defined as the difference in concentrations:

$$\Delta S = C - C^* \qquad (2.3)$$

or as the ratio between the concentrations:

$$S = \frac{C}{C^*} \qquad (2.4)$$

or alternatively as relative supersaturation:

$$\sigma = \frac{\Delta S}{C^*} = S - 1 \qquad (2.5)$$

- C is the supersaturation concentration
- C^* is the equilibrium concentration from the solubility

The exceeding of the supersaturation limit is the driving force of this process, as it leads to the formation of the first solid nuclei within the solution due to instability. The system, being unstable, seeks to return to equilibrium by crystallization. [31]

Generally, the solubility of a solute in a specific solvent is a function of temperature and increases with it. The correlation between these two variables is visible in solubility curves. Solubility curves indicate the maximum concentration of solute that can be dissolved at a specific temperature. These curves are useful for describing the state of the solution, as they help determine whether the system is in a state of supersaturation. If in a state of supersaturation, crystallisation may be triggered. Between these two states exists a region known as metastable zone, where the system can maintain supersaturation for a certain range without triggering nucleation. The width of this state varies depending on the system being studied. [44]

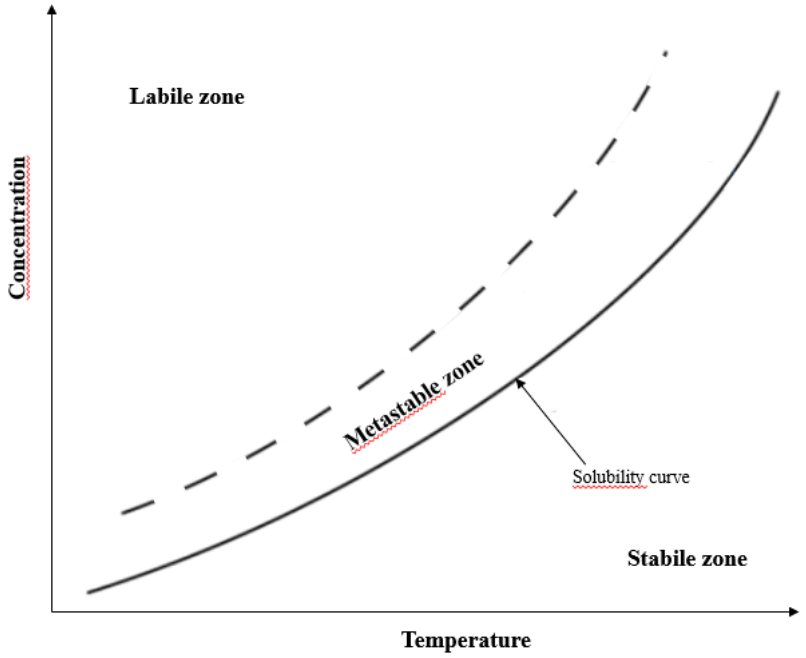

Figure 2.8: Solubility curve and the presence of metastable and labile zones. Modified from [45]

From the Figure 2.8, it is possible to identify the stability zone below the solubility curve and the unstable or labile zone above it. Under stable conditions, no nuclei form within the system. Between the solubility curve and the super-solubility limit lies the metastable zone that is the kay to obtain high quality crystal products. [45] Once the super-solubility limit is exceeded, the system enters the labile or unstable zone, where primary nucleation can occur. The duration of time spent in either of the two zones beyond the solubility curve determines the number of crystals in the system and their size. [45]

It is important to define the metastable zone width (MSZW) because it determines the nucleation behaviour of the system. [46] Based on this region, the operating conditions for crystallisation processes can be defined.

Nucleation, which is the formation of the first particles of the new phase, can be classified as primary or secondary, depending on whether there are crystals of the same nature in the primitive phase. Primary nucleation can be homogeneous or heterogeneous. Homogeneous nucleation is a spontaneous phenomenon that depends solely on supersaturation and occurs in the absence of suspended particles. Heterogeneous nucleation, on the other hand, depends not only on supersaturation but also on the presence of system heterogeneities (solid particles, dust, container walls). [31] Secondary nucleation can occur where there is already presence of crystals in solution.

There are two controlling mechanisms in this case:

- existing crystals serve as nucleation sites if they have defects in their structure (impurities, vacancies, dislocations)
- nucleation may occur at lower levels of supersaturation because crystals prefer to grow on already crystalline surfaces rather than at the interface between the liquid and solid phases (resulting in lower energy expenditure for bond formation).

Generally, this form of nucleation is unfavoured because it can lead to the formation of undesirable crystalline phases and non-uniform particle size distributions. Temperature, pressure, composition, and cooling rate influence the likelihood and extent of this phenomenon. [47]

Growth follows the nucleation phase. It involves diffusion of molecules dispersed in the solvent towards one of the growing crystals, where they are incorporated via a reaction step. The growth rate corresponds to the rate at which the particle size changes over time. This process is

controlled by diffusion, which is the transport of molecules from the bulk of the liquid to the surface of the particle, and by surface integration, which is the incorporation of molecules into the crystalline structure.

In this study, to selectively obtain the polymorphs of curcumin of interest, a crystal engineering approach was applied. This approach is based on the relationship between molecular chemistry and crystallographic structure and the specific physical and functional properties of the resulting particles. Crystal engineering involves the study of intermolecular interactions within the context of crystal packing, aiming to understand how these interactions influence the bulk and surface properties of solids, with the goal of designing new materials with tailored physical and chemical characteristics. [48] The main objective is to control molecular interactions and, consequently, the properties of crystalline materials, such as solubility and bioavailability, to modulate crystallisation and obtain structures with desired characteristics that can be applied in fields such as pharmaceuticals, nanotechnology, and materials engineering. [49]

Several crystallisation techniques can be employed and are classified based on the method used to induce supersaturation. Cooling, solvent evaporation, antisolvent, and chemical reaction are the most common techniques. Solvent evaporation involves the removal of the solvent through evaporation, resulting in the concentration of the solution and triggering crystallisation. The reaction crystallization technique involves the mixing of two reactants, leading to the formation of a product whose solubility is rapidly exceeded, thereby initiating the formation of crystals. [50]

Cooling is a crystallisation method that precipitates a solute from a solution by lowering the temperature, capitalizing on the temperature-dependent solubility of many substances. The process starts with a supersaturated or near-saturated solution, where the solute is fully dissolved at an elevated temperature. As the solution gradually cools, the solubility of the solute decreases, reaching the saturation point. At this stage, the solution can no longer contain all the solute in dissolved form, leading to the formation of solid nuclei. Once the nuclei have formed, the solute starts to aggregate around these nuclei, leading to crystal growth. The speed and quality of crystal growth depend on the cooling rate, the solute concentration, and other operational parameters. [51] The process is influenced by the cooling rate, which determines the size of the crystals, the degree of supersaturation, and the presence of impurities. The latter directly affects the nucleation temperature.

Antisolvent crystallisation is a technique used to precipitate and crystallise a solute from a liquid solution by adding another solvent, called an antisolvent, which is miscible with the original solvent but in which the solute has low solubility. Starting with a solution where the solute is dissolved, the antisolvent is gradually added. As the antisolvent mixes with the original solvent, it lowers the solubility of the solute, leading to supersaturation. This condition is essential for crystallisation to occur. This crystallisation technique has the advantage of being carried out at temperatures close to room temperature. [12] Additionally, the change in solvent composition can favour one crystalline structure over another. For these reasons, antisolvent crystallisation is also used for crystallising thermolabile substances. [12]

2.6 Analysis and characterization of solid particles

Solubility tests were conducted using the Crystal 16 apparatus (Technobis), followed by High-Performance Liquid Chromatography (HPLC) measurements to assess the solubility conditions of curcumin in ethanol/water mixtures, allowing for the design of crystallisation experiments. The properties of Pickering particles determine the stability, effectiveness, and microstructure of emulsions. For this reason, the shape, concentration, wettability, and size of all the obtained crystals were determined. For each crystalline form obtained, the following characterisation tests were performed: Raman spectroscopy and Powder X-ray Diffraction (PXRD) to identify the actual polymorphic form; Differential Scanning Calorimetry (DSC) to assess the thermal behaviour of the two polymorphs; Optical Microscopy and Scanning Electron Microscopy (SEM) to examine particle shape and size distribution (PSD) of the crystals and then three phase contact angle measurements to evaluate the wettability of the powder.

2.6.1 Crystal 16

The Crystal 16 instrument permits to conduct parallel experiments controlling the temperature and monitoring the turbidity of the samples. It is extensively used to optimise crystallisation processes, particularly for solubility studies, solvent screening, and crystallisation studies of chemical and pharmaceutical compounds. It is designed to work at small-scale, allowing for the simultaneous crystallisation of multiple samples under controlled conditions. The Crystal 16 is equipped with 16 individual reactors, each of which can hold a small amount of solution

(typically 1-2 mL per reactor). This allows for simultaneous experiments on 16 samples, reducing the time required for solubility and crystallisation tests.

Each sample is subjected to a controlled heating and cooling programme, which is essential for determining the solubility curve of the compound. Temperature changes are applied precisely, with programmable rates, to induce either dissolution or crystal formation. During the experiment, the Crystal 16 monitors the turbidity of the solution via an optical probe that measures light transmission through the sample. This allows the identification of the points at which solute dissolution occurs (when the solution becomes clear) and crystallisation begins (when the solution turns opaque). The data collected during the heating and cooling cycle allow the generation of solubility and metastable zone curves, which are crucial for optimising the purification process or the production of crystalline compounds. For example, the saturation point, and the onset of nucleation can be easily identified.

2.6.2 High Performance Liquid Chromatography

High-performance liquid chromatography (HPLC) is a fast, precise and cost-effective technique used to characterize the composition of a liquid mixture. [52] A graphical representation is reported in Figure 2.9. The constituents of the mixture are separated based on their differing affinities with a stationary phase and the mobile phase. The stationary phase is packing material that is placed inside the chromatographic column. The mobile phase is a solvent pumped into the column at high pressure, transporting the sample under examination along the column. As the analyzed mixture pass through the column, its components interact with both phases and depending on whether they have a greater affinity for the stationary phase or the mobile phase, they will have a longer or shorter retention time. At the bottom of the column, there is a UV-Vis spectrophotometer that measures the absorption of light at a specific wavelength, producing a signal. The detector produces a signal whose intensity varies proportionally with the concentration of the compound being analysed. From the accumulation of these signals, a chromatogram is obtained, which is a graph that correlates the signals intensity with time.

Each peak corresponds to a separate compound, and the area under the peak can be correlated to the concentration of the compound in the analyzed mixture. It is important for the peaks to be distinct and narrow to ensure that accurate chromatography has been performed. In the case

of overlapping peaks, it is advisable to repeat the experiment, modifying the affinity criteria so that the compounds are clearly separated. [52]

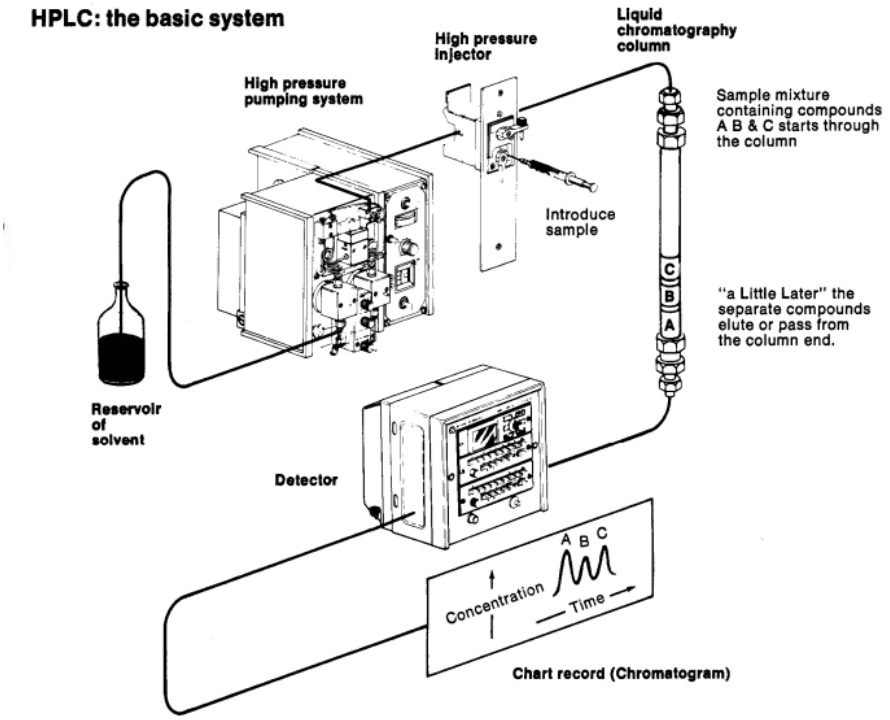

Figure 2.9: High-Performance Liquid Chromatography (HPLC) system [52]

2.6.3 Raman Spectroscopy

Raman spectroscopy is a non-destructive analytical technique that provides detailed information about chemical structure, polymorphism and crystallinity. [53] When a substance is irradiated by a beam of monochromatic light, only a small fraction of this light is scattered. Most of the radiation will retain the same energy as the source, resulting in elastic scattering (Rayleigh scattering). However, a minimal amount (approximately one photon in ten million) of the scattered light will exhibit a different energy compared to that of the incident source, leading to inelastic scattering (Raman scattering). In this process, an exchange of energy occurs between the photon of the incident radiation and the matter, causing the latter to enter an excited state. Part of this energy is used to activate a vibrational motion. Subsequently, the matter returns to its ground state, emitting a photon whose energy is reduced by the amount necessary to activate the vibrational motion. Raman scattering is closely related to the vibrational modes

of a substance; since these are influenced by the mass of the atoms, the bonding forces, and the symmetries, it follows that the Raman spectrum of a material serves as a fingerprint, allowing for its unique identification. [54]

The scattered light is collected by a detector and analysed (Figure 2.10). The variations in energy of the scattered light correspond to different molecular vibrations, generating a Raman spectrum that displays intensities as a function of frequency. The bands in the spectrum correspond to various vibrational modes of the molecules. The positions and intensities of the bands in the spectrum can provide information about the chemical structure, symmetry, and molecular interactions of the sample.

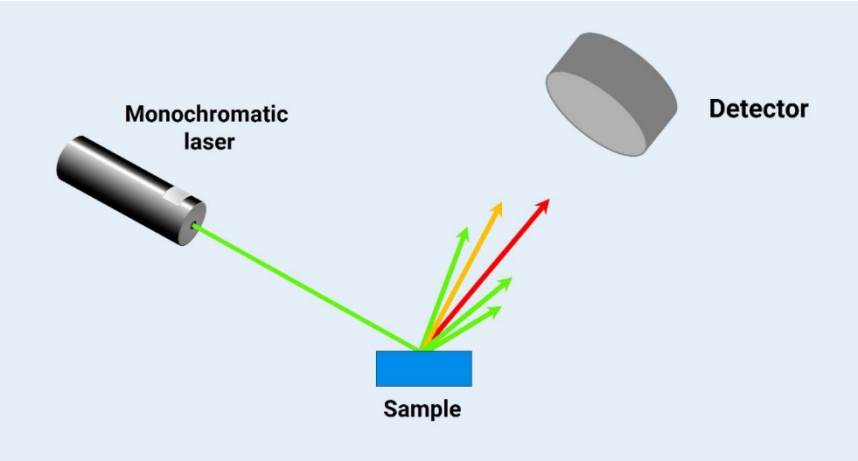

Figure 2.10: Operating principle of Raman spectroscopy [55]

This technique has applications in the medical and biological fields, in pharmaceuticals, in nanotechnology, and in materials science. Raman spectroscopy is a non-destructive technique and can be used in situ, making it particularly useful for rapid and real-time analyses.

2.6.4 Powder X-ray Diffraction

Powder X-ray Diffraction (PXRD) is a technique used for discrimination of different crystalline structures. The analysis of a sample via PXRD allows for the identification of its phase, purity and crystal size. [69] The crystals to be analysed must be in powder form so that they are oriented in all directions. The powder is uniformly distributed on a support (often a glass plate or sample holder) to prevent aggregation and ensure homogeneous measurement. An X-ray source, such as an X-ray tube, is used to generate the X-rays required for diffraction. There are

several configurations (e.g., θ-θ, θ-2θ) depending on the type of analysis to be conducted. The X-rays are directed towards the sample.

When the X-rays strike the crystal planes, they are diffracted at specific angles according to Bragg's law:

$$n\lambda=2d\sin\theta \qquad (2.6)$$

- n is an integer
- λ is the wavelength of the X-rays
- d is the interplanar spacing
- θ is the angle of diffraction

A detector measures the intensity of the diffracted X-rays as a function of the angle of diffraction, generating a diffractogram. The peaks in the diffractogram correspond to specific crystal planes. The position (angle) and intensity of the peaks can be compared with databases of crystalline structures (e.g., PDF, Powder Diffraction File) to identify the phases present in the sample.

2.6.5 Differential Scanning Calorimetry

Differential Scanning Calorimetry (DSC) is a thermal analysis technique that imposes temperature ramps and registers the difference between the amount of heat required to increase the temperature of a sample and a reference material. Colorimetry is a primary technique for determining the enthalpy associated with a process and the relationship between temperature and the properties of a substance. [57]

Two cells are used: one containing the sample to be analysed and an empty one. These are placed on a thermoelectric disc surrounded by a furnace. Both cells are subjected to a controlled heating or cooling programme at a predetermined rate. Heat is supplied to the cells through the thermoelectric disc. As the sample undergoes thermal transitions (such as melting), it absorbs or releases heat. The DSC measures the difference in heat flow between the sample and the reference to keep both at the same temperature. The difference in energy required by the sample and the reference to match the temperature corresponds to the amount of heat absorbed or released by the sample (an endothermic or exothermic process, respectively). [57]

The data are displayed on a DSC thermogram (heat flow vs temperature or time). Peaks on the curve indicate the points at which thermal transitions occur. For example, an endothermic peak (which requires heat) may indicate melting, while an exothermic peak (which releases heat) may indicate crystallisation or chemical reactions. The areas under the peaks can be integrated to calculate the energy (enthalpy) involved in the transitions. The position of the peaks indicates the transition temperatures, such as the melting or crystallisation point. This technique is generally used to determine the melting point, the temperatures at which the sample begins to degrade or undergo significant changes, and in general, to characterise the thermal properties of materials.

2.6.6 Polarized light microscopy

The polarised light optical microscope provides information about details of the crystal's population such as shape, size distribution and the presence of aggregation or secondary nucleation. The microscope works by illuminating the sample with polarised light, which enhances the contrast of birefringent materials. The sample is placed on a microscope slide and is observed in transmitted or reflected light, depending on the nature of the particles and their contrast. Transmitted light is used if the particles are transparent, while reflected light is useful for opaque particles. Images of the particles are captured with a camera connected to the microscope or with an integrated digital acquisition system. [60]

In this study, images captured using the optical microscope were analyzed to perform Particle Size Distribution (PSD). The assessment of the PSD provides information on how the particles in a sample vary in size. It is usually represented as a curve or table that shows the percentage or frequency of particles relative to their size. The particle size can be expressed in terms of equivalent diameter, which represents the size of a particle based on its shape (generally spherical) or another measurable physical parameter. PSD can be measured in various ways, including laser diffraction, sieving, sedimentation and image analysis. [58]

The PSD using microscopy is a direct method that allows for visualisation and measurement of the particle sizes, aspect ratio (AR) and morphologies present in a sample. This approach is particularly useful for larger particles, generally in the range of a few to hundreds of micrometres. The process involves multiple stages, from sample preparation to data collection and analysis. The sample should be prepared well dispersing and distributing the powder on a

surface or suspended in a liquid, without agglomerates. Good dispersion is essential to ensure that the particles do not overlap and are easy to measure. If the sample is solid or in powder form, it can be dispersed on a slide with the help of a dispersing agent. If, as in this case, the sample is a suspension or an emulsion, a small amount is placed on a slide or on a special support for microscopes. An optical microscope with appropriate resolution and magnification based on the size of the particles to be analysed is used. Images of the particles are captured with a camera connected to the microscope or with an integrated digital acquisition system. The selection of representative images of the sample is influential: since this technique cannot be automated, it is prone to error, as it depends on the operator's ability to accurately identify the crystals and the selection of a suitable image. Therefore, it is crucial to choose images that are truly representative of the sample showing well-dispersed and uniformly distributed particles. This is followed by the segmentation of identifiable particles in the chosen images.

Feret's diameter is a parameter used in various fields, such as the pharmaceutical industry, construction materials, and materials technology (Figure 2.11) to indicate the size of the particles. Understanding the distribution of particle sizes and shapes can influence the reactivity, solubility, and mechanical properties of materials.

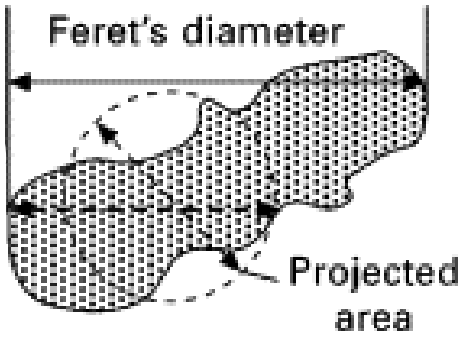

Figure 2.11: Feret diameter [59]

The aspect ratio (AR) indicates the ratio between two typical dimensions of a particle, specifically the length compared to the width. It is commonly used in various contexts, such as design, engineering, photography, and materials science. In chemistry and materials engineering, the AR of particles is crucial for determining their properties, such as flowability,

absorption, and distribution in mixtures. A high AR indicates longer or elongated particles, while a low AR suggests more symmetrical and rounded particles. [58]

The distributions of Feret diameter and AR are then represented with a histogram. However, image acquisition and manual analysis require extended periods for accurate analysis, the choice of samples significantly influences the results obtained, and the margin of error is amplified by the resolution of the optical microscope.

2.6.7 Scanning Electron Microscope (SEM)

The crystal size distribution can be determined using a Scanning Electron Microscope (SEM). This technique allows for precise observation of the sample's morphology, reaching magnification levels close to 500000x. It operates based on the interaction between an electron beam and the atoms making up the sample's surface. A source, typically a tungsten filament, generates an electron beam via thermionic emission. This beam is then directed through a series of electromagnetic lenses that focus it onto the surface of the sample under examination.

The interaction between atoms and electrons generates signals that are detected by a detector. Their intensity is subsequently converted into brightness for the corresponding pixel. Among the possible signals are secondary electrons and backscattered electrons. Secondary electrons have low energy and are useful for obtaining high-resolution images that reveal the surface morphology. In contrast, backscattered electrons are deflected after interacting with the sample, providing information on the sample's compositional contrast. Inside the SEM, a vacuum of $10^{-4} - 10^{-6}$ Torr is maintained to limit interactions between air gas molecules and the electrons. [61]

2.6.8 Three phase contact angle measurement

The wettability of a solid surface by a liquid is described by three-phase contact angle. This contact angle is specific to each system, forming at the interface between the solid/liquid/gas phases, and it directly depends on the interfacial tensions between them. [62]

It is described by Young's equation:

$$cos\theta = \frac{\gamma_{SV} - \gamma_{SL}}{\gamma_{VL}} \qquad (2.7)$$

- θ is contact angle
- γ_{SV} is the solid-vapour interfacial tension
- γ_{SL} is the solid-liquid interfacial tension
- γ_{LV} is the liquid-solid interfacial tension

Depending on the measured contact angle value, perfect wettability is observed if θ = 0°, high wettability when 0° < θ < 90°, low wettability if 90° < θ < 180°, and non-wetting when θ = 180° (Figure 2.12).

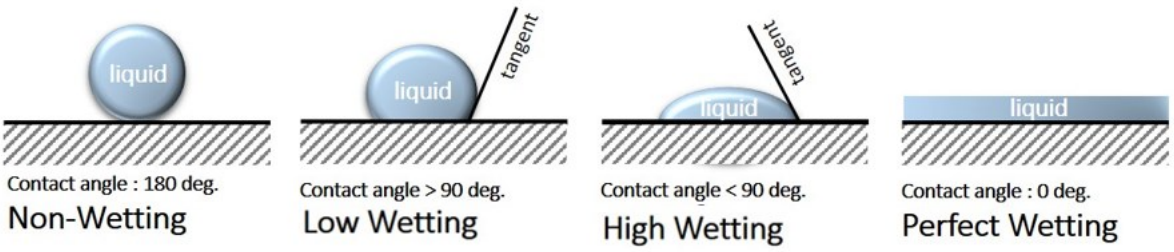

Figure 2.12: Different values of contact angle. Modified from [63]

It can be measured using different techniques such as the sessile drop, the Wilhelmy plate, and liquid penetration. The Wilhelmy plate is based on the immersion of a thin sample plate into the liquid. The adhesive force between the two phases generates a lift of the plate, and through the Young-Laplace correlation, it is possible to measure the contact angle. The liquid penetration technique is based on the absorption of the liquid by a porous surface; based on the depth reached by the liquid, it is possible to derive the contact angle.

In this study, the sessile drop method is applied, which involves depositing a droplet of liquid onto the solid sample being examined. The powder is compacted into a disc by applying a pressure of 200 bar. A high-speed camera records the greyscale image and transfers it to analysis software. The edges are then highlighted, and the shape of the droplet is described using a

geometric model. The measured value corresponds to the angle between the tangent to the droplet profile and the surface of the sample. Although this is a simple and reliable technique for flat and smooth surfaces, the presence of surface roughness, liquid penetration into the pores, and swelling can hinder the measurement of the contact angle (Figure 2.13). [62]

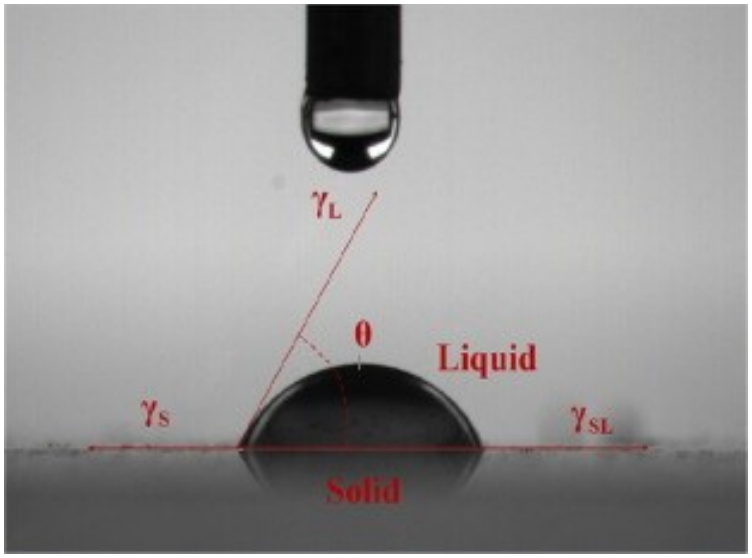

Figure 2.13: Sessile drop method [64]

3. Materials and methodology

3.1 Materials

Curcumin (IUPAC (1E,6E)-1,7-ais (4-hydroxy-3-methoxyphenyl)-1,6-heptadiene-3,5-dione name) is a bright yellow-orange powder and was supplied by Thermo Scientific (Massachusetts, USA), with a purity grade of more than 98%. The curcuminoid mixture was used without further purification, as any impurities present did not impact the experiments. Hence, it will be referred to as raw curcumin throughout the rest of the discussion.

At each stage of the process, water was purified and deionized using the Milli-Q apparatus from Millipore Corporation (Massachusetts, USA). The solvent used for crystallisation was Ethanol (99.98%) purchased from Sigma-Aldrich.

Sodium Carboxymethyl Cellulose (CMC) 700000 average Molecular weight and k-carrageenan were supplied by Sigma Aldrich.

Medium-chain triglycerides (MCT) oil was chosen to produce the emulsions.

3.2 Solubility of curcumin

The solubility of raw curcumin was measured using a Crystal 16 apparatus (Technobis) by measuring the transmissivity values of turbidity for each reactor.

Five ethanol water mixture (80:20 by weight) stock solutions were prepared in 10 mL vials, each with a curcumin concentration ranging from 0.13 mg/g to 0.95 mg/g (Table 3.1). Curcumin was previously ground in a mortar using an agate pestle to reduce the influence of particle size. The samples were agitated with a magnetic anchor at 900 rpm for an hour to equilibrate.

Twelve 1.5 mL vials were subsequently filled with the samples and placed in the Crystal 16 system. For each concentration tested, a minimum of two repetition were performed.

Four cycles were set with temperature ramps having first a heating ramp up to 75°C and then a cooling ramp up to 1°C with a rate of 0.3 °C/min (Figure 3.1). The lower limit temperature was chosen to avoid the formation of ice (given the high amount of water in the vials) and the higher one to avoid the evaporation of the solvent (ethanol).

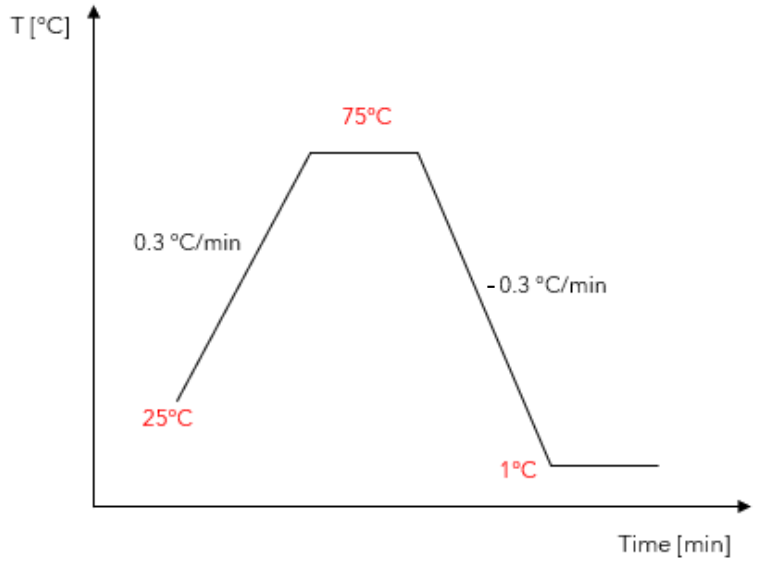

Figure 3.1: Temperature ramp set in Crystal 16

The same experiment was then carried out changing the ratio between the two solvents (70:30 by weight). The amount of water in the solution was reduced to promote the solubility of curcumin. The number of vials per concentration, their arrangement within the Crystal 16 and the number of cycles set are the same as in the previous case.

Table 3.1: Curcumin concentration in Crystal 16 experiment vials

	SOLUB_80_20 (Ratio 80:20 by weight)	**SOLUB_70_30** (Ratio 70:30 by weight)	**SOLUB_70mix_30** (Ratio 70:30 by weight)
Vials	CUR concentration in solution [mg/g]	CUR concentration in solution [mg/g]	CUR concentration in solution [mg/g]
1	0.13	0.19	0.19
2	0.13	0.19	0.19
3	0.25	0.38	0.38
4	0.25	0.38	0.38
5	0.38	0.57	0.57
6	0.38	0.57	0.57
7	0.38	0.57	0.57
8	0.38	0.57	0.57
9	0.51	0.75	0.75

10	0.51	0.75	0.75
11	0.63	0.95	0.95
12	0.63	0.95	0.95

A third measurement was then carried out in water-ethanol 70:30 mix. The samples were prepared as described above. For this measurement a single cycle was carried out to avoid re-dissolving a different polymorphic form precipitated in the cooling step. The limit temperature has remained unchanged.

Upon completion of the experiments, the solubility curves were generated using CrystalClear software, based on the "clear points": the temperatures at which the solution achieves 100% light transmission (completely clear). The solubility data were then linearised using the Van't Hoff equation:

$$ln(x) = -\frac{\Delta H}{R}\left(\frac{1}{T} - \frac{1}{T_0}\right) \qquad (3.1)$$

- x is sample molar fraction
- ΔH is enthalpy of dissolution
- T_0 starting temperature
- T saturation temperature of molar fraction x

The quantification of curcumin in ethanol/water mixtures with different ratios was performed with a High-Performance Liquid Chromatography (HPLC) system (Shimadzu 20A Nexera). A Kinetex core-shell C18 column (5 µm, 150 × 4.6 mm) from Phenomenex, paired with a photodiode array detector. The absorbance of curcumin and the solvents was previously assessed, and a wavelength of 425 nm was chosen. The mobile phase consisted of acetonitrile and 0.1% formic acid in a 50/50 (v/v) ratio. An isocratic elution technique was utilized, maintaining a flow rate of 0.8 mL/min and setting the column oven temperature to 40 °C. The injection volume was 10 µL. [65]

The area of interest for this study is between ethanol/water ratios of 0.2 and 0.4 by weight.

A calibration curve was established by preparing nine solutions of curcumin at varying concentrations (ranging from 0.1 to 100 µg/mL) in ethanol, prepared by serial dilutions from a mother solution of 100 µg, as reported in Table 3.2.

Table 3.2: Curcumin concentration for HPLC calibration curve

Curcumin Concentration [μg/mL]	100	50	15	10	5	2.5	2	1	0.5	0.1

The vials were then left to stir for 10 minutes to achieve homogeneity. For each concentration, three 1 mL vials were prepared.

The analytes were prepared dispersing an excess of curcumin, previously ground in a mortar, in ethanol/water mixtures in different ratios (Table 3.3) selected to evaluate the solubility of curcumin under these conditions. The vials were maintained in agitation for two hours. The dispersions were then filtered with a 0.22 μm syringe filter. The filtrate was then subjected to HPLC measurements. The calibration curve obtained was then used as a reference to quantify the solubility of a specific concentration of curcumin in solutions with a variable ethanol/water Milli-Q ratio.

Table 3.3: Points to test for HPLC solubility curve

Ratio Milli-Q water/EtOH [w/w]	1:2.5	1:3.3	1:5	1:7.5	1:10	1:12.5	1:15	1:17.5	1:20

HPLC measurements were conducted twice, changing the analytes preparation. In the first case, a stock solution of 3 mg/g of curcumin in ethanol was prepared and added to Milli-Q water to get the desired ethanol-water ratio, resulting in the precipitation of the curcumin. In the second case, a solution of ethanol and water was prepared first, and then an excess of curcumin was added. These two methods were chosen because the curve obtained from the first experiment showed anomalous results compared to former analysis conducted on the same system. [5] The HPLC measurement values obtained for each ratio were averaged, and from these interpolations, the solubility curve was derived.

Then, the curcumin solubility was evaluated in aqueous solutions at different pH values, via thermogravimetric analysis. Three experiments were carried out: one in an acidic environment, one basic and one neutral. In all three cases, an excess (70 mg) of curcumin was introduced in 150 g of solution of known pH (previously measured with a pH meter). The acidic environment was obtained using an HCl solution (pH = 1.02), a phosphate buffer (pH=6.8) was chosen for the neutral environment and baking soda (pH=8.5) for the basic environment. In turn, each of the solutions was placed in a 250 mL jacketed reactor. The temperature was set to 25°C (Huber

Ministat 230). After 2.5 hours equilibration four withdrawals were made with a syringe and membrane filter (cut-off 0.22 μm). 5 mL of the filtrate solution were placed on weighing boats and left to evaporate. A sample of the above-mentioned solutions were also collected in 1.5 mL vials for HPLC quantification. Then, the dispersion was brought to 37°C and also in this case four samples were taken. The system was evaluated at room temperature and body temperature to understand the behaviour of curcumin if it is inserted into an oral drug.

3.3 Curcumin crystallization experiments

Two different techniques were chosen to obtain the respective forms of curcumin of interest. Form I was obtained through cooling crystallization, whereas form III was produced using the antisolvent method. In both cases, it was possible to reproducibly obtain curcumin crystals of the desired form.

3.3.1 Cooling crystallization

Starting from the solubility curves described above, a concentration of 0.57 mg/g of curcumin in ethanol-water mixture 70:30 by weight was chosen for the design of the experiment (Table 3.4). The crystallization was carried out in a 1L jacketed reactor. The amount of dispersion was set to 500 g composed by 350 g of Milli-Q water, 150 g of ethanol, and 285 mg of curcumin (0.57 mg/g) and then a temperature ramp was set as reported in Figure 3.2 with a temperature control unit (Huber Ministat 230). The ramp was set this way because, according to the solubility tests, curcumin begins to solubilise only over 40°C, so the slope of the ramp was adjusted with a double gradient: 0.5°C/min to accelerate the heating process during initial phase and 0.3°C/min to allow curcumin to adapt to the temperature change. [66] The final temperature was set to 6°C to avoid the formation of unwanted ice crystals. During the process a probe was used to monitor the process temperature and a turbidimeter for the turbidity of the suspension. The speed of mixing was set to 240 rpm to ensure thorough mixing and to prevent vortex formation.

Table 3.4: Conditions of cooling experiments

	Curcumin Concentration in solution (mg/g)	Curcumin (mg)	EtOH (g)	Milli-Q (g)	Total mass (g)
COOL_CUR_1	0.57	285	150	350	500
COOL_CUR_2	0.57	285	150	350	500

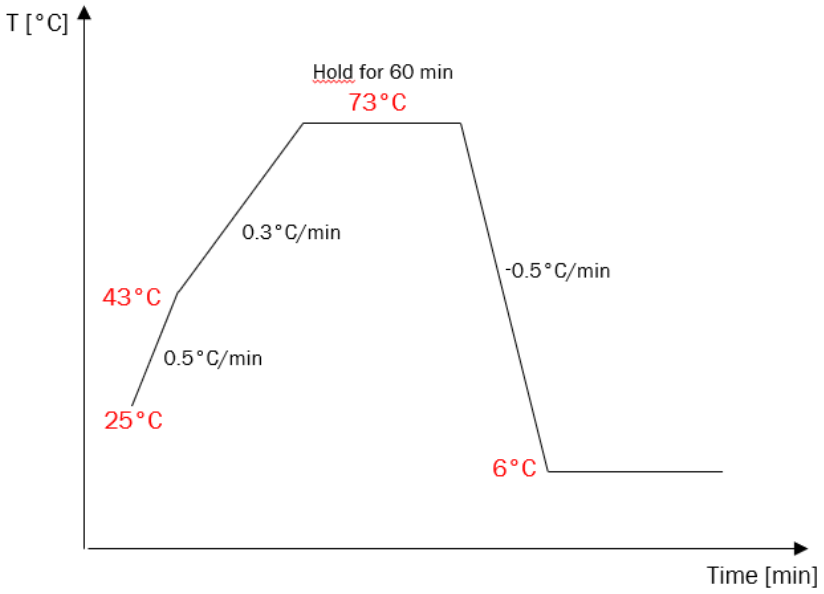

Figure 3.2: Temperature ramp for cooling crystallization

3.3.2 Antisolvent crystallization

Antisolvent crystallization technique was used to obtain curcumin polymorph form III. First, the curcumin was gently ground using a mortar. Subsequently, the curcumin, ethanol, and water were weighed according to the quantities outlined in Table 3.5.

Table 3.5: Conditions of antisolvent experiments

	CUR CONC in EtOH (mg/g)	SOLV/ ANTIS Ratio by weight	EtOH (g)	Milli-Q (g)	Time of mixing (min)	Stirring (rpm)	Total mass (g)	T EtOH Solution (°C)
ANTISOLV_1	7.25	1:2.5	142.86	357.14	5	15000	500	35
ANTISOLV_2	11.07	1:2.5	142.86	357.14	5	15000	500	55
ANTISOLV_3	7.25	1:5	83.33	416.67	5	15000	500	35
ANTISOLV_4	11.07	1:5	83.33	416.67	5	15000	500	55

A solution of ethanol was prepared in which a known quantity of curcumin was dissolved. The solution was then stirred with a magnetic stirrer and heated (conditions on Table 3.5). Based on the concentration of curcumin in the solution, the solute was dissolved warming the solution, according to the curcumin solubility curve previously measured and reported in the literature. [11] This solution was covered with a layer of Parafilm to prevent ethanol evaporation and stirred on a magnetic plate to promote homogenisation. [11]

This solution was then poured in one step with the Milli-Q water, maintained in agitation using an IKA Ultraturrax T25 digital mixer (Germany) at 15000 rpm to minimise the formation of a concentration gradient within the beaker. After 5 minutes of stirring, the solution was filtered through a filter paper disc with the assistance of a SC 920 G vacuum pump from KNF (Germany) to expedite the process. The filtration was carried out twice to achieve a sufficiently clear filtrate. The crystals were then left to dry overnight in the air and subsequently collected in a vial.

3.3.3 Effect of polymers on curcumin surface properties

To evaluate the effect of additives on the surface properties of curcumin crystals, experimental trials have been carried out with the addition of polymers in solution. Carboxymethyl cellulose (CMC) and k-carrageenan were chosen for these tests. Their effect on the resulting crystals was tested both in cooling and antisolvent crystallization.

Firstly, to evaluate the effect of CMC on curcumin crystals, experiments were carried out with both polymorphic forms of curcumin of interest.

A cooling crystallization experiment was carried out in a jacketed reactor maintaining the same conditions described above adding the polymer of interest (Table 3.6). The polymer was previously dispersed in the aqueous solution mixing it with an Ultraturrax homogenizer at 25000 rpm for few minutes. This step was essential to prevent the polymers from forming a gel in the aqueous solution. It is known that, at low concentrations, polymers limit aggregate formation and keeps curcumin suspended, improving particle distribution during cooling and promoting more uniform crystallization. Subsequently, the ethanol and curcumin previously weighed were added to the aqueous polymer solution.

Then, was made the same experiment with k-carrageenan maintaining the same conditions and quantities.

Table 3.6: Conditions of cooling experiments with polymers in solution

	CUR CONC in solution (mg/g)	**Amount of polymer (%wt)**	**CMC (g)**	**K-CAR (g)**	**EtOH (g)**	**Milli-Q (g)**	**Total mass (g)**
COOL_CMC	0.57	CMC 0.05	0.25	-	149.92	349.83	500
COOL_KCAR	0.57	KCAR 0.05	-	0.25	149.92	349.83	500

To assess the effect of both polymers on curcumin form III, four experiments were conducted with different polymer concentrations (0.1%wt and 0.05%wt) using the antisolvent technique. The operating conditions are reported in Table 3.7. The polymer was weighed and dissolved in a known volume of Milli-Q water. To prevent polymer aggregation in the water, this system was stirred at 25000 rpm (using an Ultraturrax) for few minutes until the polymer was fully dispersed in the water. The ethanol solution was heated and quickly poured into the aqueous solution, which was still being stirred. The system was then kept stirring at 15000 rpm for 5 minutes, after which the solution was immediately filtered using filter paper and a vacuum pump. The filter was then left to air-dry.

Table 3.7: Conditions of antisolvent experiments with polymers in solution

	CURC CONC in EtOH (mg/g)	SOLV/ ANTIS Ratio by weight	Polymer (g)	EtOH (g)	Milli-Q (g)	Time (min)	Stirring (rpm)	Total mass (g)	T (°C)
ANTISOLV_ 005CMC	7.25	1:5	CMC 0.25	83.29	416.45	5	15000	500	35
ANTISOLV_ 01CMC	7.25	1:5	CMC 0.5	83.25	416.25	5	15000	500	35
ANTISOLV_ 005KCAR	7.25	1:5	KCAR 0.25	83.29	416.45	5	15000	500	35
ANTISOLV_ 01KCAR	7.25	1:5	KCAR 0.5	83.25	416.25	5	15000	500	35

By conducting the cooling and antisolvent experiments with both polymers, it was possible to assess and compare the behaviour of CMC and k-carrageenan during the crystallisation of curcumin for both polymorphs.

3.4 Characterization of curcumin crystals

Particle properties are crucial for the stability, effectiveness, and overall functionality of Pickering emulsions. [3] For this reason, the solid particles obtained were characterised by using a range of techniques. Raman and PXRD, DSC measurements, SEM and optical microscope images to assess the morphology and PSD. Contact angle measurements were carried out to evaluate powder wettability.

Raman Spectroscopy

Raman spectroscopy was used to gather information about the molecular structure of the samples and to determine whether the desired polymorphic form had been obtained. The instrument used was a LabRAM HR Evolution spectrometer from HORIBA Scientific.

A 785 nm laser was used as the excitation source, and the Raman signal was captured with a Synapse Plus BIDD Detector (1024 x 256 pixels) equipped with a 300/nm grating. No filters

were applied, and the laser power was set to 100% of its maximum capacity. Several milligrams of the material were placed on a glass slide, with the powder gently pressed using a 5X objective. The sampling parameters were configured for 5 acquisitions with an exposure time of 0.5 seconds.

Powder X-Ray Diffraction

X-ray diffraction (PXRD) was conducted on the obtained crystals to provide further insights into their crystalline structure and to compare their diffractograms with those available in the literature for the various polymorphic forms of curcumin.

PXRD analysis was carried out using a Panalytical X'Pert PRO diffractometer in Bragg–Brentano mode with Cu Kα radiation (λ = 1.5406 Å). The samples were placed onto a silicon zero-background sample holder. Diffraction patterns were recorded across a 2θ range of 4° to 40°, using a step size of 0.026° and an acquisition time of 180 seconds for each step. The resulting diffraction data were subsequently compared to simulated X-ray patterns derived from the crystal structures of the polymorphs available in the Cambridge Structural Database (CSD), where refcodes BINMEQ13, BINMEQ12, and BINMEQ07 correspond to Forms I, II, and III, respectively.

This technique enabled a detailed analysis of the crystal lattice of curcumin powders and identification of the polymorphic forms present, complementing the Raman analysis previously performed.

Differential Scanning Calorimetry

Differential Scanning Calorimetry (DSC) was carried out using a Hitachi NEXTA DSC 200 under an inert nitrogen atmosphere (50 mL/min).

An aluminium pan containing approximately 3 mg of sample powder was prepared. The pan was then sealed using a specialised press. After sealing, the pan and an empty reference pan were placed inside the machine's chamber in diametrically opposite positions. A temperature program was established to heat the pans from 20°C to 200°C at a rate of 10°C per minute.

Scanning Electron Microscopy (SEM)

Scanning Electron Microscopy (SEM) was performed to further understand the size distribution and morphology of crystals obtained from previous experiments. A Zeiss Merlin Field Emission Gun Scanning Electron Microscope was used. The powders were immobilized on a strip of double-sided platinum conductive tape to improve conductivity and consequently image quality. The procedure was performed at 30 mA for 30 seconds. In the various images, the visible particles were segmented by hand. The images were then uploaded to the ImageJ.exe software.

Particle Size Distribution

After obtaining crystals of form I and form III using the respective methods previously described, the particle size distribution (PSD) was measured. This process involves taking a sample of the solution and examining it under an optical microscope. For each sample, a minimum of five representative image is captured. The image is then transferred to a computer, where the particles in the sample are manually outlined.

A reference scale is added to the image.

Figure 3.3: Main steps of Particle Size Distribution, in order: optical microscope image, manual selection of particles, particles identification and characterization by ImageJ.exe

Using software (ImageJ.exe), it is possible to evaluate the characteristics of the identified particles. Feret's diameter and aspect ratio (AR) are calculated for multiple representative samples from various experiments. Feret's diameter can be defined as the average distance measured between pairs of parallel lines tangent to the particle's projected outline. [58]

The ellipsoidal and elongated shape of the particles allowed to approximate their shape with the "Fit Ellipse" command and the minimum and maximum lengths were considered for the calculation of the Feret diameter and the aspect ratio. At least 300 particles were evaluated to obtain adequate screening of each sample.

The same results were then processed in Matlab R2023b, where the hist3 function allowed for the creation of three-dimensional size distribution graphs, considering frequency as well as the lengths of the major (L1) and minor (L2) axes.

The same method was adopted to assess the droplet size distribution in emulsions.

Contact Angle

The curcumin crystal powder obtained was utilized to measure the contact angle using the sessile drop method. The measurements were conducted at room temperature with a DSA25 drop shape analyzer from Krüss Scientific. A hydraulic press was used to create compressed disks of curcumin powder. During this process, two tracing paper disks were placed between the plates to ensure the formation of smooth and homogeneous disk surfaces. The powder was pressed at 200 bar for 30 seconds. Following this, droplets of MCT oil and water (2 µL) were deposited using a micro syringe, and the behaviour of the drops was recorded with a camera. This measurement allowed us to determine whether to use water-in-oil or oil-in-water emulsions based on the properties of the crystals.

3.5 Emulsification and emulsion characterization

Given the results of the contact angle experiments for the samples tested, it was decided to prepare water-in-oil (W/O) emulsions. Milli-Q water and MCT oil were used to produce the emulsions. Four different water percentage incorporation (range 5 – 20%wt) were chosen to evaluate the effect of the curcumin crystals on the size of the water droplets (Table 3.8). It is known that, in Pickering emulsions, the particles size is about an order of magnitude smaller than the droplets in the dispersed phase to favour the packing of the solid and form a barrier that limits the formation of clusters. [5]

A vial was prepared with MCT oil in which 20 mg of curcumin (0.4wt%) was added and dispersed stirring with the Ultraturrax at 10000 rpm for 3 minutes. Milli-Q water was subsequently added to the dispersion and mixed for 1 minute at 1000 rpm.

Table 3.8: Composition of W/O emulsions

Water concentration (%wt)	Oil (g)	Water Milli-Q (g)
5	4.73	0.25
10	4.48	0.5
15	4.23	0.75
20	3.98	1

Form III previously obtained was tested in emulsions with different water ratio (range 5 – 10%wt). See Table 3.9.

Table 3.9: Conditions of experiments made with form III

	Water concentration (%wt)	Curcumin crystal used	Presence of Polymers
EMU_5_A_1	5	ANTISOL_1	NO
EMU_5_A_3	5	ANTISOL_3	NO
EMU_5_A_01C	5	ANTISOL_01CMC	YES
EMU_10_A_1	10	ANTISOL_1	NO
EMU_10_A_3	10	ANTISOL_3	NO
EMU_10_A_01C	10	ANTISOL_01CMC	YES
EMU_15_A_1	15	ANTISOL_1	NO
EMU_15_A_3	15	ANTISOL_3	NO
EMU_15_A_01C	15	ANTISOL_01CMC	YES
EMU_20_A_1	20	ANTISOL_1	NO
EMU_20_A_3	20	ANTISOL_3	NO
EMU_20_A_01C	20	ANTISOL_01CMC	YES

Form I was tested as stabilizer only for emulsions with 10%wt of water (Table 3.10). Operating conditions were changed as the mixing speed of Ultraturrax (from 10000 to 15000 rpm), the amount of curcumin (from 20 to 60 mg, respectively o.4 and 1.2wt%) and the mixing time

(varying from one to four minutes). All these tests were carried out to define the effect of these conditions on the stability of the W/O emulsion.

Table 3.10: Conditions of experiments made with form I

	Water concentration (%wt)	**Curcumin (mg)**	**Curcumin crystal used**	**Mixing time (min)**	**Stirring (rpm)**
EMU_10_C_1	10	20	COOL_CUR_2	1	10000
EMU_10_C_2	10	20	COOL_CUR_2	4	15000
EMU_10_C_3	10	60	COOL_CUR_2	4	15000

To assess the droplet size distribution, images of the samples were obtained with an optical microscope.

4. Results and discussion

4.1 Solubility curves

To determine the solubility of curcumin in water/ethanol solutions, an HPLC measurement was carried out. Starting from a series of curcumin ethanol solutions with known concentrations (range 0.1 – 100 µg/mL), two calibration curves were obtained (Figure 4.1 and 4.2) to reduce the error from interpolation. From this, it was possible to select nine points to test to derive the solubility curve.

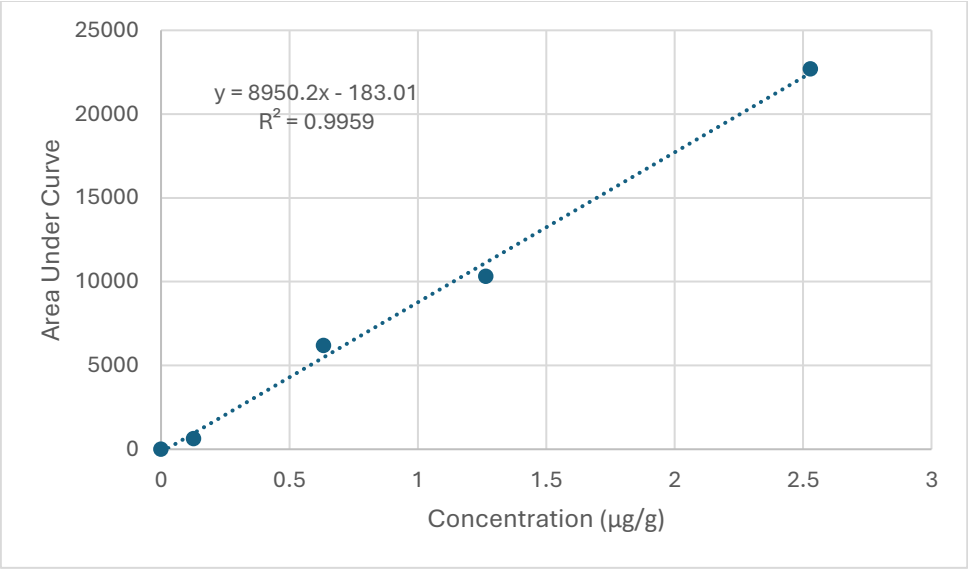

Figure 4.1: Calibration curve of curcumin concentration (first part)

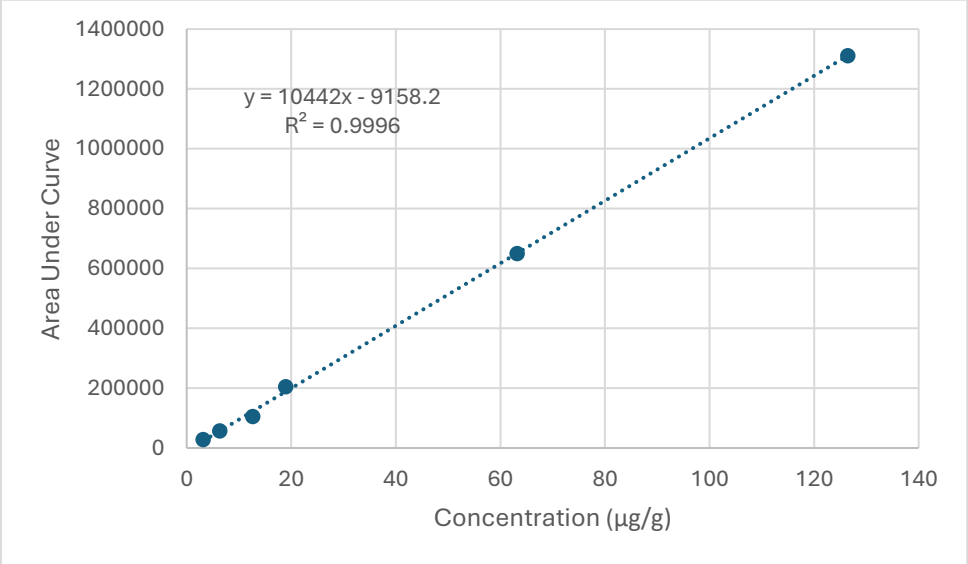

Figure 4.2: Calibration curve of curcumin concentration (second part)

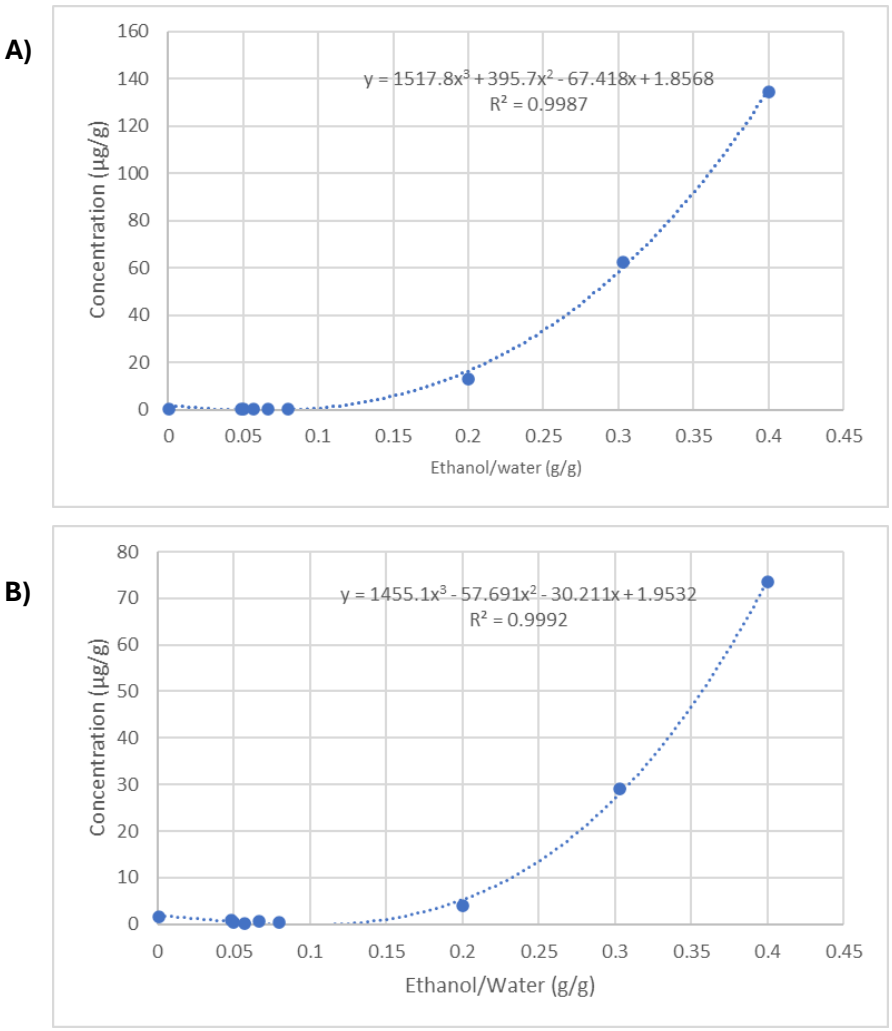

Figure 4.3: Solubility curve of curcumin as a function of increasing water content: A) Case conducted by preparing a stock ethanolic solution with curcumin, followed by the addition of Milli-Q water B) Experiment repeated by initially preparing a solution of ethanol and Milli-Q water, to which curcumin was subsequently added

The HPLC experiment was first conducted by preparing a stock ethanolic solution with curcumin, followed by the addition of Milli-Q water which caused the precipitation of curcumin in the system. It was deduced that the kinetics had been favoured the formation of polymorph form III, which has a higher solubility than the most stable form I. So, sample preparation was modified, and the experiment was repeated by initially preparing a solution of ethanol and Milli-Q water, to which curcumin was subsequently added. Three samples were prepared for each test point. The HPLC measurement values obtained were averaged, and from these interpolations, the solubility curve was derived (Figure 4.3). The curve trend for both experiments is comparable. Still, in first case (Figure 4.3 A), for higher ethanol/water ratios, the concentration of solubilized curcumin is significantly higher compared to previous measurements conducted on the same system. [5]

Based on the HPLC results, the solubility curves of curcumin in ethanol-water solution were obtained using the Crystal 16, as described in Chapter 3. Upon completion of the experiments, the solubility curves were generated using CrystalClear software, based on the "clear points": the temperatures at which the solution achieves 100% transmissivity (completely clear). These temperatures were then averaged according to their corresponding concentrations, and the standard deviation (SD) was calculated.

The solubility data were displayed in Figure 4.4, which correlated the average solubilisation temperature with the concentration of curcumin in the solution. The curves from the initial experiments (see Table 3.1 in the Methodology chapter), which involved multiple heating and cooling cycles, were not satisfactory. In fact, after the first heating and cooling cycle, the polymorphic change in the precipitate may occur. Additionally, the Crystal 16 consistently recorded transmittance close to 100% during these experiments, although some particles were visible. This was likely because curcumin accumulated around the anchor magnet and the meniscus surface in some vials, causing the system to detect turbidity only when the curcumin detached and fell.

The third experiment with a 70:30 ratio by weight, however, demonstrated improved solubilisation of curcumin in solution. The data from this test (Table 4.1) were analysed to obtain a solubility curve correlating saturation concentration and temperature, approximated with a linear function (Figure 4.4).

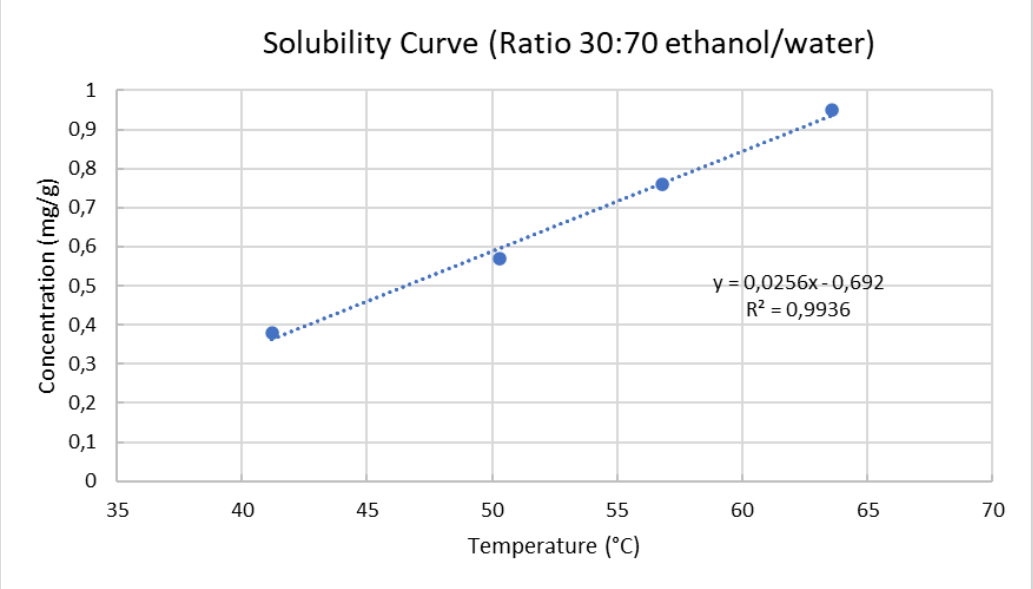

Figure 4.4: Solubility curve of curcumin

The coefficient of determination R^2 had a value close to unity, indicating a high degree of accuracy in the interpolation of the experimental data.

Table 4.1: Mean temperature and Standard Deviation (SD) of each curcumin concentration

Mean Temperature (°C)	CUR Concentration (mg/g)	SD (°C)
41.2	0.38	1
50.3	0.57	0.9
56.8	0.76	0.35
63.6	0.95	0.7

The points of the curve were then interpolated using Van't Hoff's equation to produce the solubility graph shown in Figure 4.5.

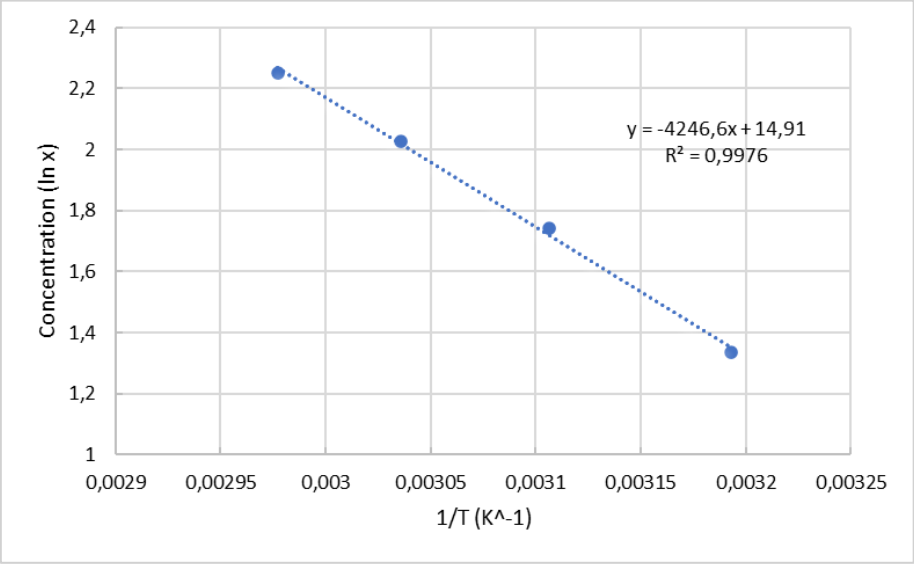

Figure 4.5: Van't Hoff solubility graph of curcumin in pure ethanol in the range 34-71°C. In the y axis, concentration of curcumin as natural logarithm of the molar fraction (x), in the x axis the reciprocal of temperature in Kelvin

The experimental data fit the Van't Hoff equation well, as the coefficient of determination is very close to unity.

Finally, the solubility of curcumin in environments with varying pH was assessed. A constant quantity of raw curcumin form I was added to three distinct aqueous solutions with different pH levels. Four samples were taken from each solution at room temperature and four at 37°C to quantify the curcumin solubilized in the different solutions at different temperatures. The system was evaluated at room temperature and body temperature to understand the behaviour of curcumin at physiological conditions. The data collected did not yield a satisfactory

quantification, as very little amount of curcumin was solubilized and that could not be significantly identified with the available balance.

The samples were left in the laboratory under a hood for the time necessary for the water to evaporate. In Figure 4.6 the three different samples after water evaporation are visible.

Figure 4.6: Samples after water evaporation of curcumin in solutions at different pH: A) acidic solution, B) neutral solution, C) basic solution

Looking at the samples (Figure 4.6) is clear that in acidic environment (A) no curcumin remains on boats. In the neutral one (B) the result is the same of the previous case, in fact, despite evaporation, at the bottom of the boat a colourless viscous liquid remains. Instead, only the samples in a basic environment (C) at a 37°C temperature seems to exhibit the presence of solubilised curcumin. Analyzing by Raman spectroscopy (Figure 4.7) the latter (C), it figured out that the majority of residue was baking soda, as reported in the literature. [70]

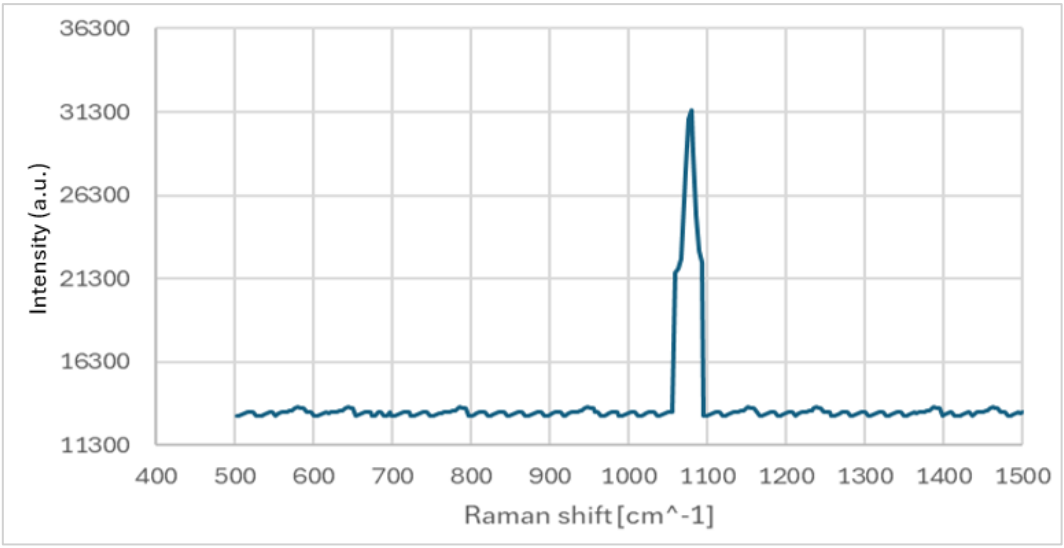

Figure 4.7: Raman spectra of the residue of sample in basic environment after water evaporation

Samples of the above-mentioned solutions were also collected in 1.5 mL vials for HPLC quantification. The samples were all colourless, except for the case of the basic solution at 37°C (Figure 4.8). In Figure 4.8 is shown the different colour of samples of curcumin in basic solutions at different temperature. It's clear that the increase of temperature favours the dissolution of curcumin. The sample of curcumin in a basic solution at 37°C was analyzed using HPLC, but the detected area under the peak was 226, which is significantly smaller than the area corresponding to the lowest point on the calibration curve (0.13 µg/g, as shown in Figure 4.1). Consequently, it was not possible to determine its solubility with certainty.

Figure 4.8: Samples of curcumin in basic solution at 37°C (on left) and at 25°C (on right)

These results confirmed curcumin's tendency to prefer basic pH environments reported in the literature.

4.2 Curcumin crystallization and crystals characterization

4.2.1 Raman spectroscopy results

This study aimed to demonstrate the applicability of crystal engineering to produce curcumin crystals in a reproducible and tuneable form through the selection of process conditions. The cooling crystallisation method was employed to produce form I of curcumin, while the antisolvent method was chosen to obtain form III.

These two techniques enabled the successful production of the desired polymorphs. The ratio of water to ethanol for the solutions was selected based on the solubility tests conducted

previously. Form I was obtained using a solution of water/ethanol (70:30 in weight), in which 0.57 mg/g of curcumin was dissolved.

The powders obtained were subsequently subjected to Raman spectroscopy. The purpose of this analysis was to confirm the successful production of the desired polymorph and to ensure the absence of chemical degradation and the crystallinity of the obtained samples during the precipitation process. The Raman spectra obtained were compared with literature data. [67]

As evidenced by the Raman spectra in Figure 4.9, maintaining consistent cooling process conditions led to the successful production of form I in both repetitions.

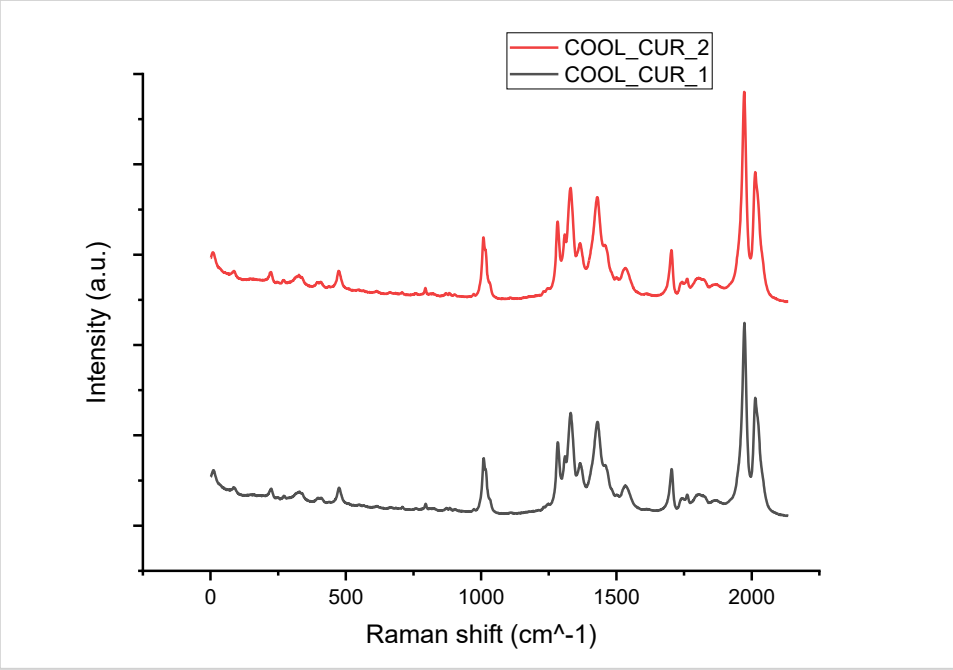

Figure 4.9: Raman spectra of curcumin polymorph obtained from cooling experiments: COOL_CUR_1 (black line), COOL_CUR_2 (red line)

Form III, on the other hand, was obtained using the antisolvent technique. Several experiments were conducted, varying the antisolvent content or the curcumin concentration. The powders were then analysed using Raman spectroscopy (Figure 4.10). As, with previous analysis, the spectra, confirms the desired polymorphic form III.

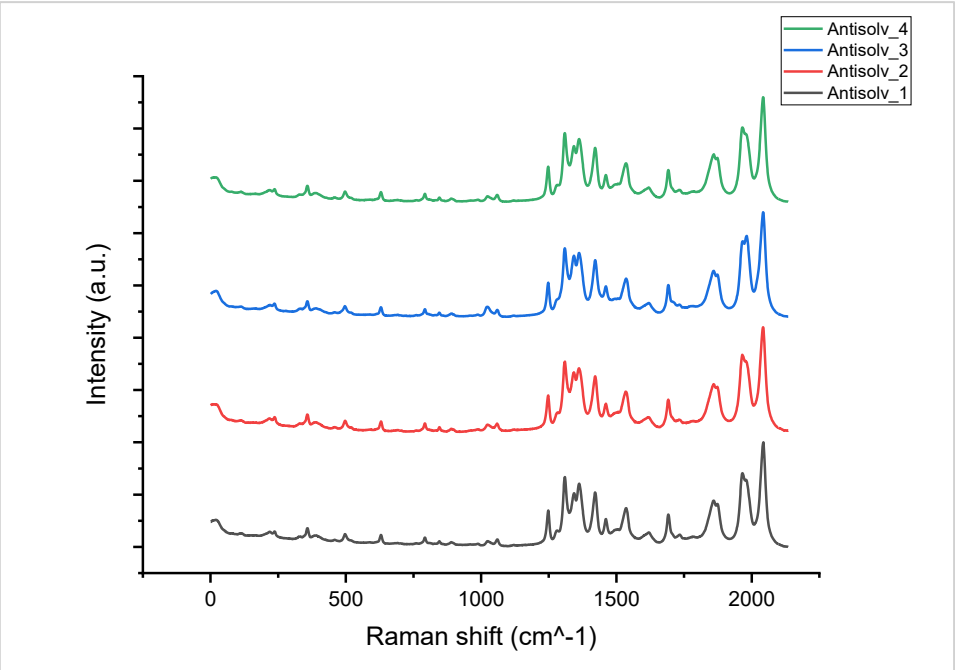

Figure 4.10: Raman spectra of curcumin Form III obtained from antisolvent experiments: ANTISOLV_1 (black line), ANTISOLV_2 (red line), ANTISOLV_3 (blue line), ANTISOLV_4 (green line)

Subsequently, the powders obtained from crystallisation experiments involving the use of polymers in solution (CMC and k-carrageenan) were characterised. In both experiments conducted with form I, the presence of the polymer did alter the appearance of the powders. As shown in Figure 4.11.

The presence of CMC has made the curcumin powder visually more compact, finer, and harder to separate from the filter. The yield, calculated as the difference between the weight of the filter at the beginning and after the accumulation of the powder, is 69% in the presence of CMC and 76% in the experiment with curcumin alone.

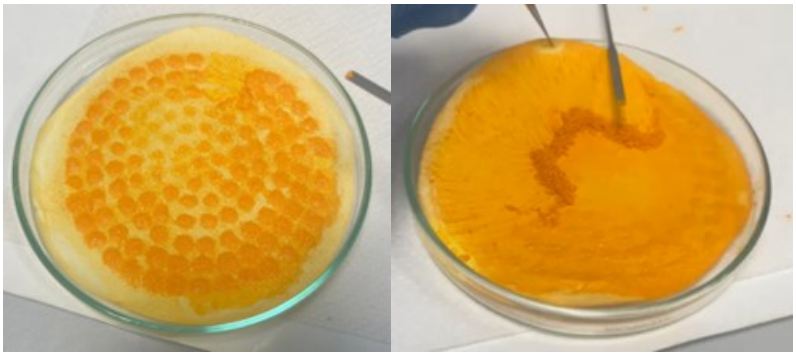

Figure 4.11: A) Curcumin form I on paper filter obtained from experiment COOL_CUR_2
B) Curcumin form I on paper filter obtained from experiment COOL_CMC

The Raman spectra indicate that, despite the presence of polymers, the same polymorphic form nucleated (Figure 4.12 and 4.13).

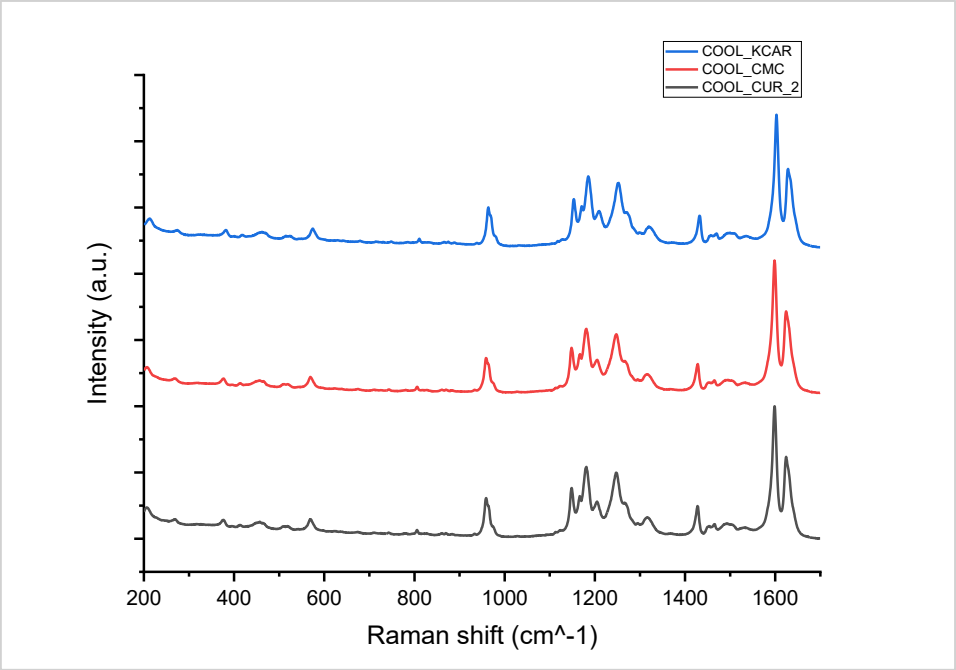

Figure 4.12: Raman spectra of experiments: COOL_CUR_2 (black line), COOL_CMC (red line) and COOL_KCAR (blue line)

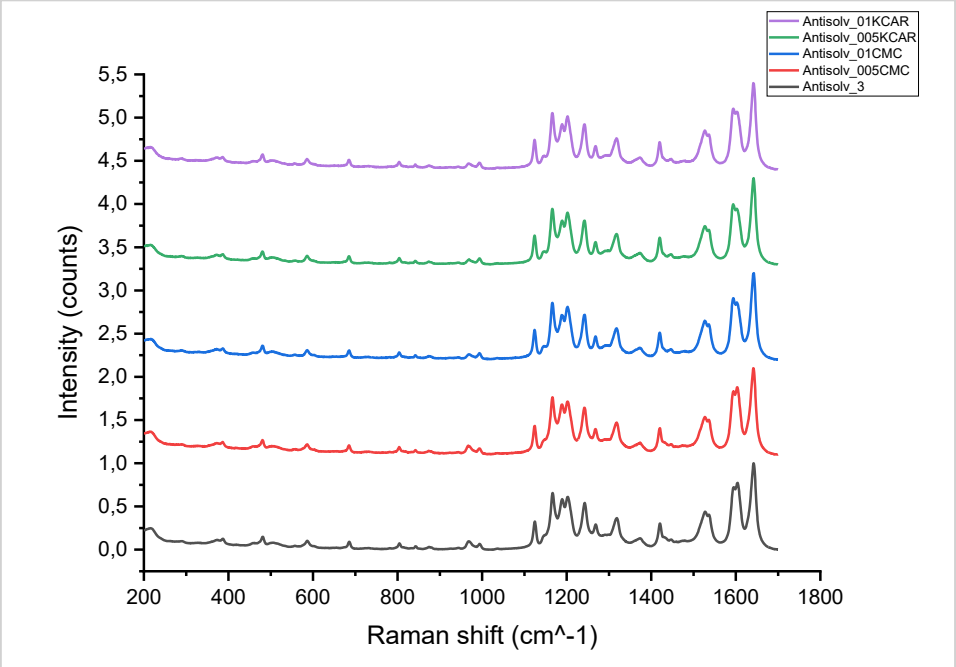

Figure 4.13: Raman spectra ANTISOLV_3 (black line), ANTISOLV_005CMC (red line), ANTISOLV_01CMC (blue line), ANTISOLV_005KCAR (green line), ANTISOLV_01KCAR (purple line)

All three solutions were filtered using vacuum pump and paper filter. The resulting powders were then analysed by Raman spectroscopy, and, as shown in the graph below (Figure 4.14), the polymorph remained unchanged. These findings demonstrated that no chemical degradation processes or phase transitions of curcumin were observed after treatment at varying pH levels.

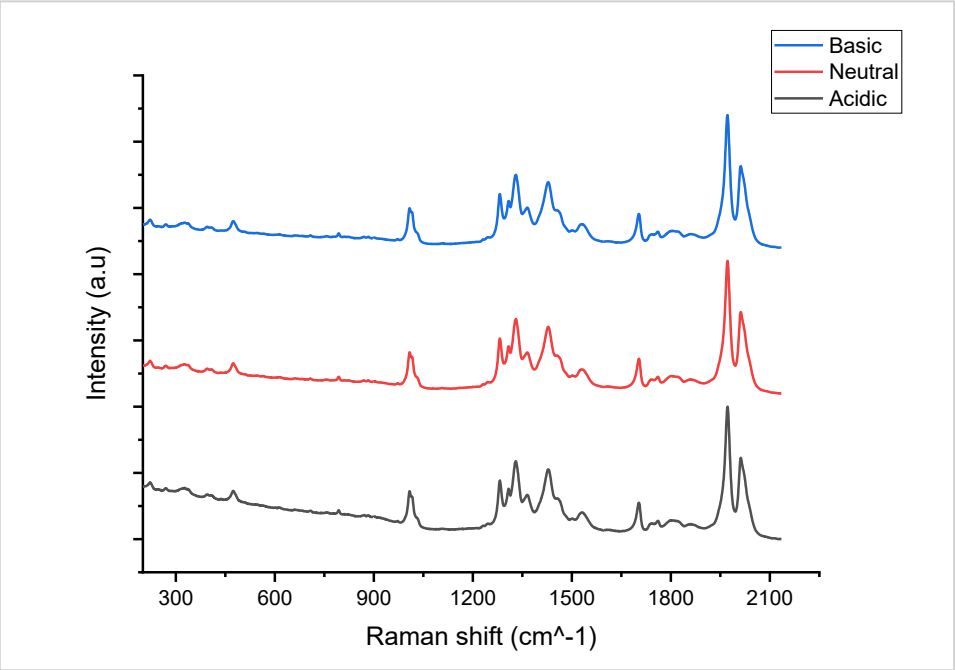

Figure 4.14: Raman spectra of curcumin in different pH environments: acidic (black line), neutral (red line), basic (blue line)

4.2.2 PXRD results

The same samples analyzed with Raman spectroscopy were then studied at PXRD to have a better understanding of potential change in crystal structure related to the addition of polymers or to the type of crystallization technique used. The diffractograms related to the cooling experiments were compared with simulated data of different curcumin polymorphs taken from the Cambridge Structural Database (CSD), refcodes BINMEQ13, BINMEQ12 and BINMEQ07 for form I, II and III, respectively.

From figures 4.15 and 4.16, it can be observed that for all cooling experiments, with or without polymers, the CMC and k-carrageenan did not alter the crystal structure. Furthermore, the peaks are pronounced, indicating high crystallinity and homogeneity.

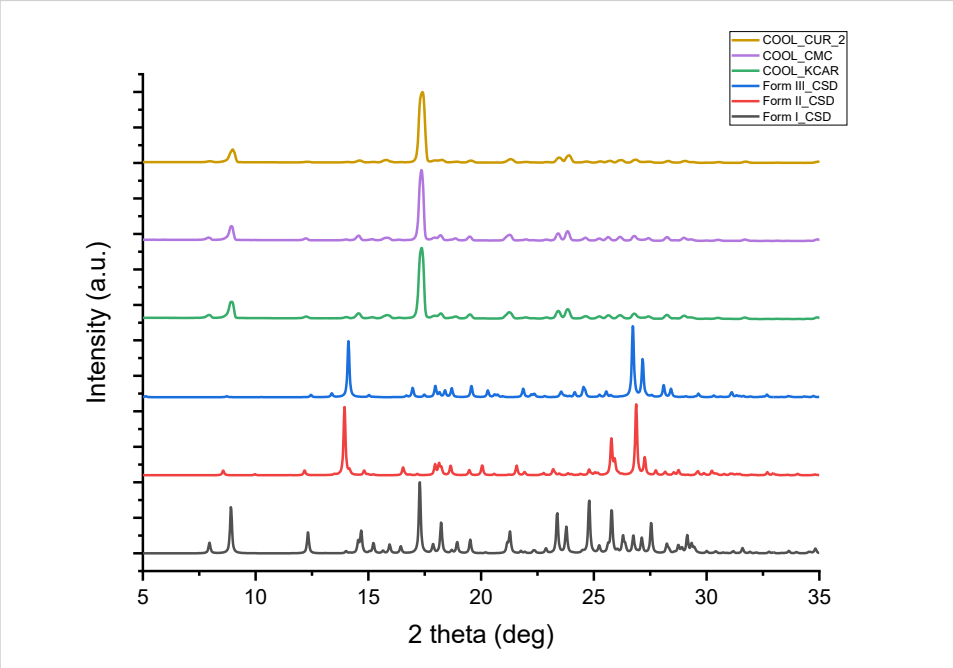

Figure 4.15: PXRD comparison between experiments COOL_CUR_2 (yellow line), COOL_CMC (purple line), COOL_KCAR (green line) and PXRD pattern of Form III from CSD (blue line), Form II from CSD (red line), Form I from CSD (black line)

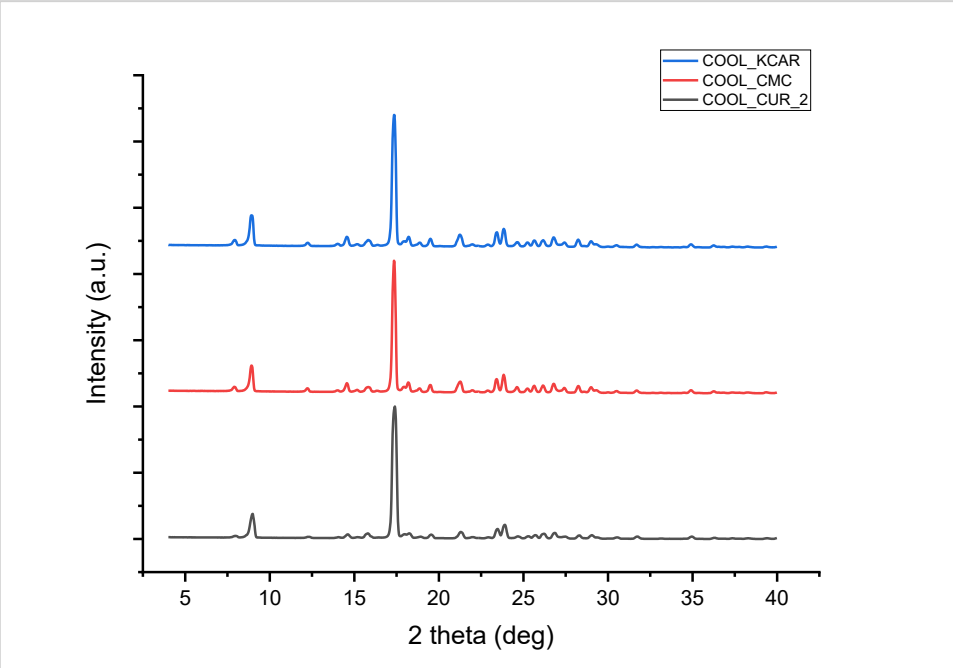

Figure 4.16: PXRD comparison between COOL_CUR_2 (black line), COOL_CMC (red line) and COOL_KCAR (blue line)

PXRD tests were also conducted for antisolvent experiments. In this case as well, the diffractograms align with the form III simulated pattern (Figure 4.17). However, it is noticeable that in the 2θ range between 20° and 35°, the peaks exhibit greater intensity in the literature reference than the other samples. Despite this, the characteristic peaks correspond, thereby confirming the successful formation of form III.

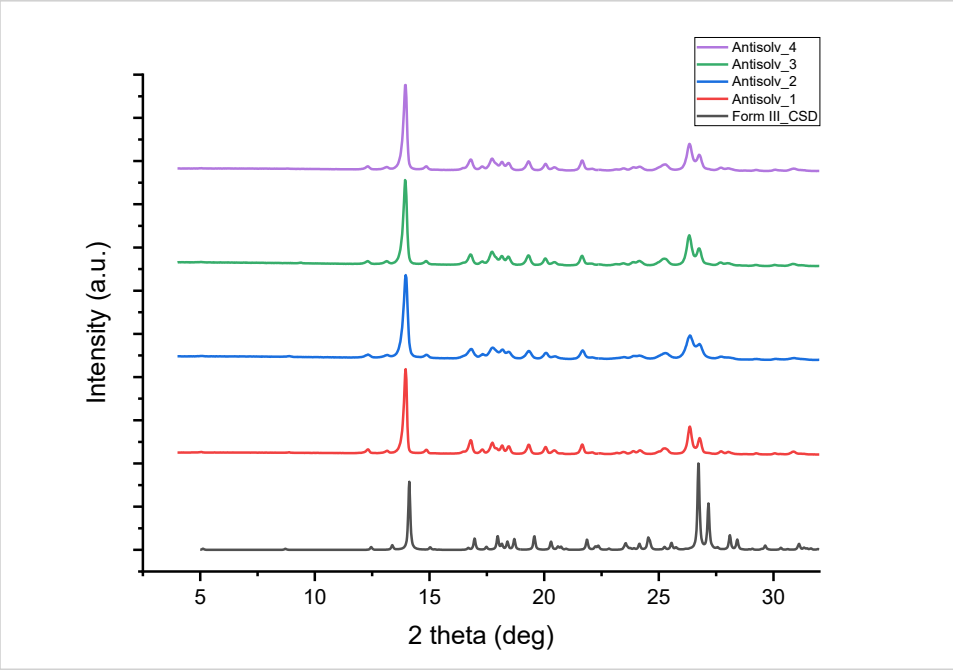

Figure 4.17: PXRD pattern of ANTISOLV_1 (red line), ANTISOLV_2 (blue line), ANTISOLV_3 (green line) and ANTISOLV_4 (purple line) compared to Form III from CSD (black line)

Antisolvent experiments were conducted with varying concentrations (0.05% and 0.1%) of CMC and subsequently k-carrageenan to assess their effects. To investigate how the amount of polymer might influence polymorphism, PXRD measurements were performed. From the spectrograms in Figures 4.18 and 4.19, the variation in the quantity of polymer in solution does not cause changes in the structure of the polymorph, and form III was always obtained.

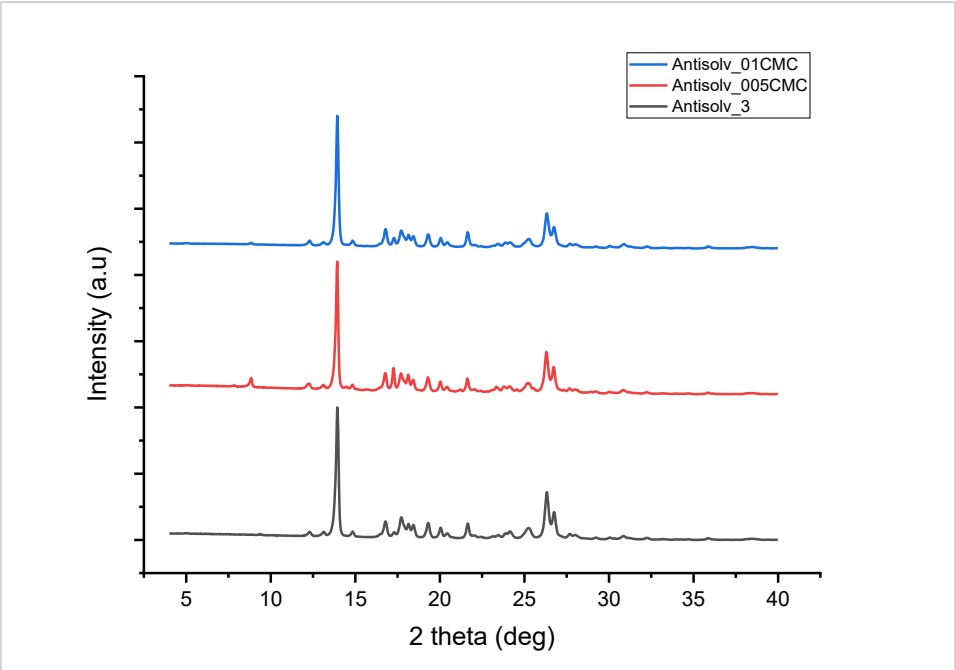

Figure 4.18: PXRD comparison between ANTISOLV_3 (black line), ANTISOLV_005CMC (red line) and ANTISOLV_01CMC (blue line)

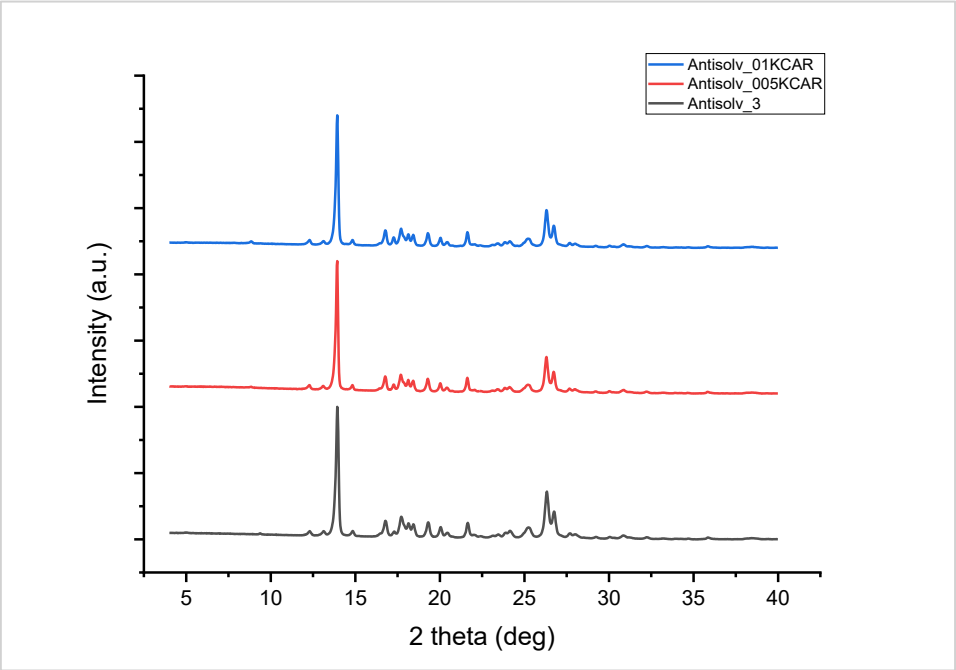

Figure 4.19: PXRD comparison between ANTISOLV_3 (black line), ANTISOLV_005KCAR (red line) and ANTISOLV_01KCAR (blue line)

4.2.3 Thermal characterization of curcumin powders

DSC analysis was carried out to study the thermal behaviour of curcumin crystals. Figure 4.20 presents the thermograms of experiment COOL_CUR_2 compared with COOL_CMC and the thermogram of pure CMC. Curcumin exhibits a melting temperature of 178.1°C, corresponding to the endothermic peak. In contrast, CMC has a melting point of 123.1°C. The COOL_CMC sample shows an endothermic peak that deviates by only a few tenths of a degree from the form I peak (178.8°C). This demonstrates the almost negligible effect of the polymer on the obtained powder.

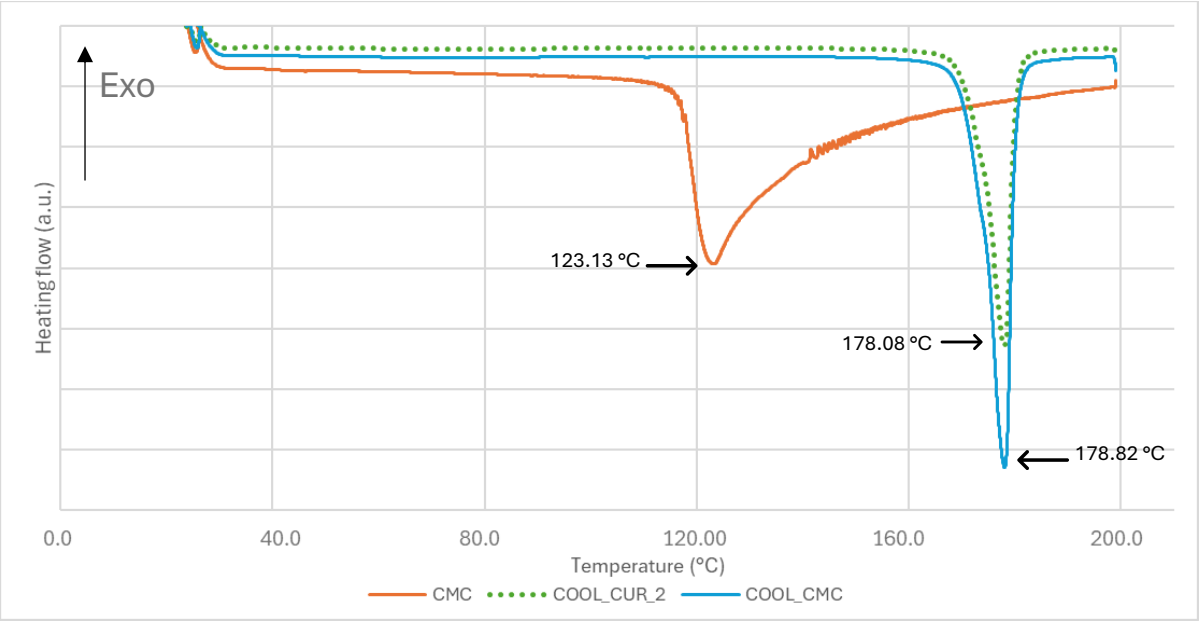

Figure 4.20: DSC thermogram of COOL_CUR_2 (green dots), CMC (orange line) and COOL_CMC (blue line)

Figure 4.21 presents the comparison with k-carrageenan. In this case as well, the melting point remains unchanged, indicating that the presence of tested polymers did not cause significant thermal effects in form I.

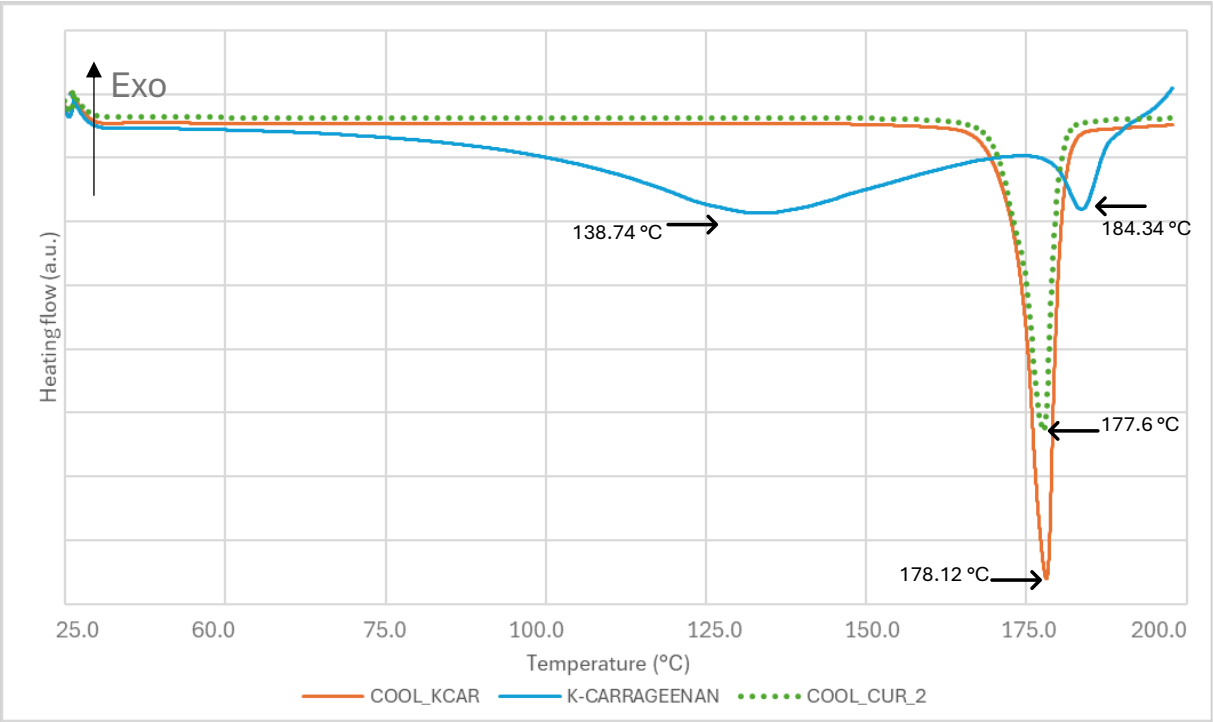

Figure 4.21: DSC thermogram of COOL_CUR_2 (green dots), K-CARRAGEENAN (blue line) and COOL_KCAR (orange line)

About form III, the crystals obtained from various experiments conducted using the antisolvent technique under different operational conditions (i.e., varying percentages of antisolvent or curcumin concentration and presence of polymers) were compared. Figure 4.22 compares the thermograms of form III obtained with a constant solvent-antisolvent ratio by weight (1:2.5) but with different curcumin concentrations. It is shown that the varying curcumin concentrations did not significantly influence the melting temperature, which remained unchanged.

A similar comparison was made in the case where the solvent-antisolvent ratio by weight was 1:5. The resulting thermograms confirms the trend (Figure 4.23). Therefore, the different solvent-antisolvent ratio slightly affects the first endothermic peak (around 166.3°C in Figure 4.22 and around 162.5 in Figure 4.23) but the thermogram are similar apart from the curcumin concentration in solution. This stability suggests that the crystallization method is effective in producing consistent polymorphs.

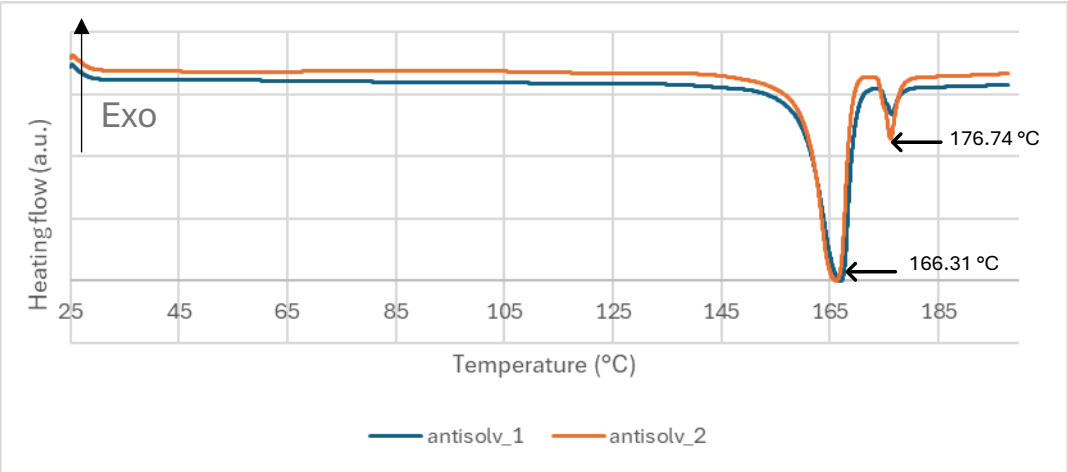

Figure 4.22: DSC thermogram of comparison between ANTISOLV_1 (blue line) and ANTISOLV_2 (orange line)

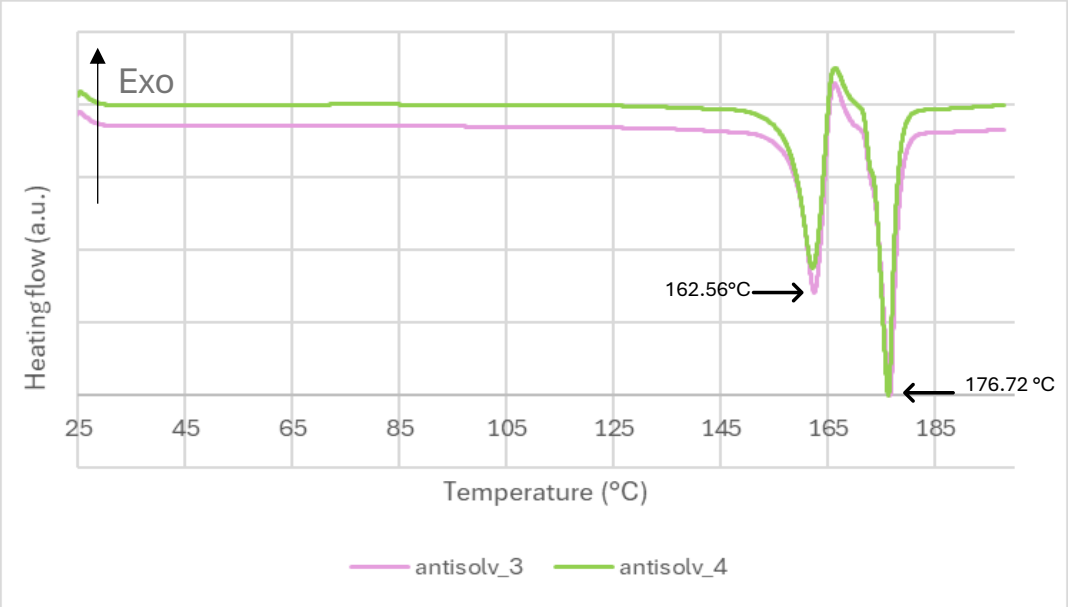

Figure 4.23: DSC thermogram of comparison between ANTISOLV_3 (pink line) and ANTISOLV_4 (green line)

Looking at the thermograms in Figures 4.24 to 4.27, it is clear that, regardless of the polymer percentage in the solution, the endothermic peaks of curcumin and polymers alone differ by a significant amount. Specifically, the curcumin shows an endothermic peak at 162.5°C, while CMC at 138.7°C and k-carrageenan at 134.9°C. The endothermic peaks of ANTISOLV_005CMC, ANTISOLV_01CMC, ANTISOLV_005KCAR and ANTISOLV_01KCAR are almost identical to those of curcumin alone. This similarity can be attributed to the substantial temperature differences between curcumin and the polymers alone, which suggests that the polymers have minimal interaction with the curcumin crystals, allowing

curcumin's thermal behaviour to remain largely unchanged. This result may be due to the low concentration of polymers or their limited interaction with the crystalline structure, which, despite the presence of polymers during crystallisation, does not undergo changes in its fundamental thermodynamic properties, such as the melting point.

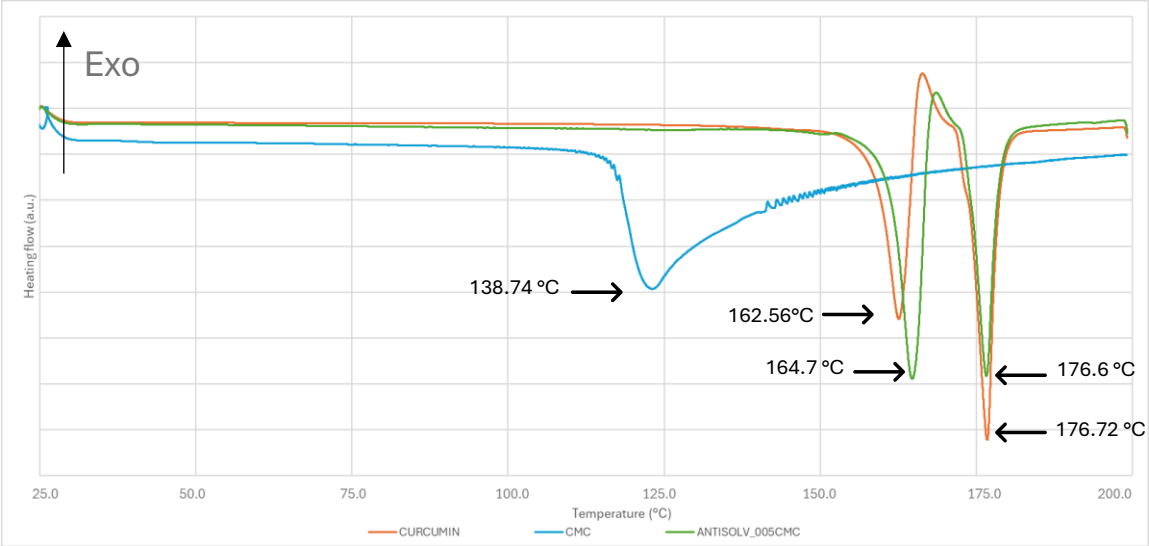

Figure 4.24: DSC thermogram of ANTISOLV_3 (orange line), CMC (blue line) and ANTISOLV_005CMC (green line)

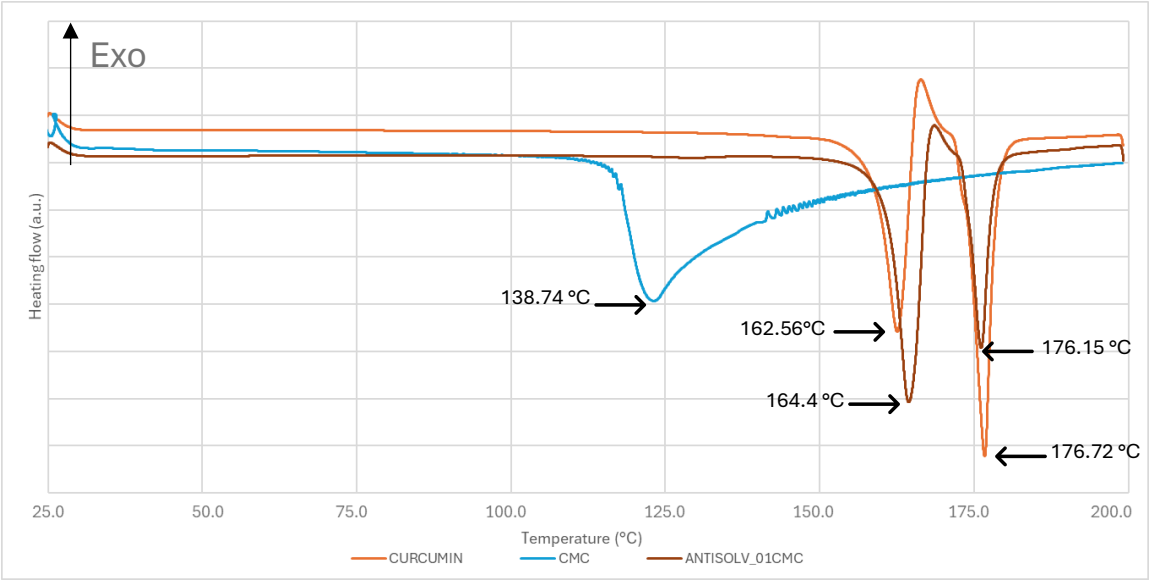

Figure 4.25: DSC thermogram of ANTISOLV_3 (orange line), CMC (blue line) and ANTISOLV_01CMC (brown line)

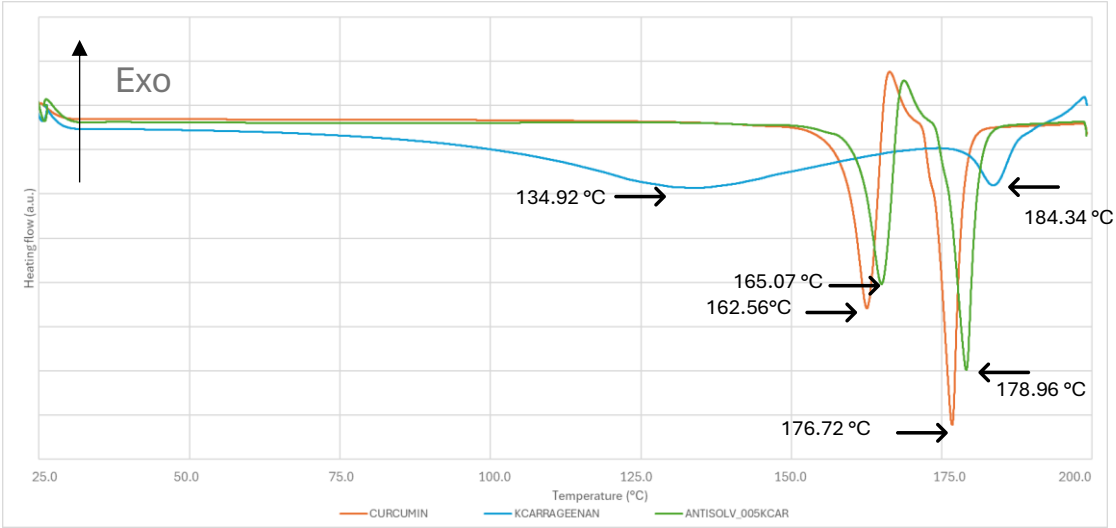

Figure 4.26: DSC thermogram of ANTISOLV_3 (orange line), KCAR (blue line) and ANTISOLV_005KCAR (green line)

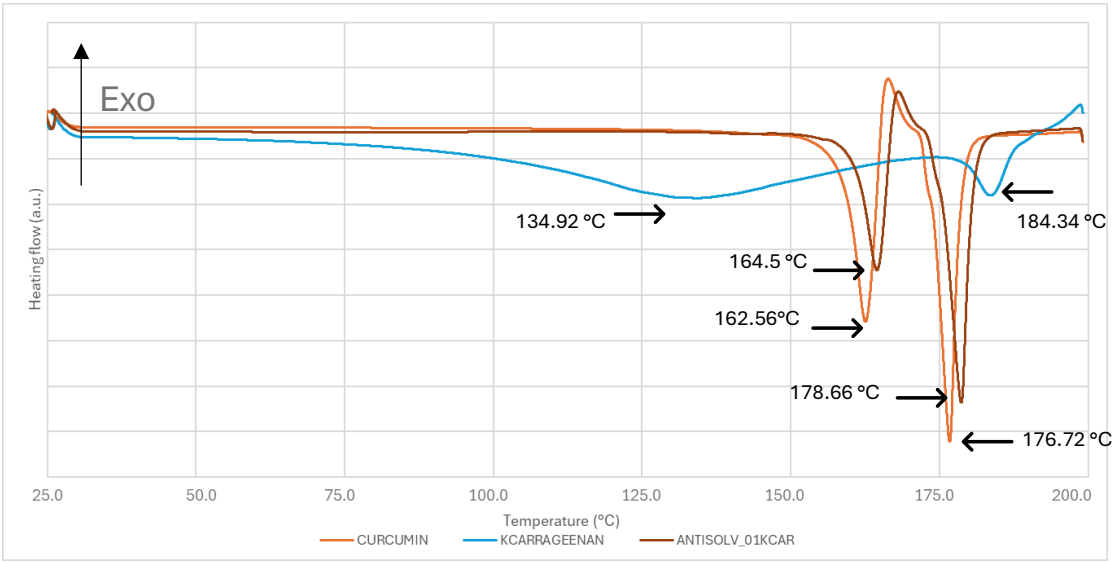

Figure 4.27: DSC thermogram of ANTISOLV_3 (orange line), KCAR (blue line) and ANTISOLV_01KCAR (green line)

4.2.4 PSD results

The polymorphs obtained from the various experiments reported in Tables 3.4 to 3.7 were then subjected to particle size distribution analysis to determine their crystal size and shape, as these properties directly influence curcumin's stabilising ability in emulsions. Samples from the different experiments were collected and observed under an optical microscope. For each sample, microscope images deemed suitable for describing the sample were selected. A 10x objective was used, and when necessary, 5x and 40x objectives were also employed. Subsequently, the visible crystals in the images were manually outlined. The images were then uploaded into the ImageJ.exe software, which facilitated the assessment of Feret diameter and aspect ratio.

Optical Microscopy and SEM were selected according to the particle size of the samples, since the two techniques are characterized by a different resolution of the images. In following Figures (4.28 to 4.33) are shown some representative images of samples.

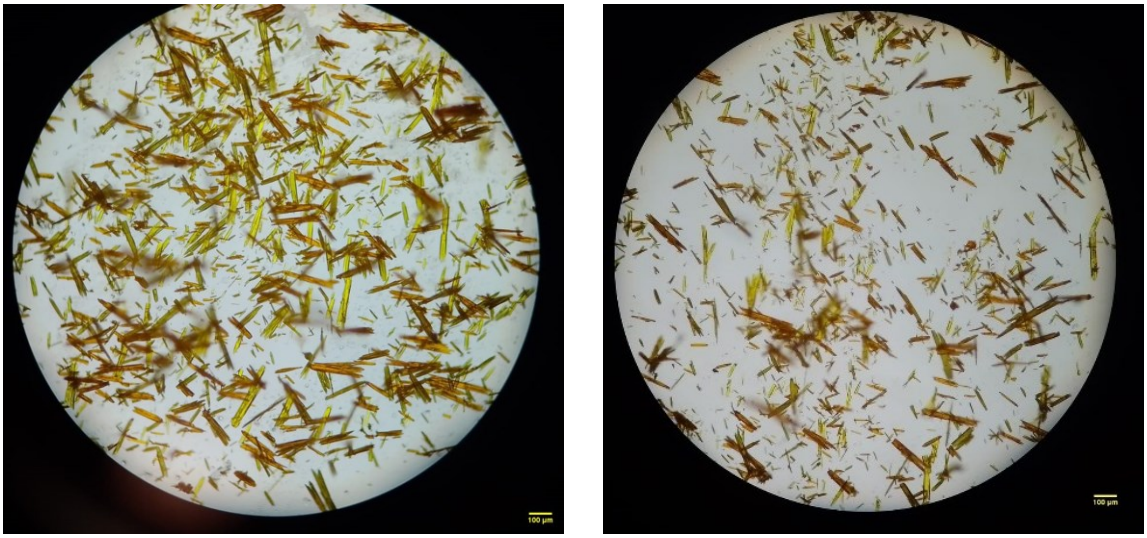

Figure 4.28: Optical microscope images of curcumin Form I (experiment COOL_CUR_2)

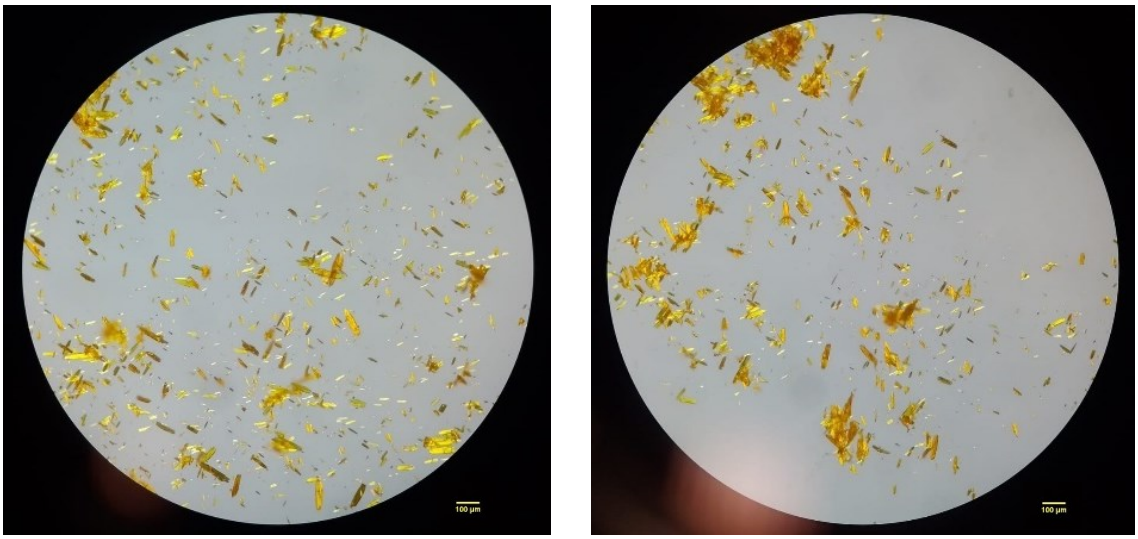

Figure 4.29: Optical microscope images of curcumin Form I (experiment COOL_CMC)

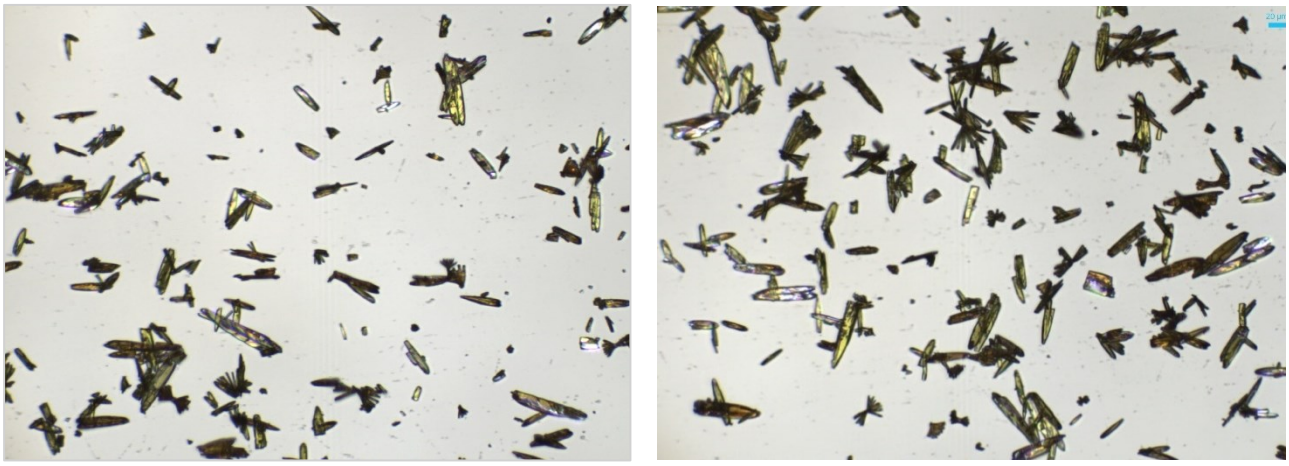

Figure 4.30: Optical microscope images of curcumin Form I (experiment COOL_KCAR)

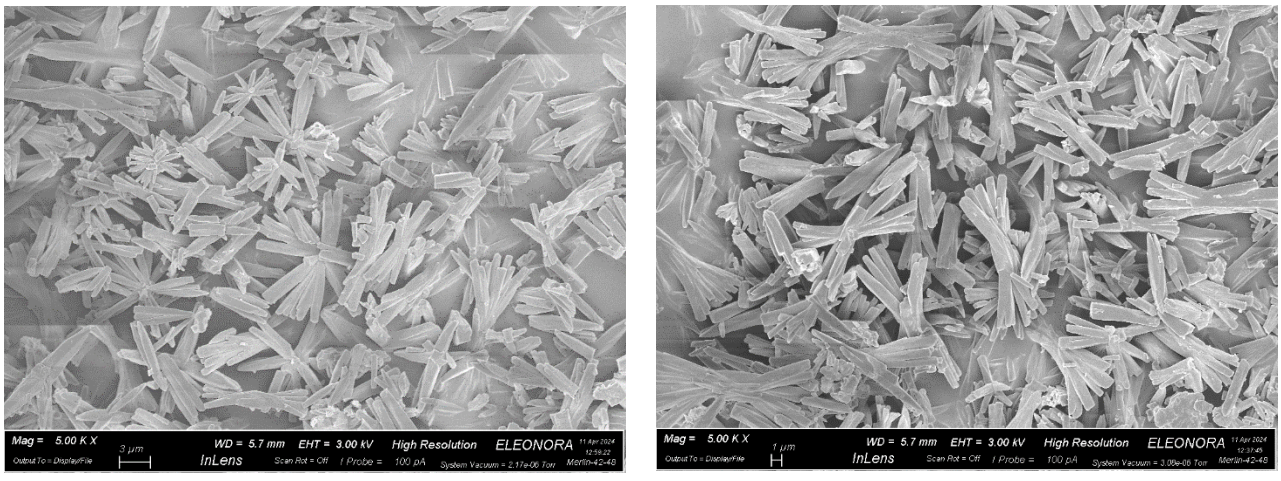

Figure 4.31: SEM images of curcumin Form III (experiment ANTISOLV_1)

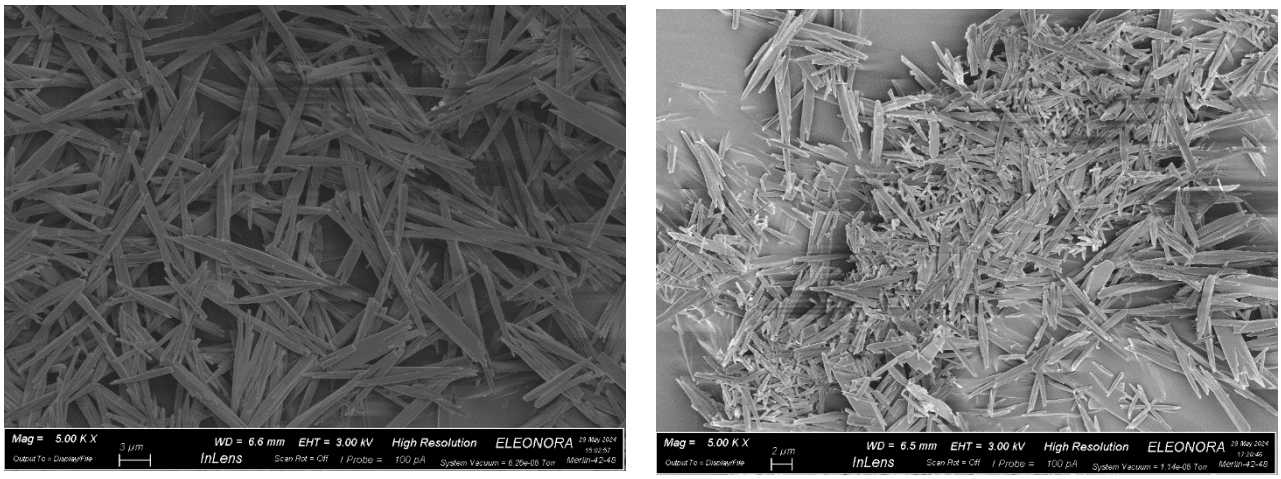

Figure 4.32: SEM images of curcumin Form III (experiment ANTISOLV_01CMC)

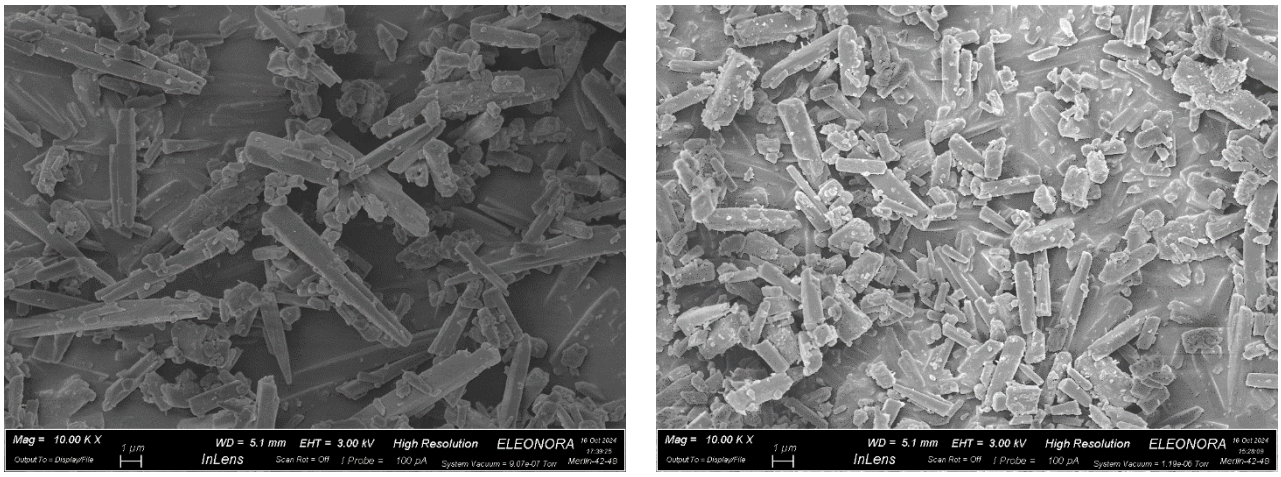

Figure 4.33: SEM images of curcumin Form III (experiment ANTISOLV_01KCAR)

Figures 4.28 and 4.31 illustrate the size and shape of the two obtained polymorphs. Form I crystals exhibit an elongated and regular shape, whereas those of form III are still needle like but often forms agglomerates, possibly due to secondary nucleation. This phenomenon may be attributed to the antisolvent crystallization method, which promotes secondary nucleation events over crystal growth. The reference scale is set at the micrometre level for the various case studies.

Particle size and shape distribution are critical parameters for emulsion stabilization. Smaller particles tend to form more compact interfacial layers, preventing droplet coalescence more effectively. The elongated, non-spherical shape observed in both form I and form III may provide additional interfacial stability by increasing the surface area coverage at the oil-water interface. The anisotropy of these particles, quantified by the aspect ratio (Table 4.2), provides

further insight into their behaviour at the interface, where elongated shapes can promote stronger steric barriers against coalescence.

In Figures 4.29, 4.30, 4.32, and 4.33, the impact of polymer presence during crystallization is visible. For form I, CMC inhibited crystal growth while promoting nucleation, resulting in smaller crystals (Figure 4.29). In the case of form III, the presence of CMC had the opposite effect, yielding larger crystals with a rectangular shape (Figure 4.32). K-carrageenan, for form III, has changed slightly the morphology of crystals that became shorter, and their aspect ratio increased proportionally to the quantity of polymer in solution (Figure 4.33).

These results highlight that the PSD is sensitive to the crystallization method and the presence of polymers. The results obtained from analysing the images from optical and SEM microscope were then processed using Origin, allowing data from each sample to be categorised by relative frequency. The Feret diameter and aspect ratio of the various samples were assessed, with the aspect ratio defined as the ratio between the dimensions of the two axes of the ellipses approximating each crystal. This data was used to generate histograms showing the relative frequency with which solid particles fell within specific size and AR ranges.

For emulsion stabilization, crystals of form I (Experiment COOL_CUR_2), form III (Experiment ANTISOLV_3 and ANTISOLV_1), and ANTISOLV_01CMC were used. Consequently, only the distributions of the Feret Diameter and aspect ratio for these samples are presented here. Additional graphs are provided in Appendix A.

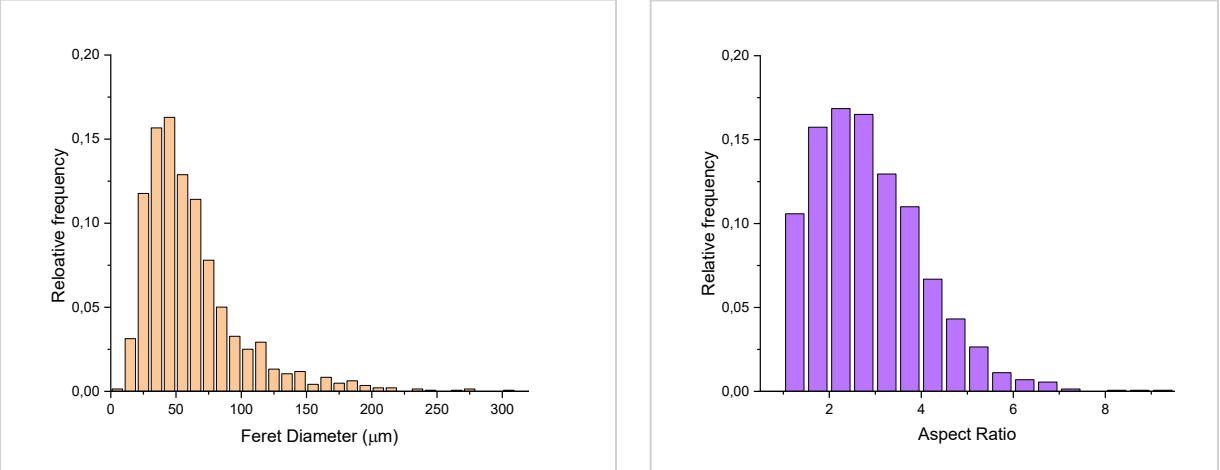

Figure 4.34: PSD (on left) and AR distribution (on right) of curcumin crystals from Experiment COOL_CUR_2

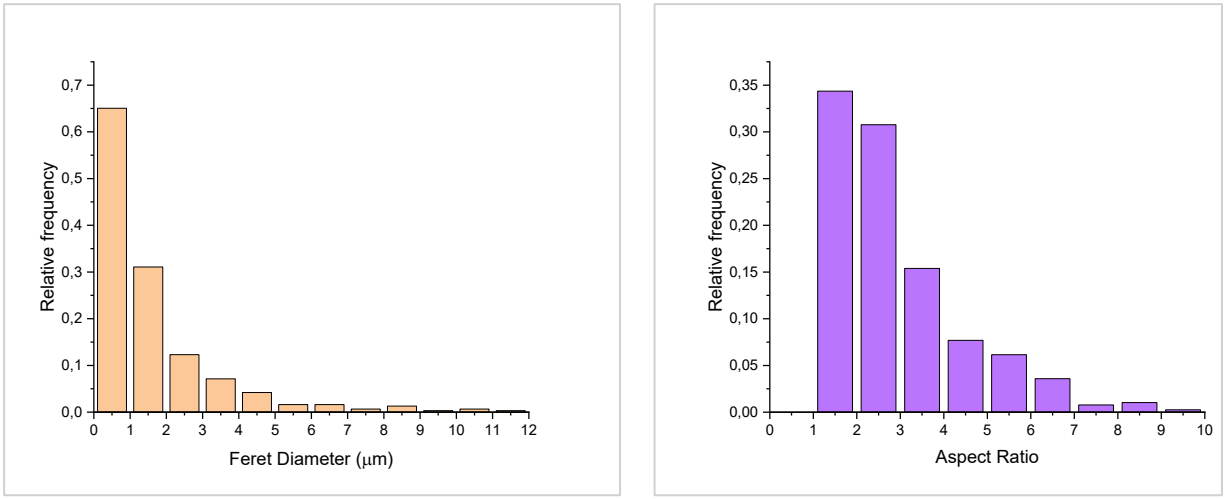

Figure 4.35: PSD (on left) and AR distribution (on right) of curcumin crystals from Experiment ANTISOLV_3

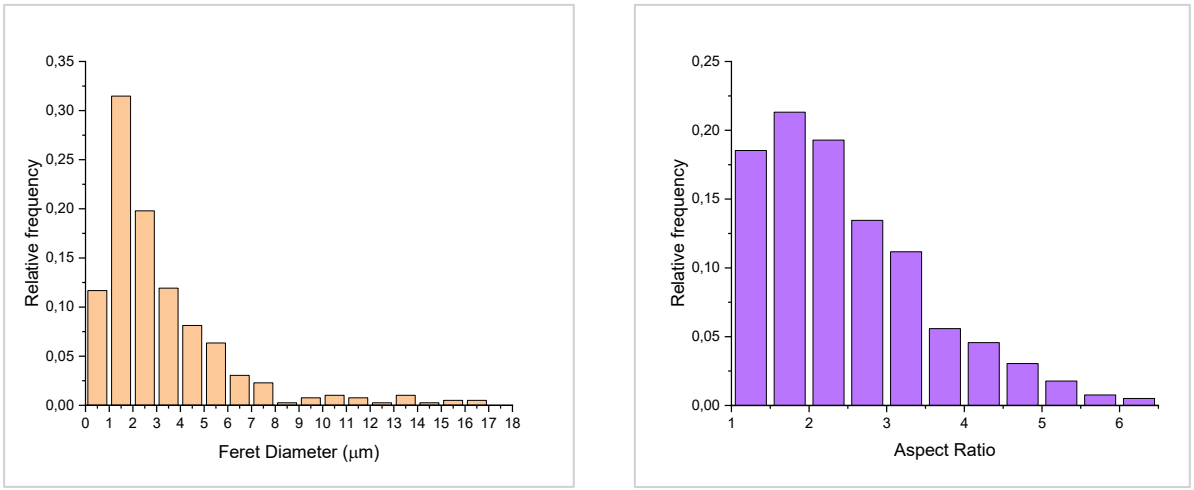

Figure 4.36: PSD (on left) and AR distribution (on right) of curcumin crystals from Experiment ANTISOLV_1

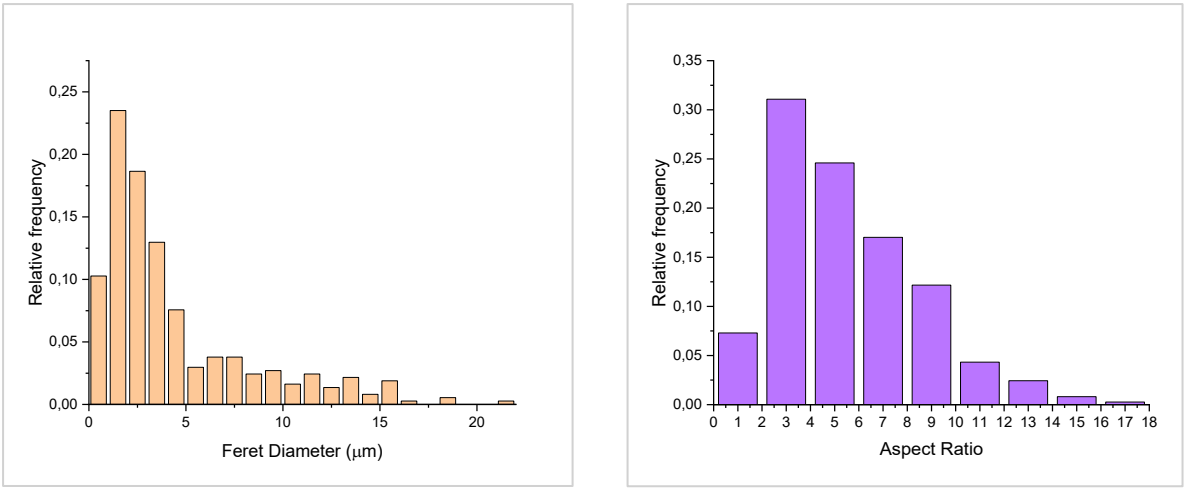

Figure 4.37: PSD (on left) and AR distribution (on right) of curcumin crystals from Experiment ANTISOLV_01CMC

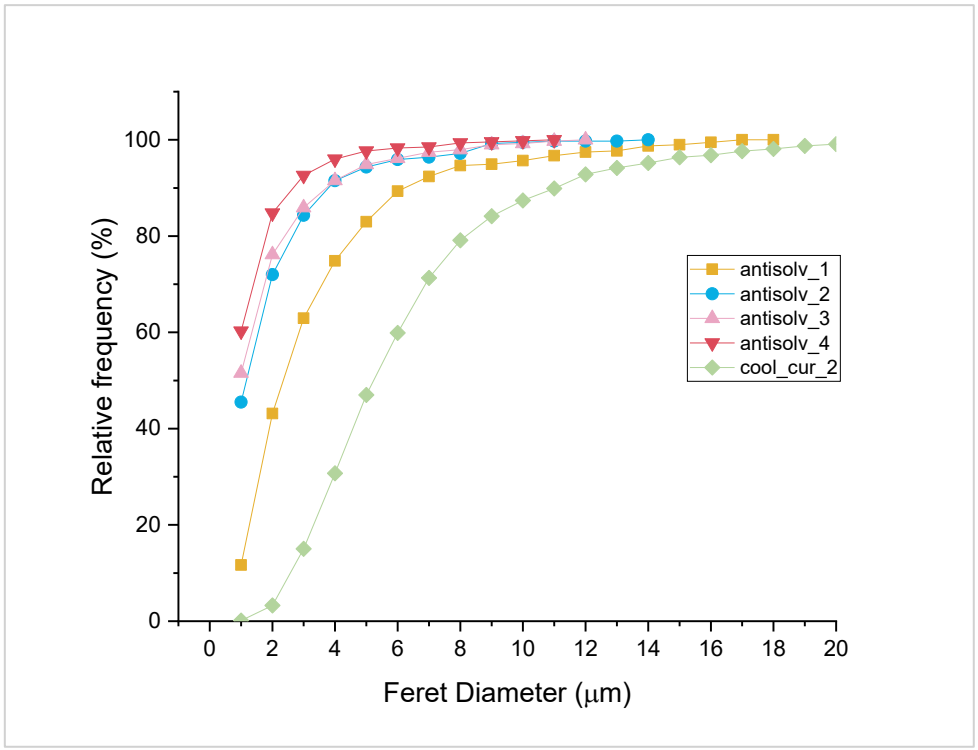

Figure 4.38: Particle size distribution represented as cumulative frequency, expressed in percentage of particles over the total number for experiments: COOL_CUR_2 (green), ANTISOLV_1 (orange), ANTISOLV_2 (blue), ANTISOLV_3 (pink), ANTISOLV_4 (red)

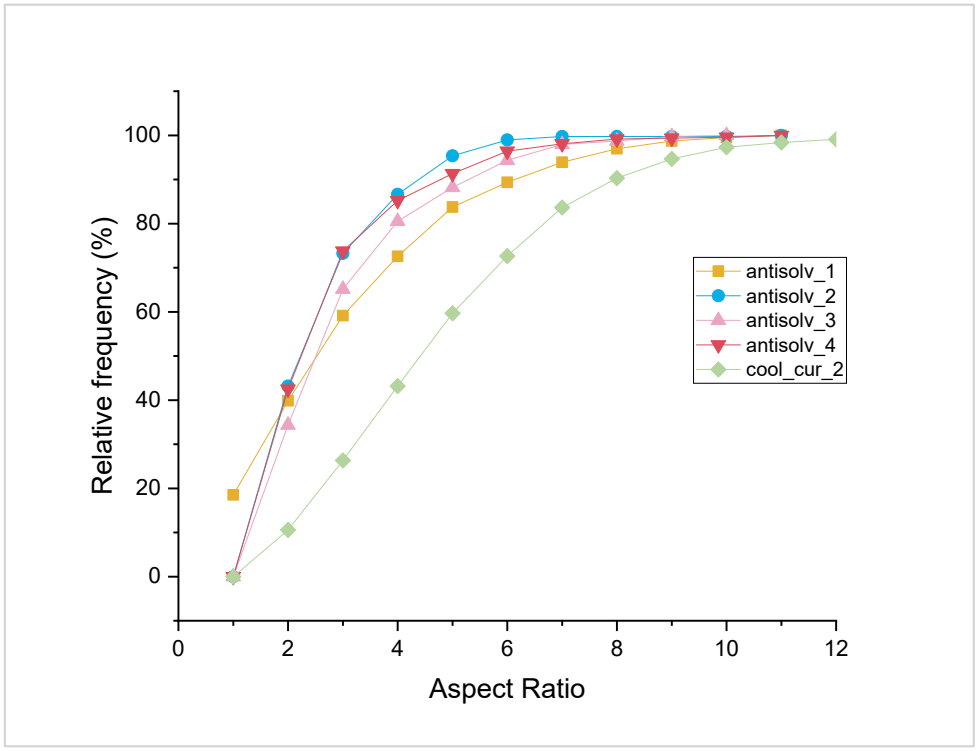

Figure 4.39: Aspect ratio as cumulative frequency, expressed in percentage of particles over the total number for experiments: COOL_CUR_2 (green), ANTISOLV_1 (orange), ANTISOLV_2 (blue), ANTISOLV_3 (pink), ANTISOLV_4 (red)

Figures 4.38 and 4.39 allow for a comparison of the samples obtained. In the antisolvent experiments, the distribution appears narrow, indicating the uniformity of crystal sizes produced. Conversely, the cooling method resulted in a broader size distribution (Figure 4.38), potentially reducing form I's effectiveness as a stabilizer due to the presence of larger particles. The greater homogeneity observed in antisolvent-produced particles is an advantage for stabilizing emulsions, as it reduces instability associated with uneven particle distributions. Figures 4.34 and 4.35 illustrate the different size distribution of the two polymorphs obtained. Form I crystals have an average size of 61.61 μm, while those of form III are around 1.6 μm. This broader range could potentially lead to reduced form I efficiency in stabilizing emulsions, as large particles are less effective in forming compact interfacial layers. To improve form I's performance, further experiments could explore methods to reduce particle size, such as modifying the cooling rates or introducing additional nucleating agents. For crystals produced via the antisolvent method, the samples obtained with a higher solvent-antisolvent ratio (1:2.5 ethanol/water, experiments ANTISOLV_1 and ANTISOLV_2) reached nearly double the size of those obtained with a lower ratio (1:5 ethanol/water ratio, experiments ANTISOLV_3 and ANTISOLV_4). Additionally, the high aspect ratio values confirm the elongated, non-spherical shape of the polymorphs (see Table 4.2).

Table 4.2: Mean Feret diameter, Aspect ratio and relative SD for all curcumin powders obtained

	Polymorph	**Mean Feret Diameter (μm)**	**SD Feret (μm)**	**Mean Aspect Ratio (μm)**	**SD Aspect Ratio (μm)**
COOL_CUR_2	FORM I	61.61	37.89	2.88	1.19
COOL_CMC	FORM I	56.47	26.79	2.35	0.92
COOL_KCAR	FORM I	32.26	20.13	9.14	4.37
ANTISOLV_1	FORM III	3.19	2.77	2.49	1.07
ANTISOLV_2	FORM III	3.49	3.71	2.52	1.24
ANTISOLV_3	FORM III	1.62	1.77	2.92	1.57
ANTISOLV_4	FORM III	1.23	1.31	2.62	1.47
ANTISOLV_005CMC	FORM III	2.77	2.23	4.38	2.34
ANTISOLV_01CMC	FORM III	4.38	3.99	5.42	2.95
ANTISOLV_005KCAR	FORM III	1.69	1.90	3.18	1.90
ANTISOLV_01KCAR	FORM III	1.24	1.39	2.27	1.11

The following graphs illustrate a comparison of the size distribution between the samples obtain with and without the presence of the polymers.

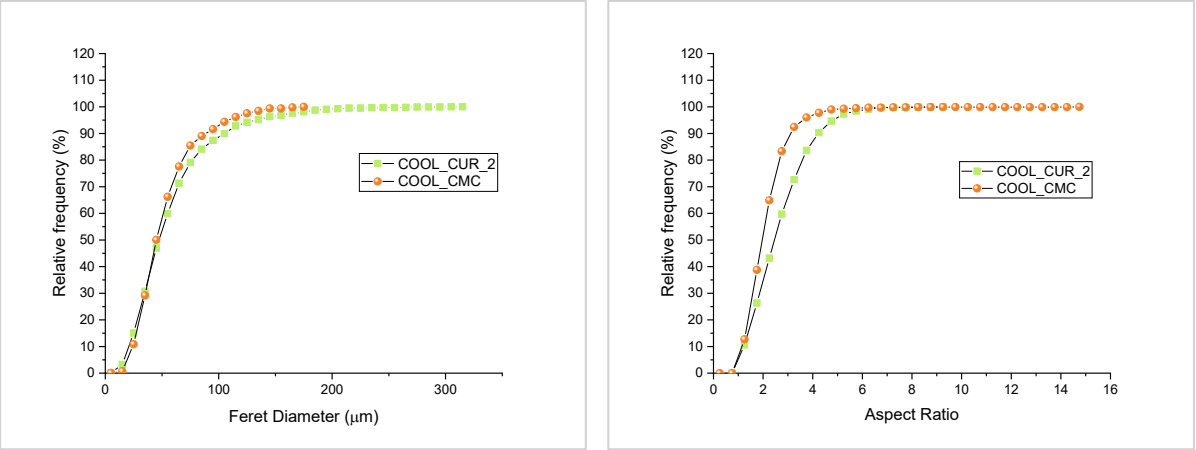

Figure 4.40: Particle size distribution represented as cumulative frequency, expressed in percentage of particles over the total number (experiments COOL_CUR_2 (orange) and COOL_CMC (green))

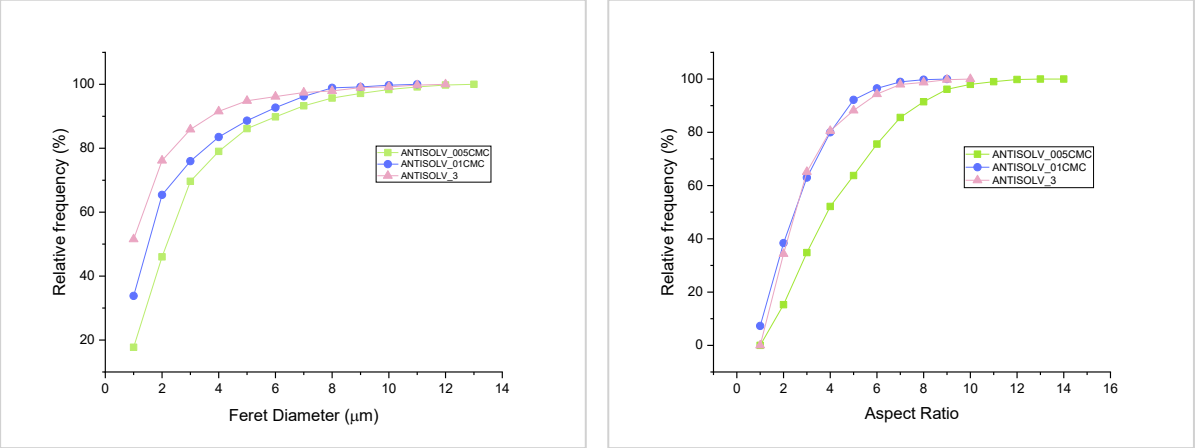

Figure 4.41: Particle size distribution represented as cumulative frequency, expressed in percentage of particles over the total number (experiments ANTISOLVENT_3 (pink), ANTISOLV_01CMC (blue), ANTISOLV_005CMC (green))

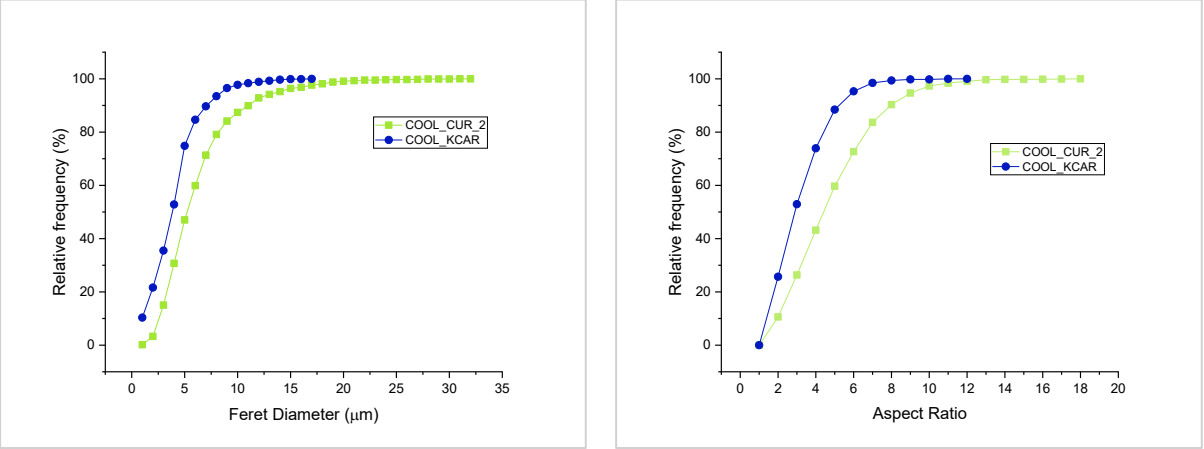

Figure 4.42: Particle size distribution represented as cumulative frequency, expressed in percentage of particles over the total number (experiments COOL_CUR_2 (green), COOL_KCAR (blue))

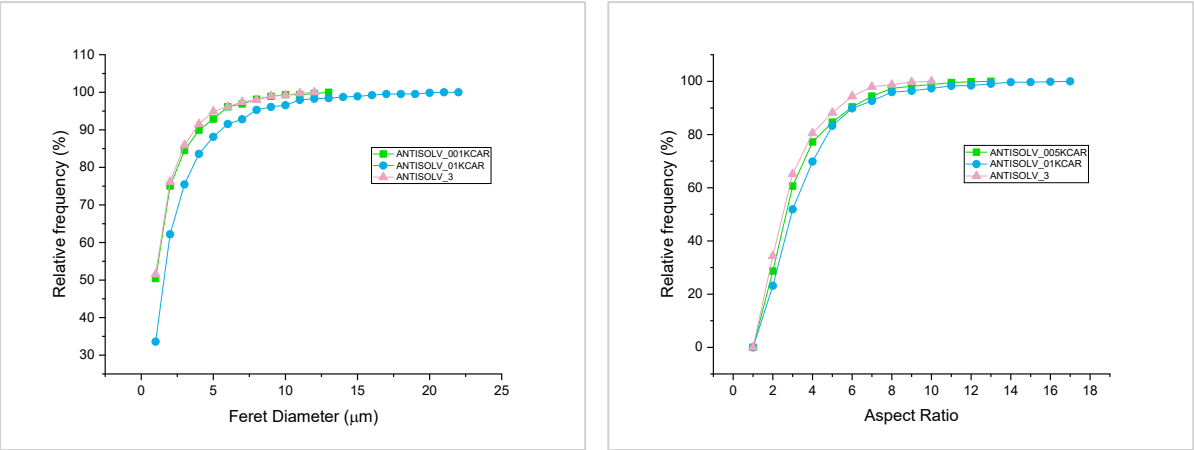

Figure 4.43: Particle size distribution represented as cumulative frequency, expressed in percentage of particles over the total number (experiments ANTISOLV_3 (pink), ANTISOLV_01KCAR (blue) and ANTISOLV_005KCAR (green))

Figure 4.40 highlights the effect of CMC presence during crystallization. For form I, CMC inhibited crystal growth while promoting nucleation, resulting in smaller crystals. In contrast, an opposite effect was observed with form III, where the presence of CMC led to larger crystal formation (Figure 4.41). The k-carrageenin instead caused the reduction of the average Feret diameter (32.26 μm) and the increase of the aspect ratio only for form I while for the other polymorph the effect was not significant (Figure 4.42 and 4.43).

Additionally, two-dimensional graphs were produced, displaying only L1 and L2 on the axes to provide a more direct view of the results. As examples, Figures 4.44 and 4.45 show the distribution from a cooling experiment, Figures 4.46 and 4.47 illustrate an antisolvent experiment, and Figures 4.48 and 4.49 shown form III obtained with 0.1% CMC. Additional graphs are provided in Appendix A.

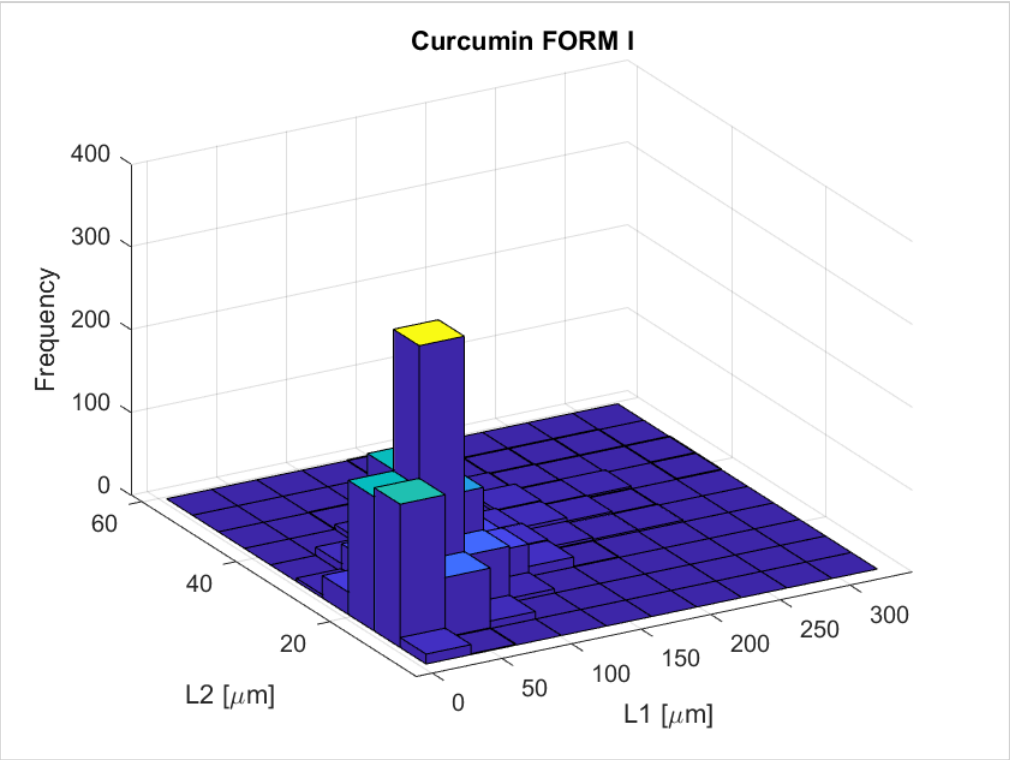

Figure 4.44: Three-dimensional distribution of dimensions considering major side (L1) and minor side (L2) of Form I obtained by cooling (experiment COOL_CUR_2)

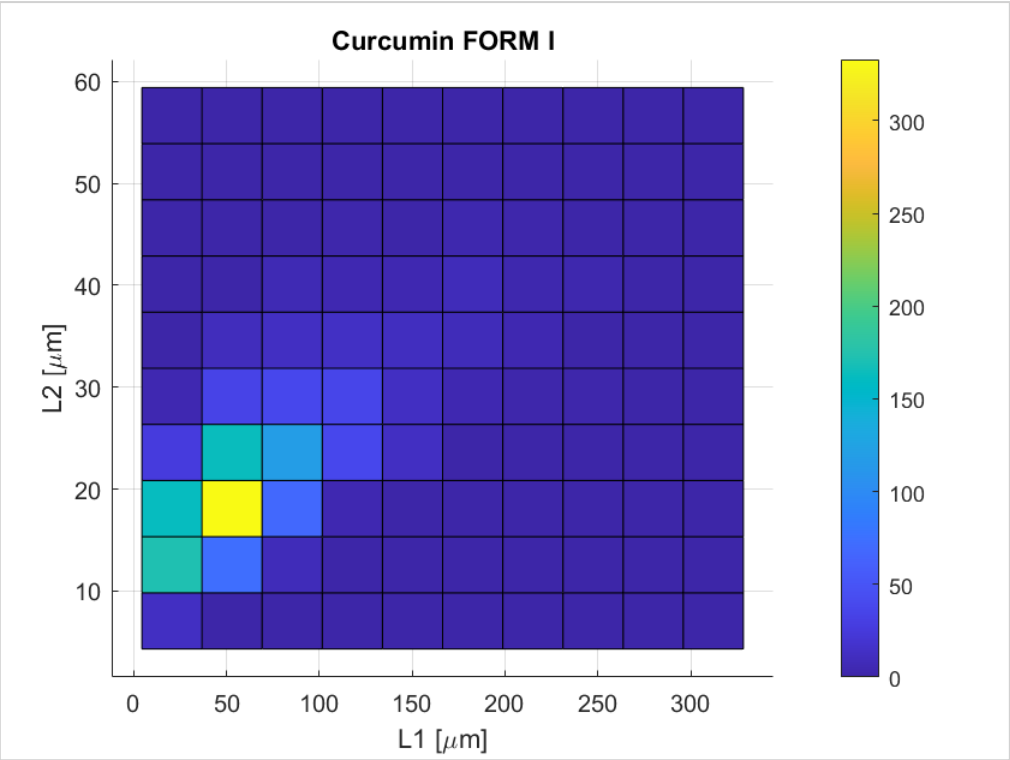

Figure 4.45: Bidimensional distribution of dimensions considering major side (L1) and minor side (L2) of Form I obtained by cooling (Experiment COOL_CUR_2)

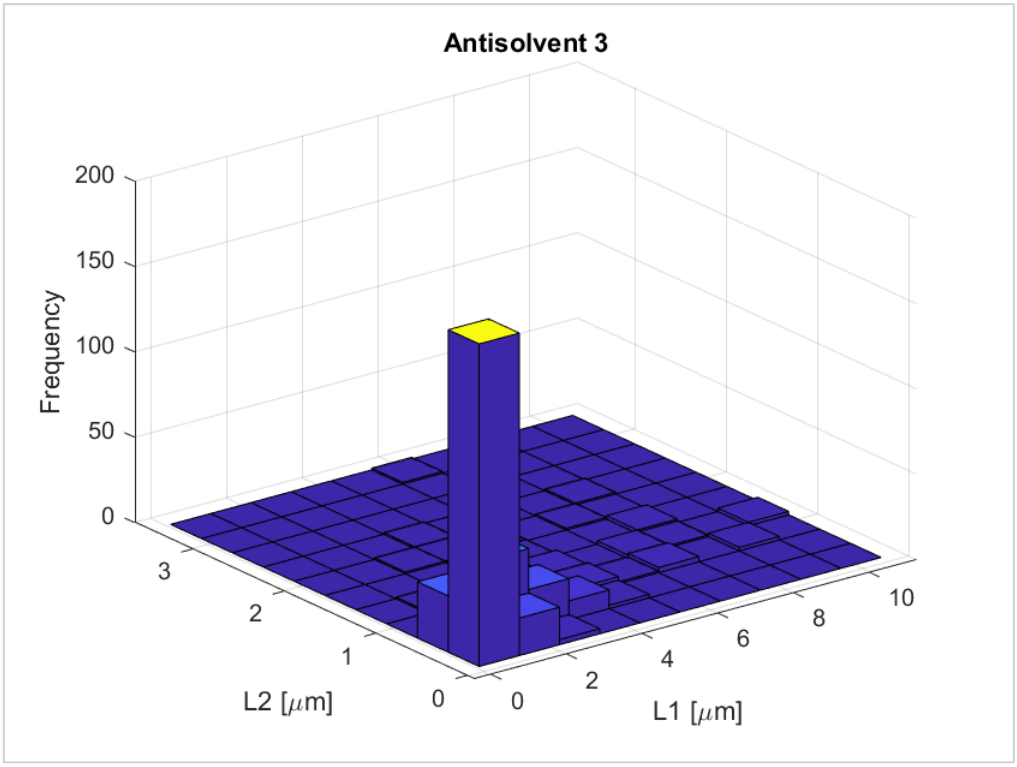

Figure 4.46: Three-dimensional distribution of dimensions considering major side (L1) and minor side (L2) of Form III obtained by antisolvent (experiment ANTISOLV_3)

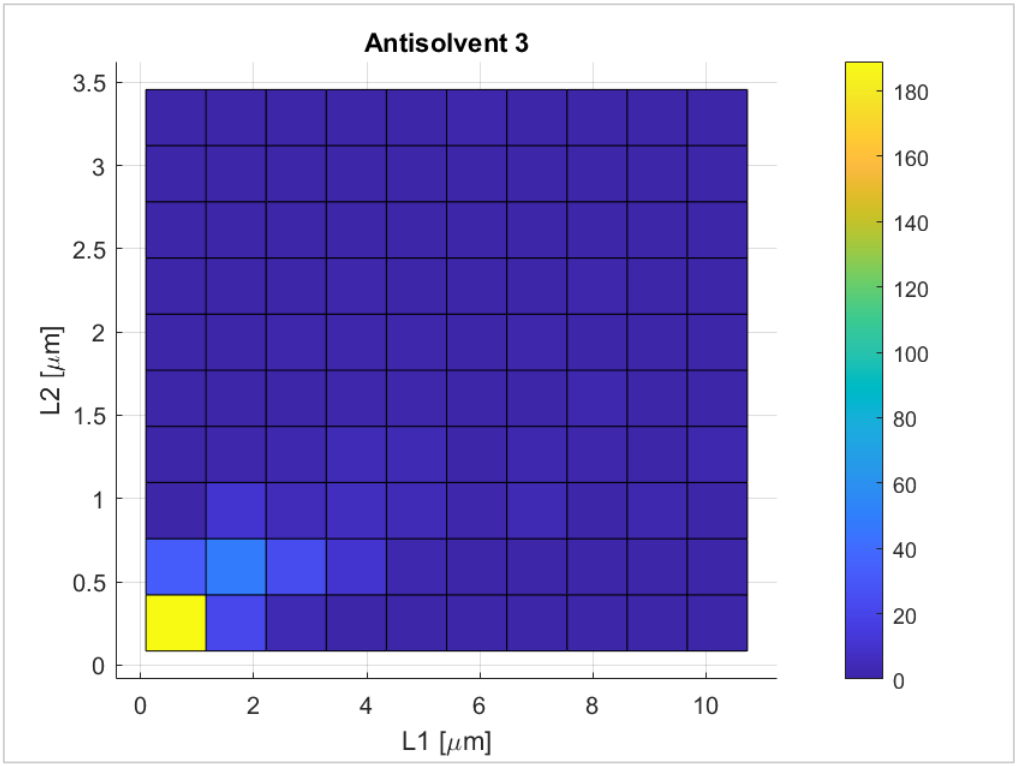

Figure 4.47: Bidimensional distribution of dimensions considering major side (L1) and minor side (L2) of Form III obtained by antisolvent (experiment ANTISOLV_3)

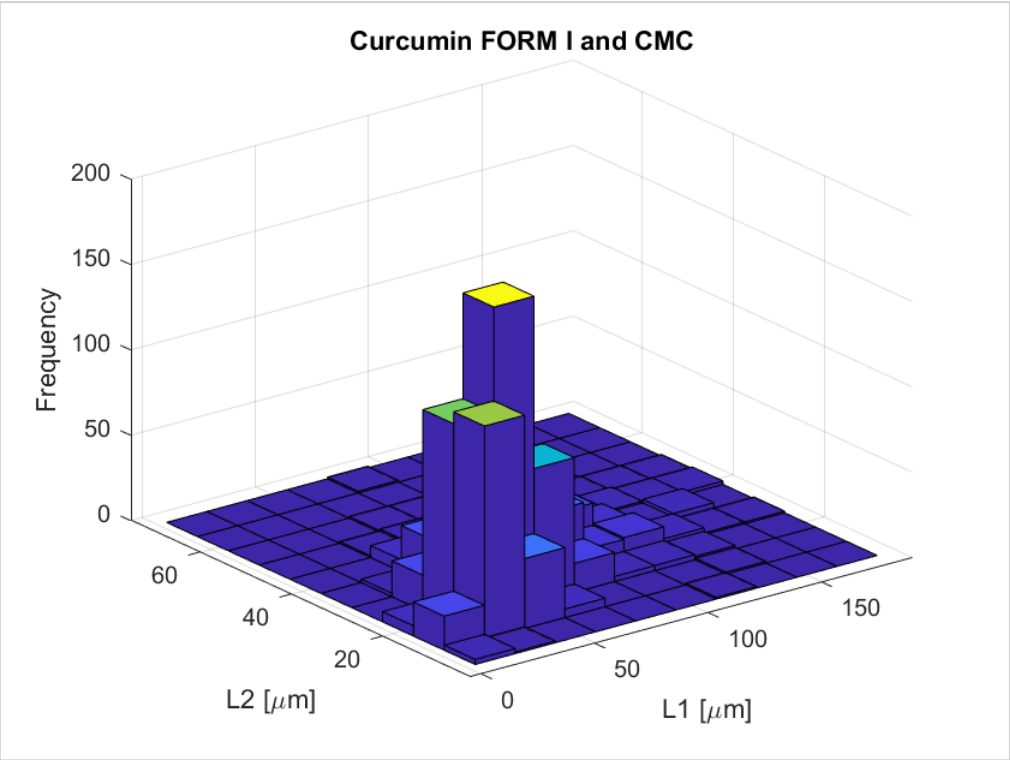

Figure 4.48: Three-dimensional distribution of dimensions considering major side (L1) and minor side (L2) of Form I obtained by cooling with 0.1%CMC (experiment COOL_CMC)

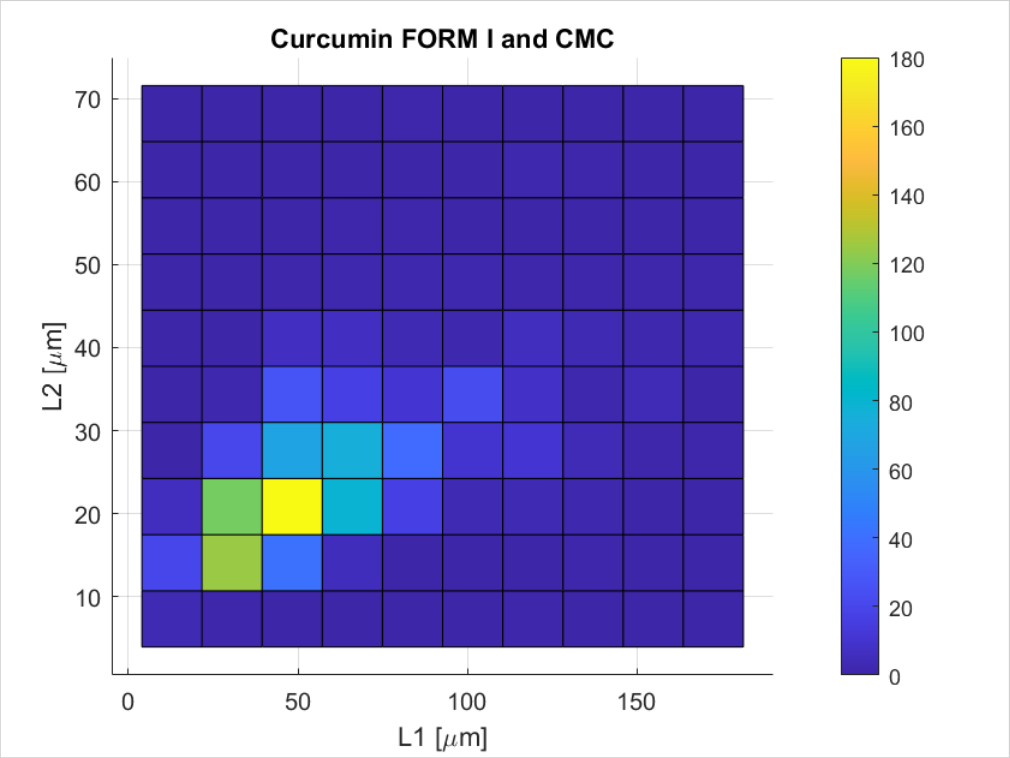

Figure 4.49: Bidimensional distribution of dimensions considering major side (L1) and minor side (L2) of Form I obtained by cooling with 0.1%CMC (experiment COOL_CMC)

The graphs (figure 4.44 to 4.49) allow for a qualitative comparison between size and shape distribution of curcumin form I and form III. It is evident that the cooling method resulted in crystals with both longer sides compared to those obtained via the antisolvent method. The average values of the major (L1) and minor (L2) axes, along with their respective standard deviations (SD), were calculated by averaging the values obtained from the dimensional analysis and are reported in Table 4.3. These results confirm the clear size difference between form I and form III.

Table 4.3: Mean major side (L1), minor side (L2) and relative SD for all curcumin powders obtained

	Polymorph	**Mean L1 (µm)**	**SD L1 (µm)**	**Mean L2 (µm)**	**SD L2 (µm)**
COOL_CUR_2	FORM I	62.98	41.03	20.88	6.83
COOL_CMC	FORM I	55.18	27.73	23.44	7.66
COOL_KCAR	FORM I	32.52	19.69	3.46	1.63
ANTISOLV_1	FORM III	3.09	2.59	1.21	0.90
ANTISOLV_2	FORM III	3.37	3.51	1.23	1.08
ANTISOLV_3	FORM III	1.61	1.73	0.49	0.37
ANTISOLV_4	FORM III	1.23	1.29	0.42	0.25
ANTISOLV_005CMC	FORM III	2.79	2.28	0.65	0.47
ANTISOLV_01CMC	FORM III	4.31	3.81	0.72	0.36
ANTISOLV_005KCAR	FORM III	1.72	1.95	0.45	0.29
ANTISOLV_01KCAR	FORM III	1.24	1.47	0.47	0.33

Despite the varying polymer concentrations, the impact on the crystal size and morphology is not particularly pronounced. It should be considered that the two different techniques used to obtain the two different polymorphic forms may have an influence in particle properties. This may suggest the need for further investigation to fully understand the optimal concentration and temperature conditions for the polymer-curcumin interaction. Such findings pave the way for future experimentation to enhance both the process and overall performance.

4.2.5 Contact angle measurements

The contact angle measurement was conducted to understand the wettability of the crystals by liquids. This property was considered because Pickering emulsions have a long-term stability influenced by particles wettability. The stability of the emulsion is increased by strong adsorption of particles with the right wettability at the interface, which prevents coalescence of drops.

For each sample, the visually most homogeneous side of the powder disk was selected to proceed with the contact angle measurement. Measurements were conducted testing both MCT oil and water.

Table 4.4: Mean contact angle and standard deviation of curcumin powders. The following values refers to the measurements conduced with water.

	Polymorph	**Amount of polymer (%)**	**Mean contact angle (°)**	**SD (°)**
COOL_CUR_2	FORM I	0	99.7	4.9
COOL_CMC	FORM I	0.05	104.2	3.5
COOL_KCAR	FORM I	0.05	107.8	1.6
ANTISOLV_3	FORM III	0	79.8	3.3
ANTISOL_005CMC	FORM III	0.05	97.4	6.5
ANTISOL_005KCAR	FORM III	0.05	101.7	2.3
ANTISOL_01CMC	FORM III	0.1	95.3	10.6
ANTISOL_01KCAR	FORM III	0.1	90.4	3.7

Table 4.4 shows the mean contact angle values and corresponding standard deviation measured for the various samples obtained. In most cases, water contact angles exceed 90°, indicating that the particles tend to favour the oil phase. This may lead to less efficient stabilization, as particles will not position themselves optimally at the interface, remaining dispersed in the continuous phase of the W/O emulsion. The results demonstrate that contact angles are higher for samples produced in the presence of polymers. In the case of form I with 0.05% CMC, the contact angle increased from 99.7° to 104.2°, suggesting a slightly more hydrophobic surface and a greater affinity for the oil phase. This could make these particles more effective in stabilizing water-in-oil (W/O) emulsions, where the aqueous phase is dispersed within the oil phase. A similar behaviour is observed in the presence of k-carrageenan (107.8°), the highest value recorded for form I.

For form III, a similar trend is observed. While the addition of polymers does not cause drastic variations in contact angle, the hydrophobicity slightly increases with k-carrageenan and CMC. This is evident from the values recorded for 0.05% CMC (97.4°) and 0.05% k-carrageenan (101.7°). Interestingly, increasing the polymer concentration to 0.1% results in more variable angles, as seen with 0.1% CMC (95.3°) and 0.1% k-carrageenan (90.4°). This variability at higher polymer concentrations may stem from uneven polymer distribution on the crystal surfaces or particle aggregation during crystallization, which could alter the consistency of surface properties. Nevertheless, the predominantly hydrophobic nature of curcumin particles is confirmed, as indicated by contact angle values consistently above 90°. These results align with the expectation [11] that curcumin-based particles are more suited for stabilizing W/O emulsions than O/W emulsions, given their tendency to favour the oil phase at the interface.

4.3 Emulsions production and characterization

Given the results of the contact angle measurements, it was decided to proceed by preparing water-in-oil emulsions with a constant amount of curcumin crystals (20 mg) from experiments COOL_CUR_2, ANTISOLV_1, ANTISOLV_3, and ANTISOLV_01CMC. These polymorphs were selected to investigate the dependence of the stabilising action on the size and shape of the solid particles and to assess the stabilising effect of a polymorph obtained in the presence of a polymer. Water-in-oil emulsions with varying percentages of water were prepared and sampled. The different samples were observed under an optical microscope, and the images deemed most representative of the systems were selected. The visible water droplets in the images were then manually identified and outlined to perform the droplet size distribution analysis. Graphs were generated to depict the relative frequency with which droplets appeared at specific sizes. This analysis aimed to assess the size of water droplets in the dispersed phase, as droplet size can influence the positioning of solid particles at the phase interface and, consequently, the stability of the system.

In Figure 4.50, representative pictures obtained from emulsion obtained using particles from ANTISOLV_3 experiments are shown. The increase in water droplet size with rising water content in the emulsion is clearly visible. Even in the transition from 5%wt to 10%wt of water content, the droplets appear larger and fewer in number. In general, this behaviour indicates reduced stability of the emulsion. The samples were named as reported in Table 3.10.

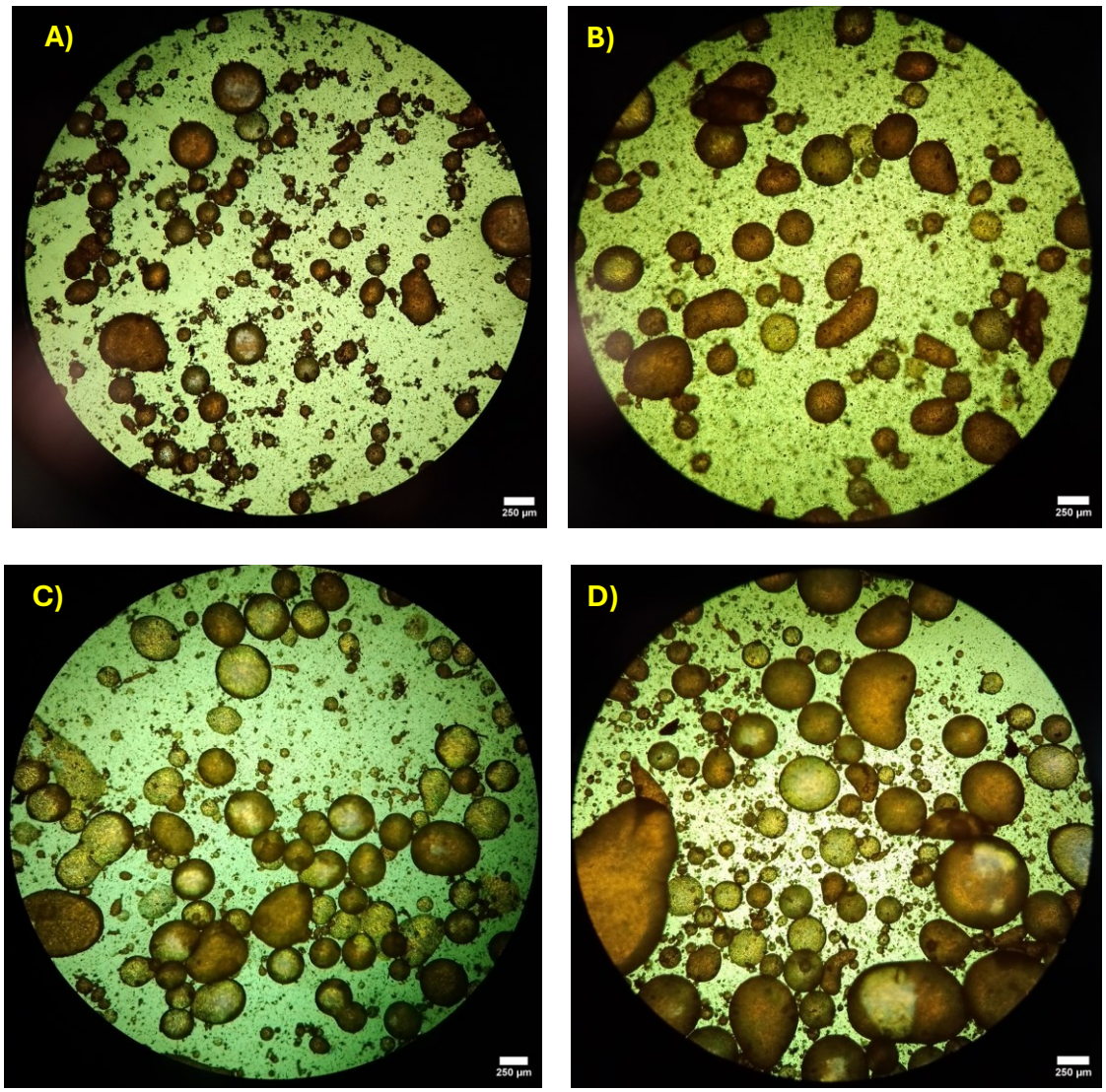

Figure 4.50: Water-in-oil emulsions with different percentage of water: A) 5% water B) 10% water C) 15% water D) 20% water stabilized with ANTISOLV_3

Figures 4.51, 4.52, 4.53, and 4.54 compare the three emulsion samples, each stabilised with different particles containing the same amount of water.

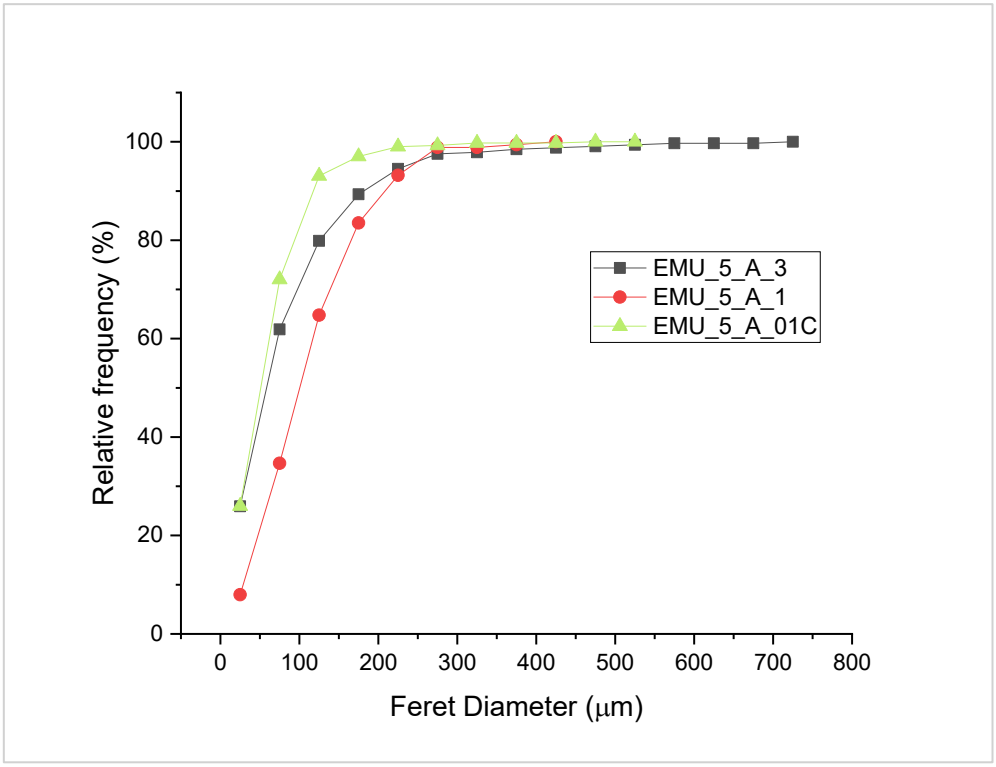

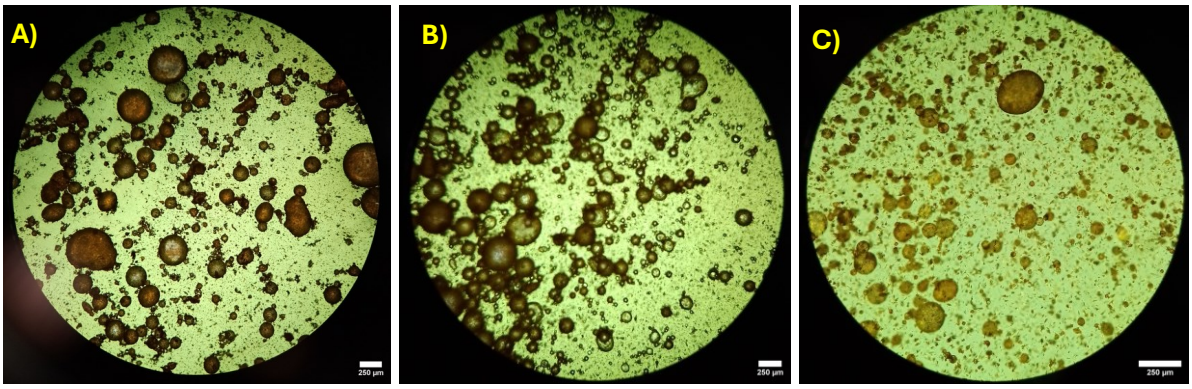

Figure 4.51: Droplet size distribution represented as cumulative frequency, expressed in percentage of droplets over the total number in emulsions with 5% of water. EMU_5_A_3 (black), EMU_5_A_1 (red), EMU_5_A_01C (blue) Images: A) EMU_5_A_3; B) EMU_5_A_1; C) EMU_5_A_01C

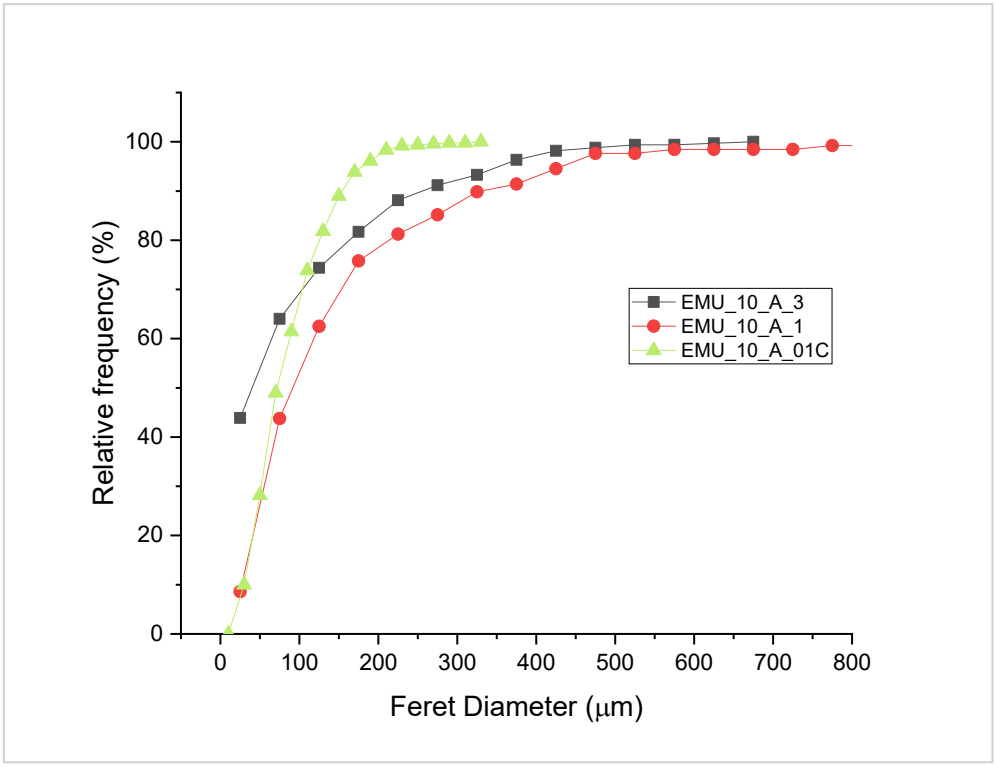

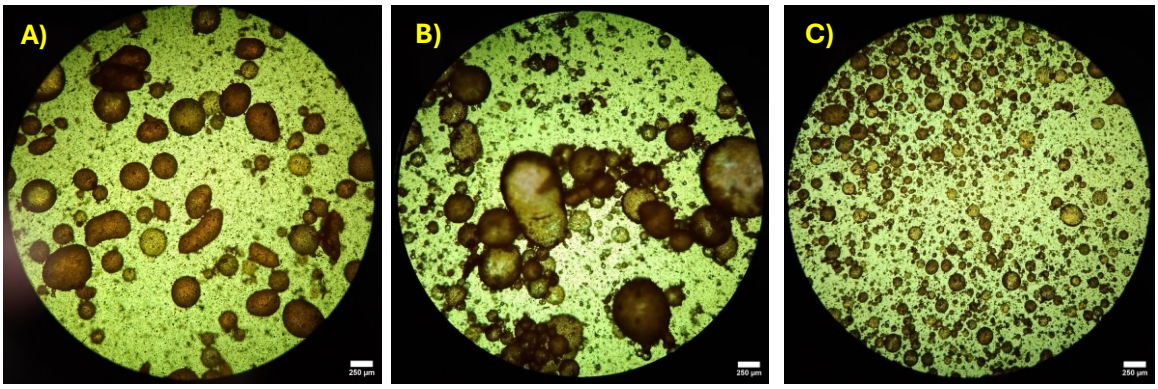

Figure 4.52: Droplet size distribution represented as cumulative frequency, expressed in percentage of droplets over the total number in emulsions with 10% of water. EMU_10_A_3 (black), EMU_10_A_1 (red), EMU_10_A_01C (blue) Images: A) EMU_10_A_3; B) EMU_10_A_1; C) EMU_10_A_01C

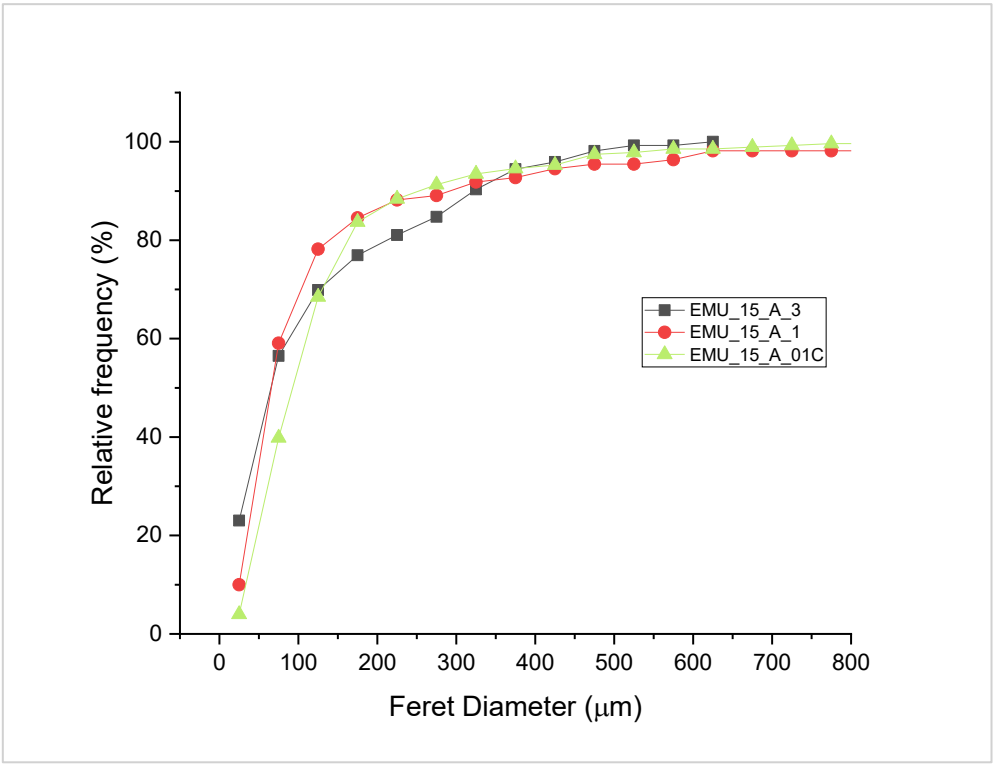

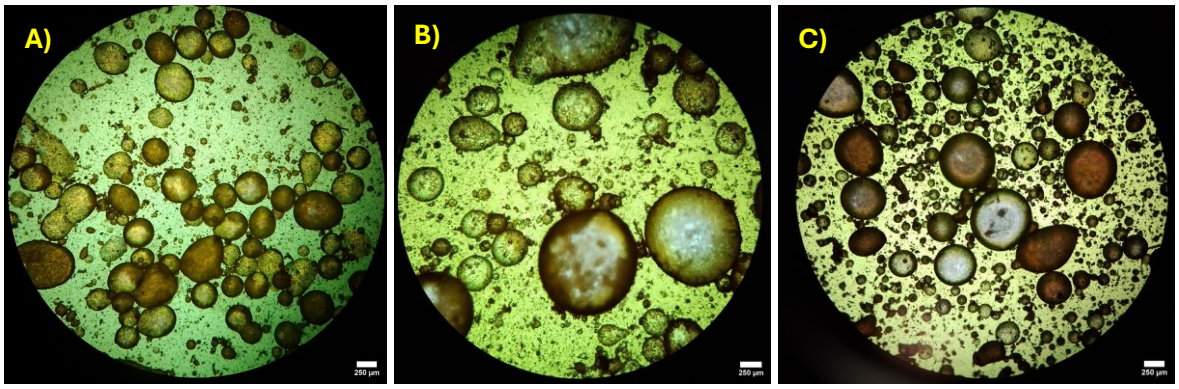

Figure 4.53: Droplet size distribution represented as cumulative frequency, expressed in percentage of droplets over the total number in emulsions with 15% of water. EMU_15_A_3 (black), EMU_15_A_1 (red), EMU_15_A_01C (blue) Images: A) EMU_15_A_3; B) EMU_15_A_1; C) EMU_15_A_01C

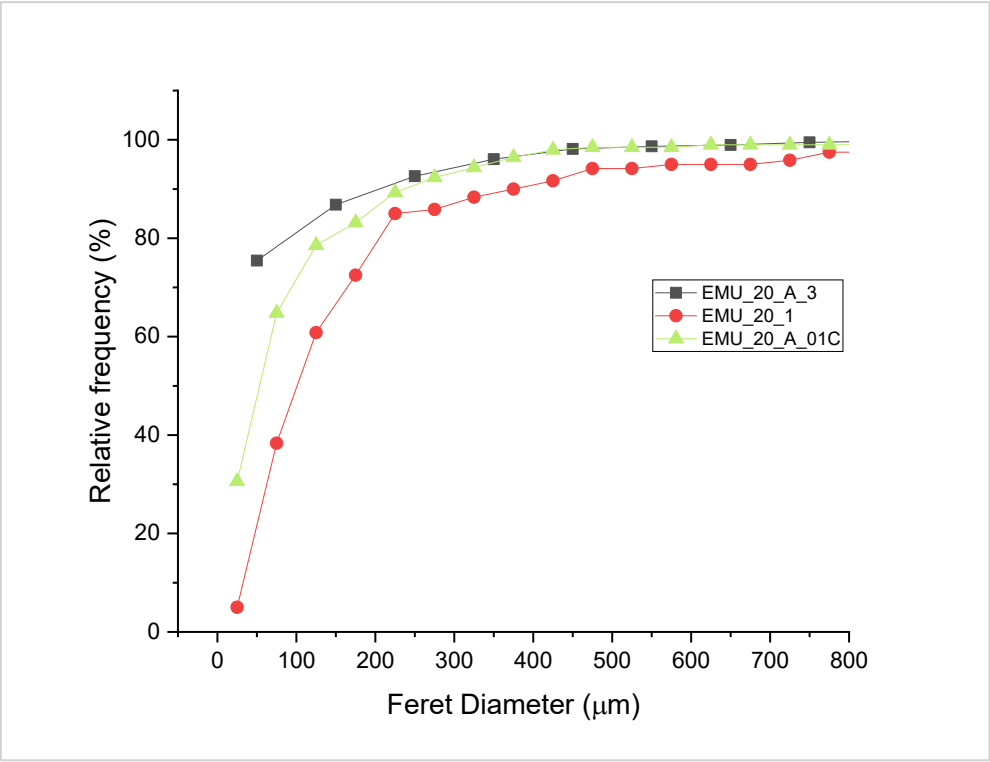

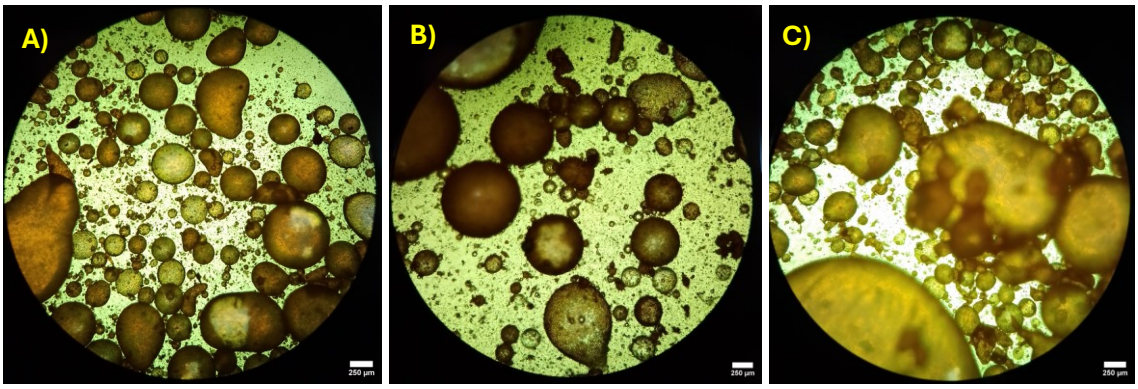

Figure 4.54: Droplet size distribution represented as cumulative frequency, expressed in percentage of droplets over the total number in emulsions with 20% of water. EMU_20_A_3 (black), EMU_20_A_1 (red), EMU_20_A_01C (blue) Images: A) EMU_20_A_3; B) EMU_20_A_1; C) EMU_20_A_01C

The rapid increase in relative frequency of droplet diameter for each sample, followed by the attainment of a plateau, indicates that most droplets are of a similar size, concentrated within a relatively narrow diameter range. As the water content in the emulsion increases (from 5% to 20%), the droplet size distribution changes across the samples, with noticeable differences in average droplet size and distribution uniformity. Generally, as the water content in the emulsion rises, droplet size increases for all samples, likely due to a higher probability of coalescence with more water present. Notably, EMU_5_A_3, EMU_10_A_3, EMU_15_A_3, and EMU_20_A_3 stabilised with particles from ANTISOLV_3 consistently show the most

uniform size distribution and a tendency to maintain smaller droplet sizes even as the water content increases, suggesting that the solid particles in this sample are more effective at preventing droplet coalescence. In contrast, EMU_5_A_1, EMU_10_A_1, EMU_15_A_1 and EMU_20_A_1, prepared with ANTISOLV_1 batch, display intermediate droplet size distributions, with greater variability and larger average sizes as water content increases. The lower effectiveness of ANTISOLV_1 particles could be linked to their larger dimensions and lower uniformity, which reduce their ability to stabilise the interface effectively. Overall, EMU_5_A_01C, EMU_10_A_01C, EMU_15_A_01C and EMU_20_A_01C prepared with ANTISOLV_01CMC particles appear to be the most effective at stabilising droplets in the emulsion, maintaining a more uniform size distribution and limiting droplet growth as water content increases, even at higher concentrations. This suggests that the presence of CMC during crystallisation enhances the stabilising efficiency of form III particles, likely by promoting more consistent particle morphology and size. For a more accurate analysis, the average Feret diameter and the corresponding standard deviation were calculated for all emulsions (Table 4.5). These values confirm the trends observed in the visual analysis, with the smallest average droplet sizes and standard deviations consistently observed for samples stabilised with ANTISOLV_01CMC particles.

Table 4.5: Mean Feret diameter and SD of droplets in emulsions with different percentage of water (from 5 to 20%) and containing different curcumin polymorph.

Percentage of water in emulsion (%)	Name of sample	Particle batch	Mean Feret diameter (µm)	SD (µm)
5	EMU_5_A_3	ANTISOLV_3	104.76	86.16
	EMU_5_A_1	ANTISOLV_1	134.16	69.79
	EMU_5_A_01C	ANTISOLV_01CMC	83.15	48.92
10	EMU_10_A_3	ANTISOLV_3	138.00	133.19
	EMU_10_A_1	ANTISOLV_1	165.58	155.66
	EMU_10_A_01C	ANTISOLV_01CMC	94.42	49.81
15	EMU_15_A_3	ANTISOLV_3	141.22	129.79
	EMU_15_A_1	ANTISOLV_1	147.73	187.93
	EMU_15_A_01C	ANTISOLV_01CMC	150.47	120.59
20	EMU_20_A_3	ANTISOLV_3	103.48	124.28
	EMU_20_A_1	ANTISOLV_1	187.66	192.92
	EMU_20_A_01C	ANTISOLV_01CMC	118.77	133.16

Upon examining the various samples under the microscope, it was observed that the solid particles tend to position themselves at the interface between the phases. In cases with a lower water content, however, the crystals remain partially dispersed within the continuous phase (see Figures 4.50). Upon observing two samples (Figure 4.55), it was found that, despite the particle distribution at the interface, the system is not stable, even in the case with the lowest water percentage, as the two phases tend to separate after a short period.

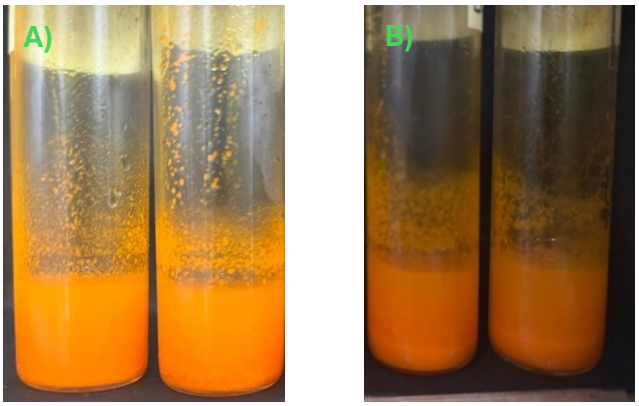

Figure 4.55: Water-in-oil emulsions of experiment: (on right) A) EMU_10_A_01C and EMU_10_A_3 just made; on left B) EMU_10_A_01C and EMU_10_A_3 after thirty minutes

With form I, since the crystals are considerably larger than those of form III, experiments were conducted using emulsions with 10% water, and the operational conditions were subsequently adjusted (see Table 3.9 in *Chapter 3*).

Microscopic analysis of the samples (Figures 4.56) revealed that crystals adsorbed at the interface between the phases, forming crystal network-like structures that caused the droplets of the dispersed phase to aggregate. In this case, the crystals are significantly larger than the water droplets, leading to the formation of crystal clusters that are unevenly distributed (Figure 4.56). This clearly demonstrates that stability was not achieved in this case, and that the size of the crystals has a notable impact on their behaviour within the emulsion.

The results confirm the tendency of curcumin particles to act as stabilisers for water-in-oil (W/O) Pickering emulsions. Analysis of various parameters, including particle size distribution, morphology, contact angles, and emulsion stability demonstrates that form I crystals obtained can’t stabilize the emulsions due to their big size. Both polymorphs exhibit stabilising properties; however, the long-term stability and resistance to coalescence are more pronounced with form III, probably due to the reduced size of the particles. These findings support the initial

hypothesis that selective crystallisation of curcumin can enhance its interfacial properties, establishing it as a viable alternative to traditional surfactants for stabilisation purposes.

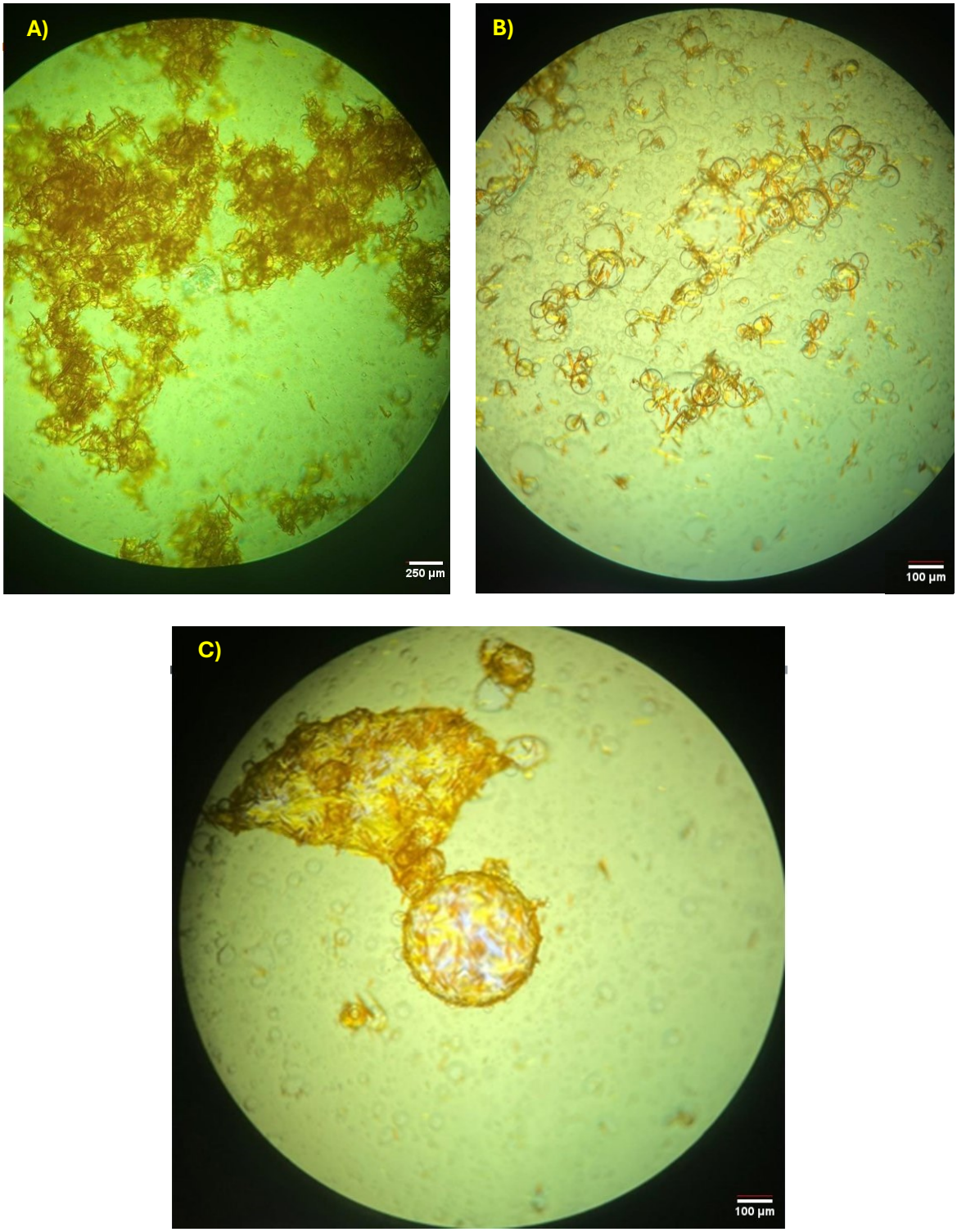

Figure 4.56: Water-in-oil emulsions of experiment: A) EMU_10_C_1; B) EMU_10_C_2; C) EMU_10_C_3

5. Conclusions and future development

The objective of this study was to apply a crystal engineering approach to produce different curcumin polymorphs, subsequently testing them as natural stabilisers in Pickering emulsions. The polymorphic form influence properties of the solid particles, such as size, shape, and wettability, which influence their stabilising effectiveness. In this study was investigate the stabilizing action of curcumin form I and III. Firstly, curcumin's solubility in water/ethanol mixtures was assessed, and the solubility curves obtained through polynomial interpolation and a Van't Hoff equation showed a determination coefficient R^2 close to unity, confirming both the reliability of the experimental data and its good fit with Van't Hoff's law. The solubility of curcumin in solutions with different pH levels was also evaluated to explore its potential for use as a modified-release drug delivery vehicle. As expected, curcumin showed a preference for alkaline environments over acidic ones, achieving partial solubilisation only when reaching temperatures near body temperature. The two crystallisation techniques selected, cooling and antisolvent, successfully yielded the desired polymorphs, though with distinct particle sizes. Both form I and form III exhibited elongated shapes and uniform size distributions. Form I reached an average size of 60 μm, while form III averaged approximately 2 μm. Additionally, the effect of polymers (carboxymethylcellulose and k-carrageenan) in solution during crystallisation was tested to determine their influence on the surface properties of the crystals. It was found that the presence of polymer, regardless of its percentage in solution (0.05 or 0.1%wt), does not determine evident changes in the size, shape or polymorphism of the curcumin crystals. For the characterization of polymorphs various analyses were conducted, including Raman spectroscopy and powder X-ray diffraction (PXRD) that confirmed the successful production of the targeted polymorphs. Thermal analyses of the crystals produced indicated that the presence of CMC and k-carrageenan had no significant impact on the thermal properties of the crystals; in fact, the melting point did not change. However, the minimal influence observed from polymers raises questions about their potential role in curcumin thermal properties, which may not be detectable via thermal analysis alone. Crystal shape and size was found to depend directly on the crystallisation process conditions. The form III obtained with the higher solvent-antisolvent ratio (1:2.5 ethanol/water by weight) is quite the double size of the same polymorph obtained with the lower ratio (1:5 ethanol/water by weight). The contact angle measurements confirmed the hydrophobic nature of curcumin, with angles consistently above 90°, regardless of the polymorph obtained. The effect of polymer presence

during crystallization was observed only in these measurements, where the addition of polymers increased the contact angle beyond 90°, promoting the positioning of the particles at the phase interface and improving system stability. This was particularly evident for Form I with 0.05% CMC, where the contact angle increased from 99.7° to 104.2°, suggesting a greater affinity for the oil phase and potentially greater effectiveness in stabilizing water-in-oil (W/O) emulsions. The stabilising action of the polymorphs in emulsion was evaluated based on particle and droplets size distribution. Results indicated that crystals with sizes comparable to the droplets (form III) positioned themselves at the water-oil interface, increasing system stability, although this arrangement was not stable in the long term. In contrast, larger crystals (form I) tended to form clusters in the continuous phase or create a network of particles that altered the size distribution of dispersed phase droplets. However, for both form I and form III, lasting stability in emulsion was not definitively achieved.

Future work could focus on modifying the crystallisation conditions tested in this study to obtain comparable size & shape crystals of both polymorphs and explore alternative crystallization techniques. Additional studies might investigate other polymers in solution, with variations in concentration, to better understand their potential impact on surface properties and interactions not detectable through thermal analysis. Moreover, it could be valuable to explore advanced surface characterisation techniques, such as X-ray Photoelectron Spectroscopy (XPS), to elucidate subtle changes induced by polymers. [68] Further experiments could also examine the production and characterisation of different curcumin crystals forms, such as co-crystals or other polymorphs to use as Pickering stabilisers. Further studies on the relationship between particle size, surface properties (such as wettability and roughness), and stabilising performance in emulsions under conditions relevant to specific applications (like pharmaceutical or food industry) could provide valuable insights for optimising these systems for industrial use.

Appendix A

Particle Size Distribution graphs

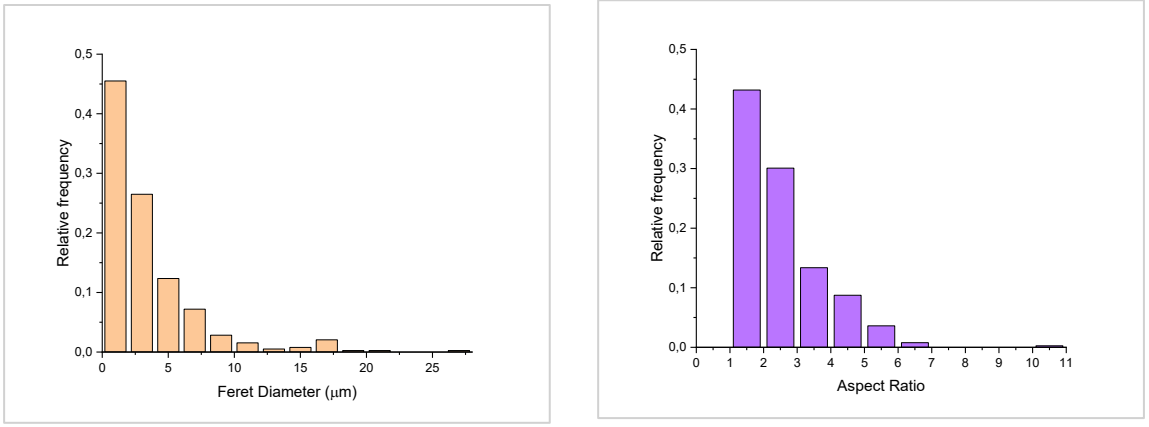

Figure A.1: PSD (on left) and AR distribution (on right) of curcumin crystals from Experiment ANTISOLV_2

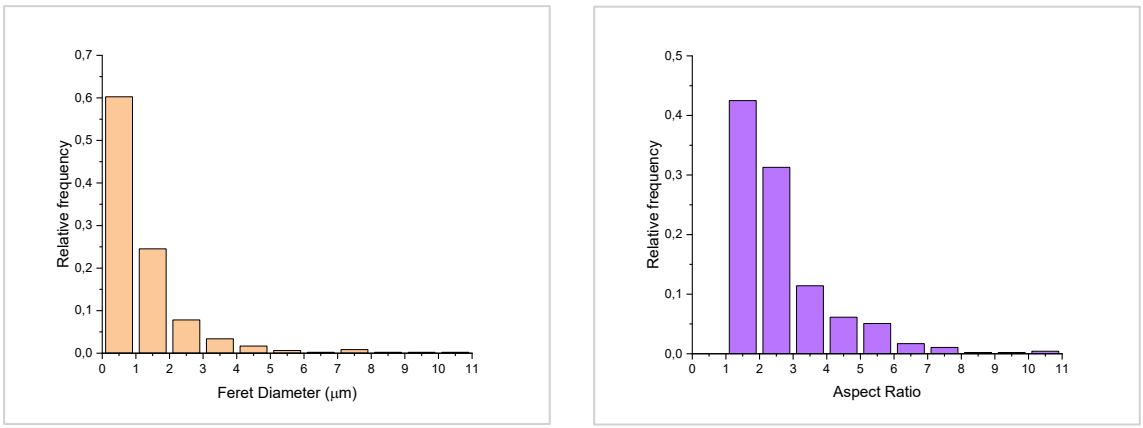

Figure A.2: PSD (on left) and AR distribution (on right) of curcumin crystals from Experiment ANTISOLV_4

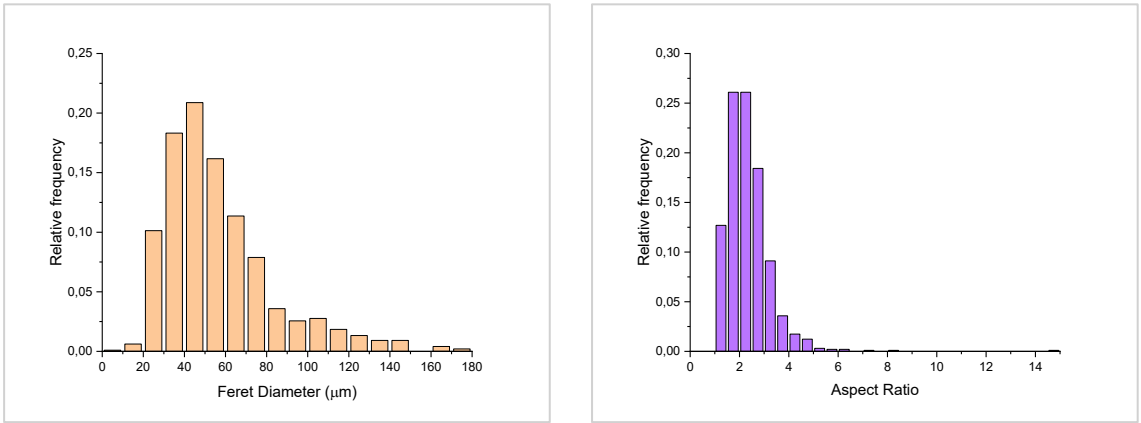

Figure A.3: PSD (on left) and AR distribution (on right) of curcumin crystals from Experiment COOL_CMC

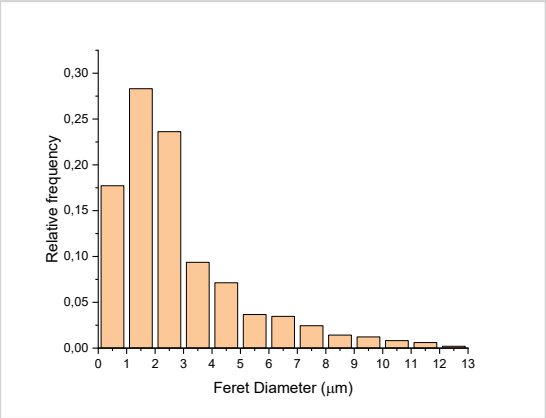

Figure A.4: PSD (on left) and AR distribution (on right) of curcumin crystals from Experiment ANTISOLV_005CMC

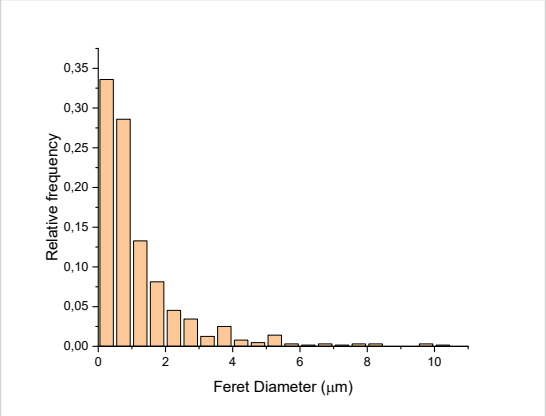

Figure A.5: PSD (on left) and AR distribution (on right) of curcumin crystals from Experiment ANTISOLV_01KCAR

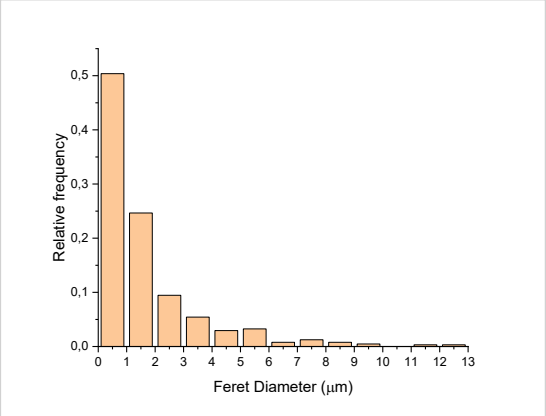

Figure A.6: PSD (on left) and AR distribution (on right) of curcumin crystals from Experiment ANTISOLV_005KCAR

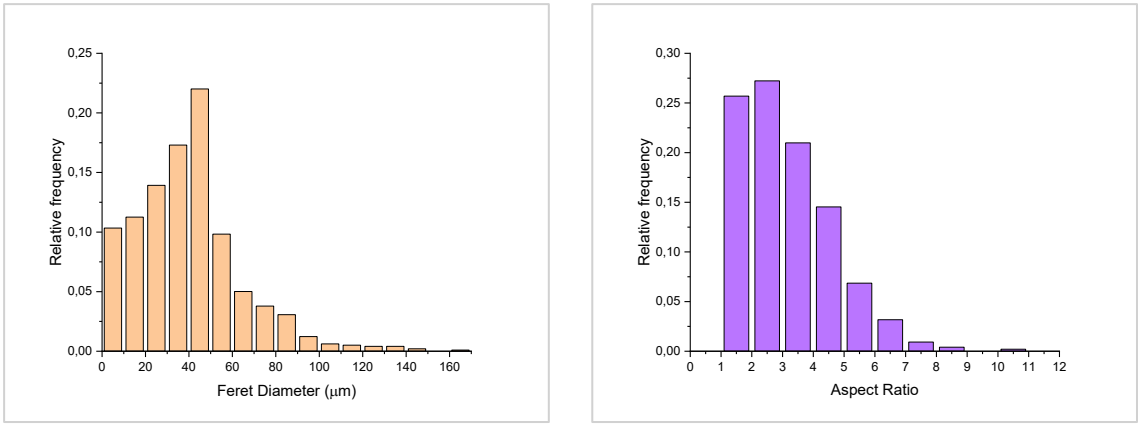

Figure A.7: PSD (on left) and AR distribution (on right) of curcumin crystals from Experiment COOL_KCAR

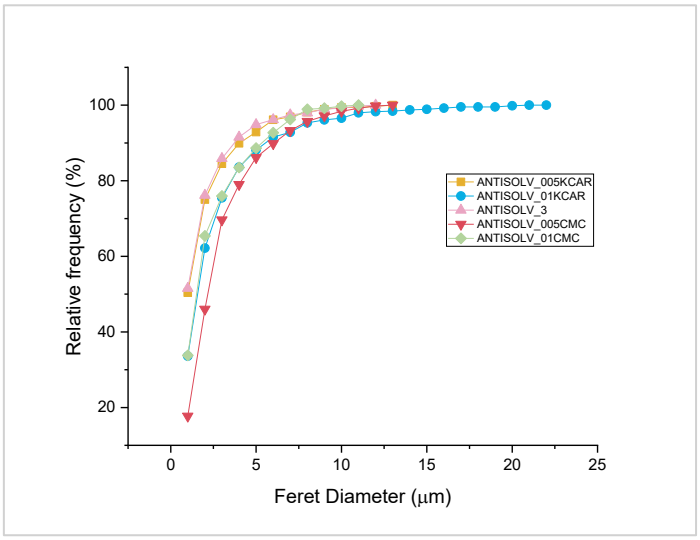

Figure A.8: Particle size distribution represented as cumulative frequency, expressed in percentage of particles over the total number (experiments ANTISOLV_3 (pink), ANTISOLV_005CMC (red), ANTISOLV_005KCAR (orange), ANTISOLV_01CMC (green) , ANTISOLV_01KCAR (blue))

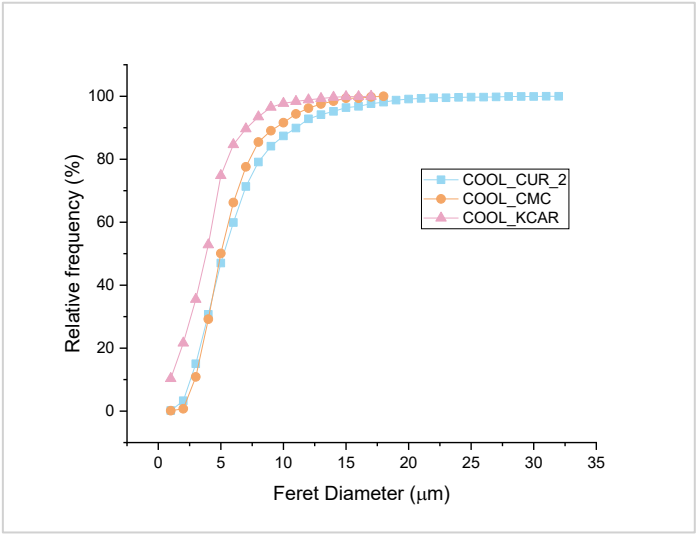

Figure A.9: Particle size distribution represented as cumulative frequency, expressed in percentage of particles over the total number (experiments COOL_CUR_2 (blue), COOL_CMC (orange), COOL_KCAR (pink))

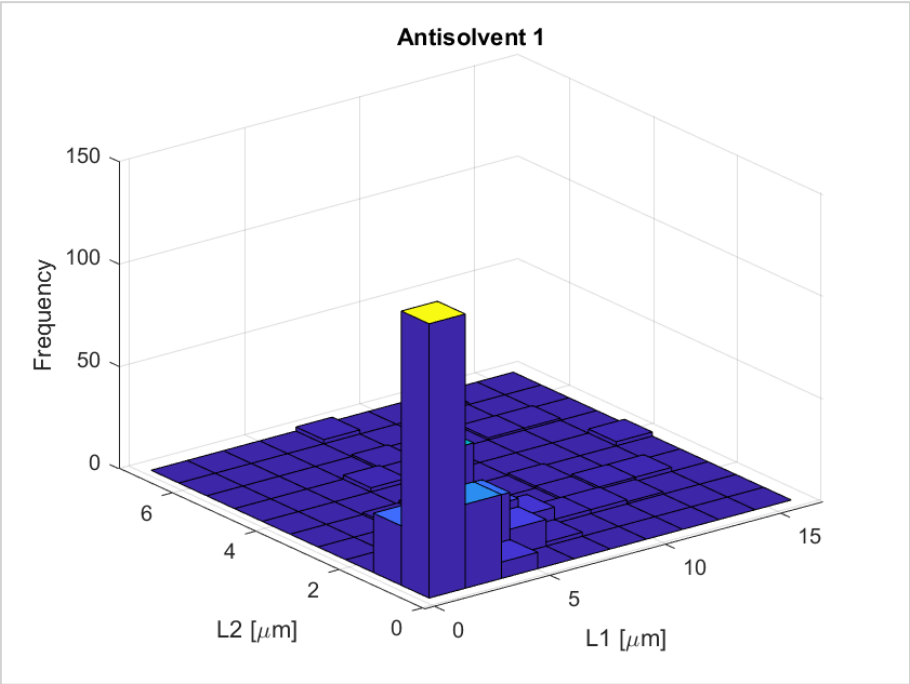

Figure A.10: Three-dimensional distribution of dimensions considering major side (L1) and minor side (L2) of Form III obtained by antisolvent (experiment ANTISOLV_1)

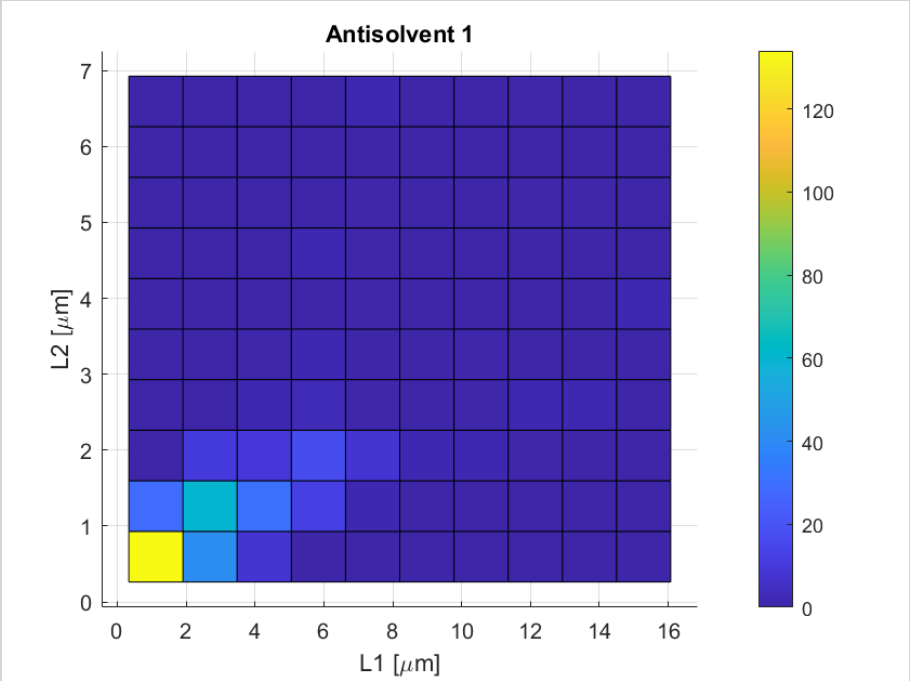

Figure A.11: Bidimensional distribution of dimensions considering major side (L1) and minor side (L2) of Form III obtained by antisolvent (experiment ANTISOLV_1)

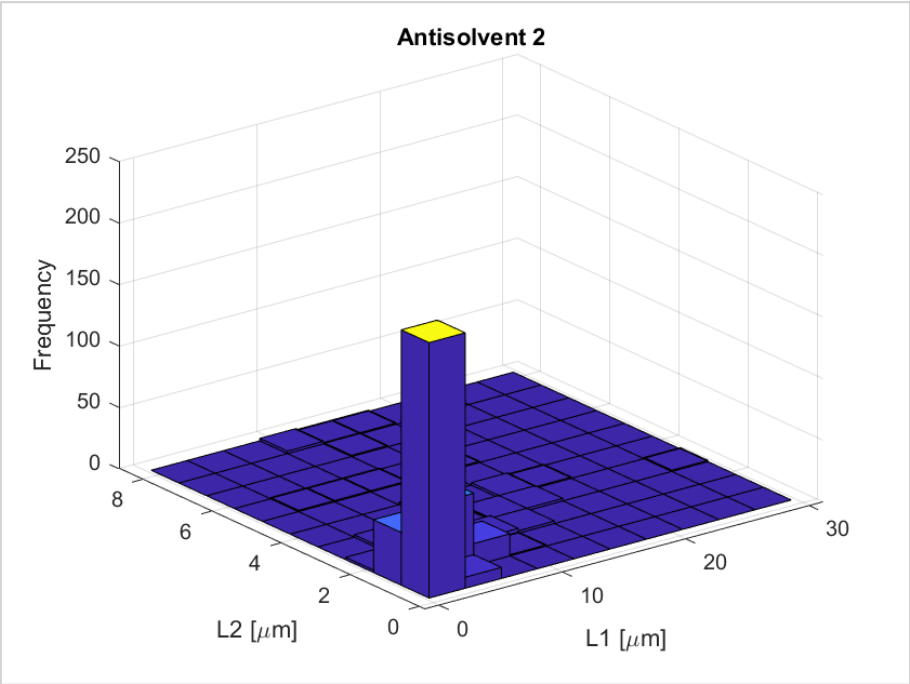

Figure A.12: Three-dimensional distribution of dimensions considering major side (L1) and minor side (L2) of Form III obtained by antisolvent (experiment ANTISOLV_2)

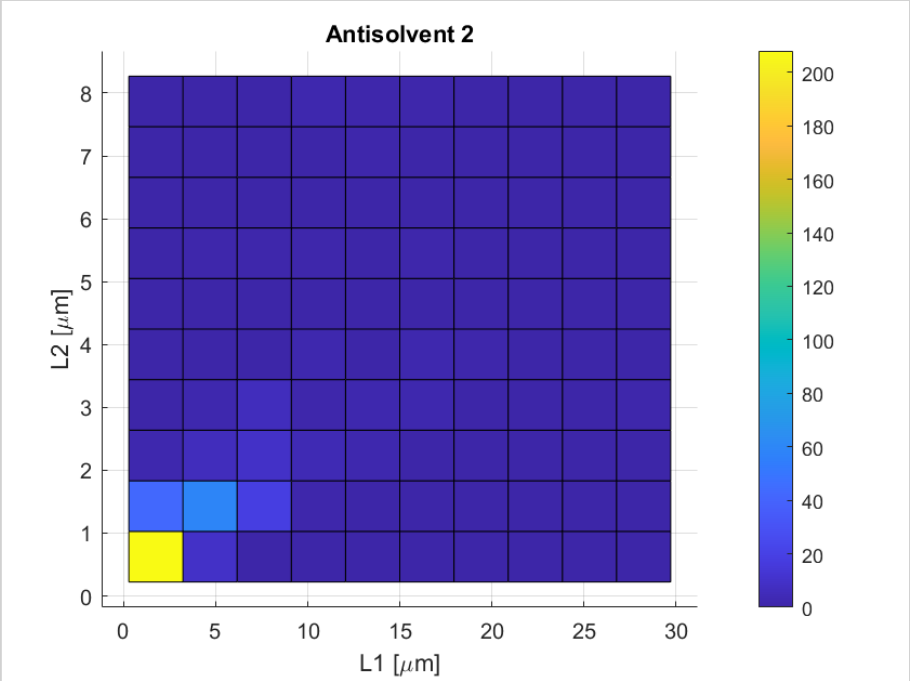

Figure A.13: Bidimensional distribution of dimensions considering major side (L1) and minor side (L2) of Form III obtained by antisolvent (experiment ANTISOLV_2)

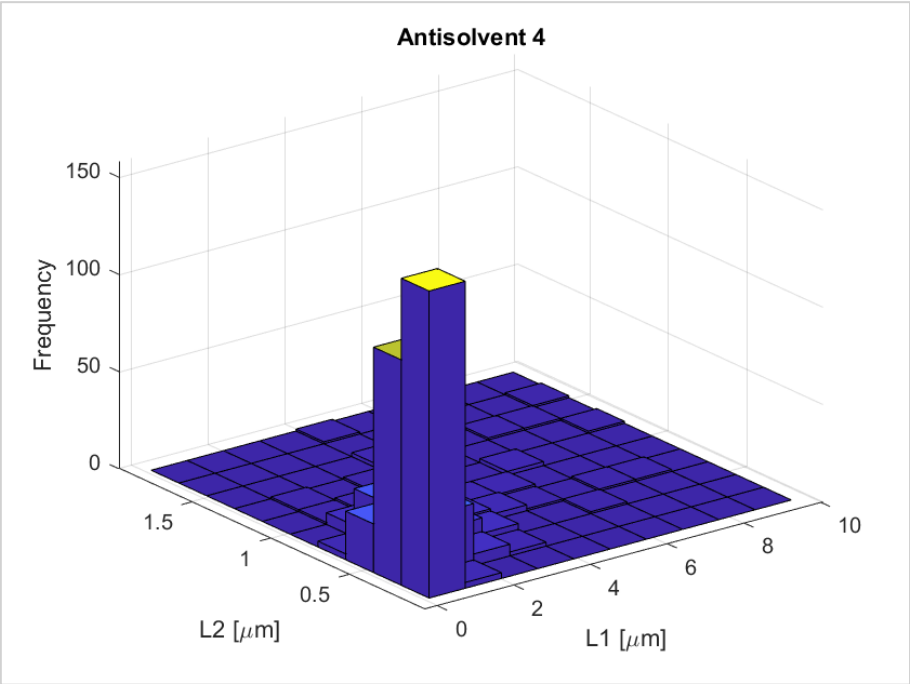

Figure A.14: Three-dimensional distribution of dimensions considering major side (L1) and minor side (L2) of Form III obtained by antisolvent (experiment ANTISOLV_4)

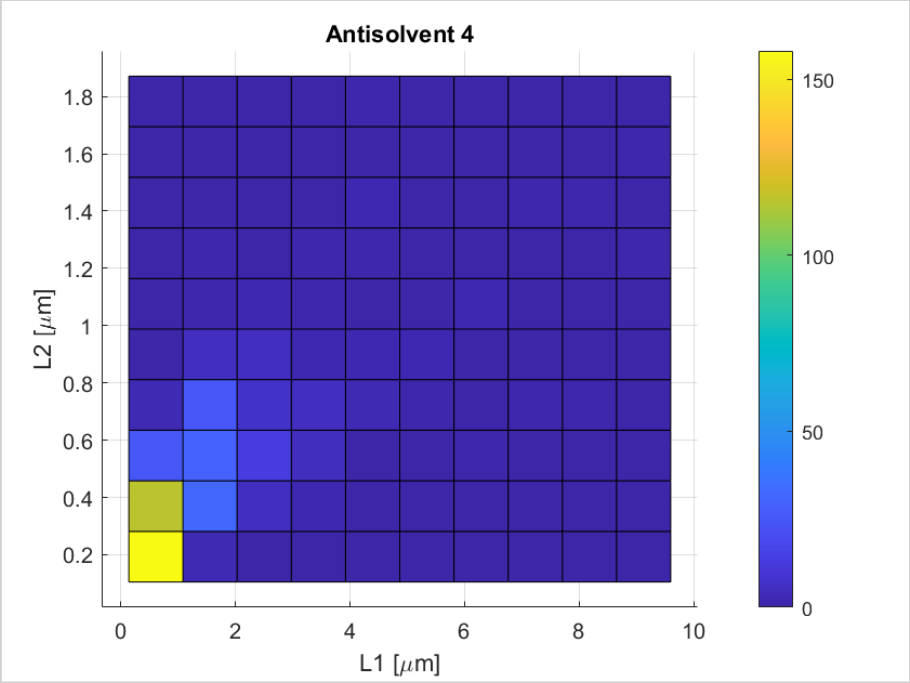

Figure A.15: Bidimensional distribution of dimensions considering major side (L1) and minor side (L2) of Form III obtained by antisolvent (experiment ANTISOLV_4)

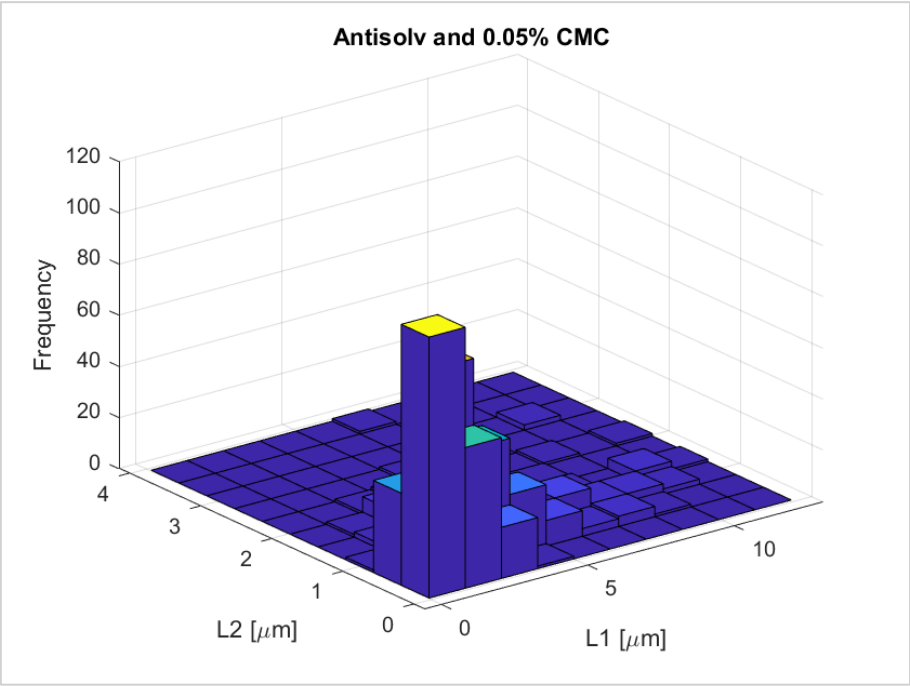

Figure A.16: Three-dimensional distribution of dimensions considering major side (L1) and minor side (L2) of Form I obtained by antisolvent with 0.05%CMC (experiment ANTISOLV_005CMC)

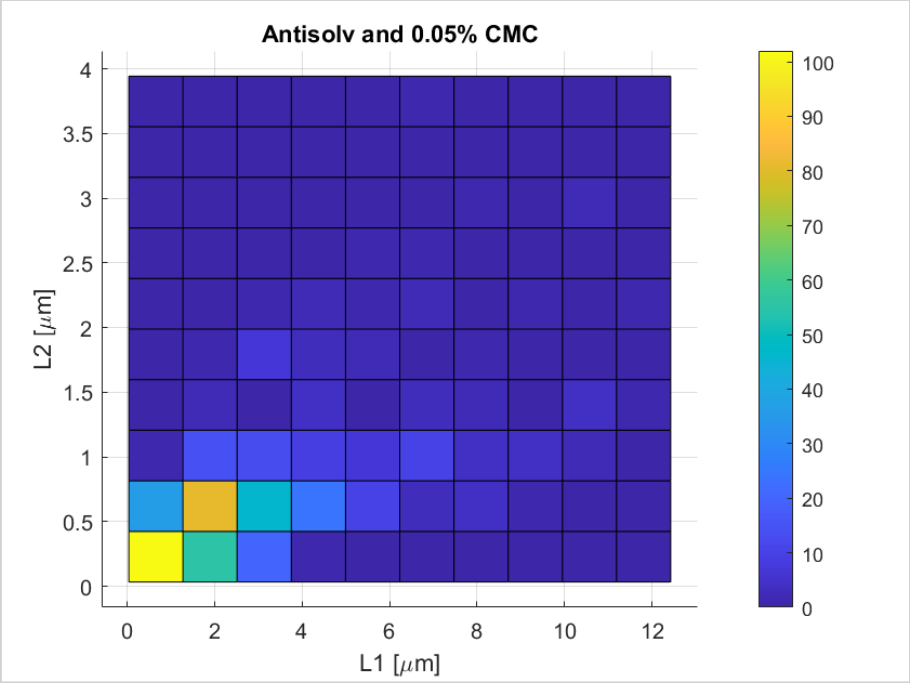

Figure A.17: Bidimensional distribution of dimensions considering major side (L1) and minor side (L2) of Form III obtained by antisolvent with 0.05%CMC (experiment ANTISOLV_005CMC)

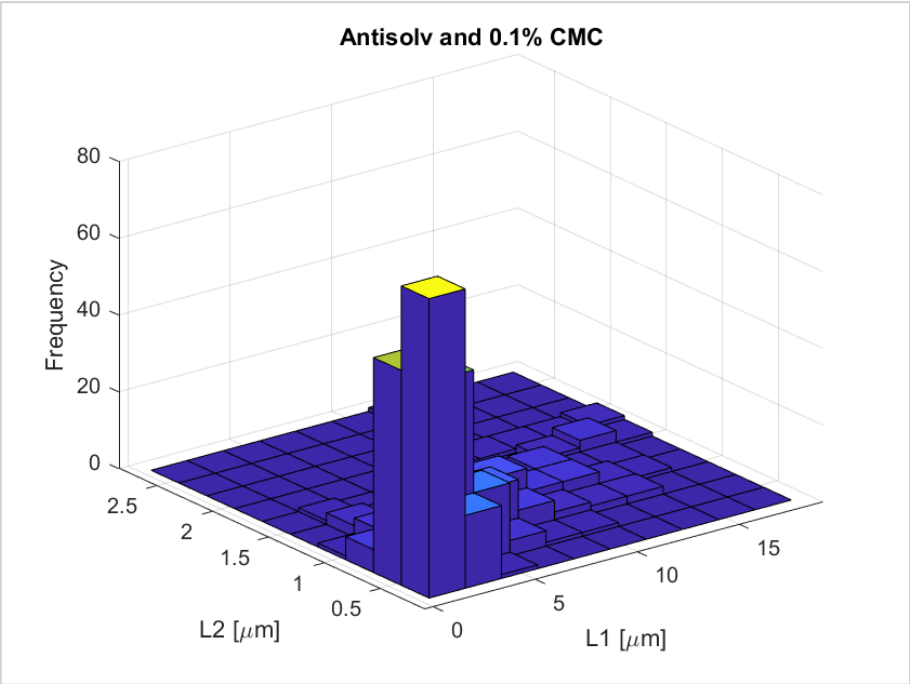

Figure A.18: Three-dimensional distribution of dimensions considering major side (L1) and minor side (L2) of Form III obtained by antisolvent with 0.1%CMC (experiment ANTISOLV_01CMC)

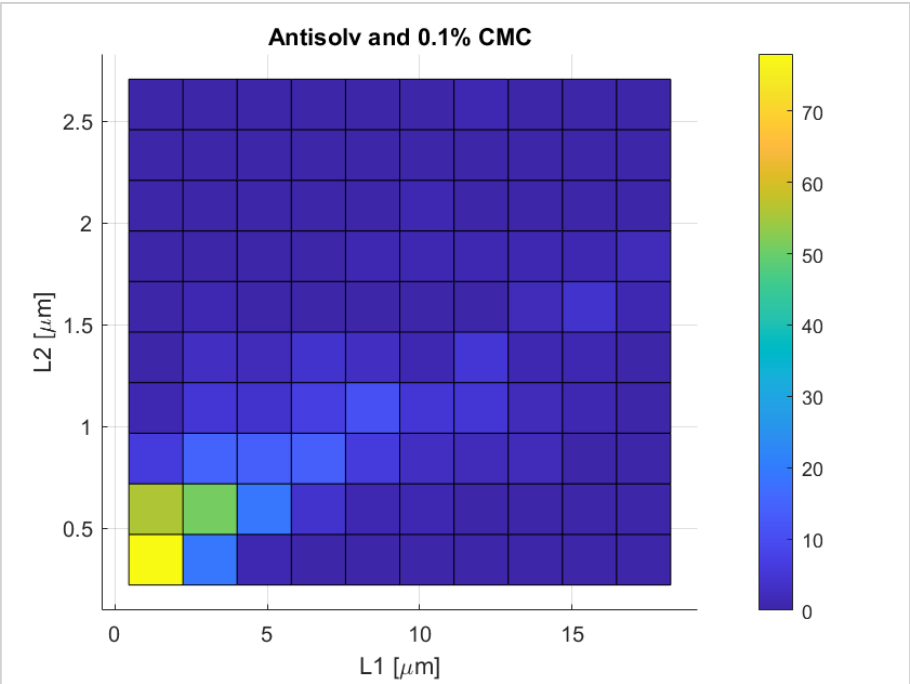

Figure A.19: Bidimensional distribution of dimensions considering major side (L1) and minor side (L2) of Form III obtained by antisolvent with 0.1%CMC (experiment ANTISOLV_01CMC)

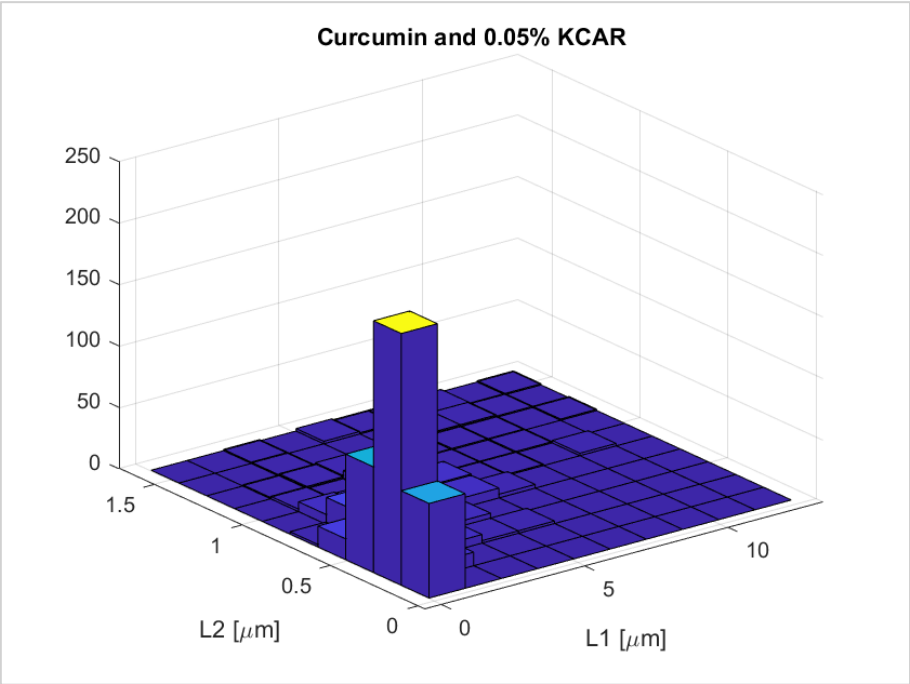

Figure A.20: Three-dimensional distribution of dimensions considering major side (L1) and minor side (L2) of Form III obtained by cooling with 0.05% KCAR (experiment ANTISOLV_005KCAR)

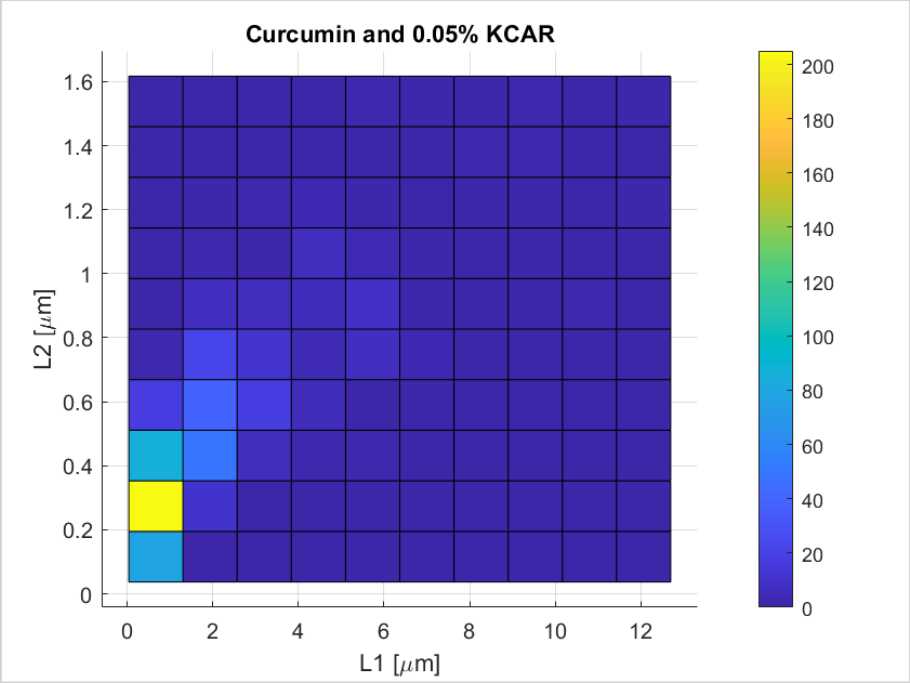

Figure A.21: Bidimensional distribution of dimensions considering major side (L1) and minor side (L2) of Form III obtained by antisolvent with 0.05% KCAR (experiment ANTISOLV_005KCAR)

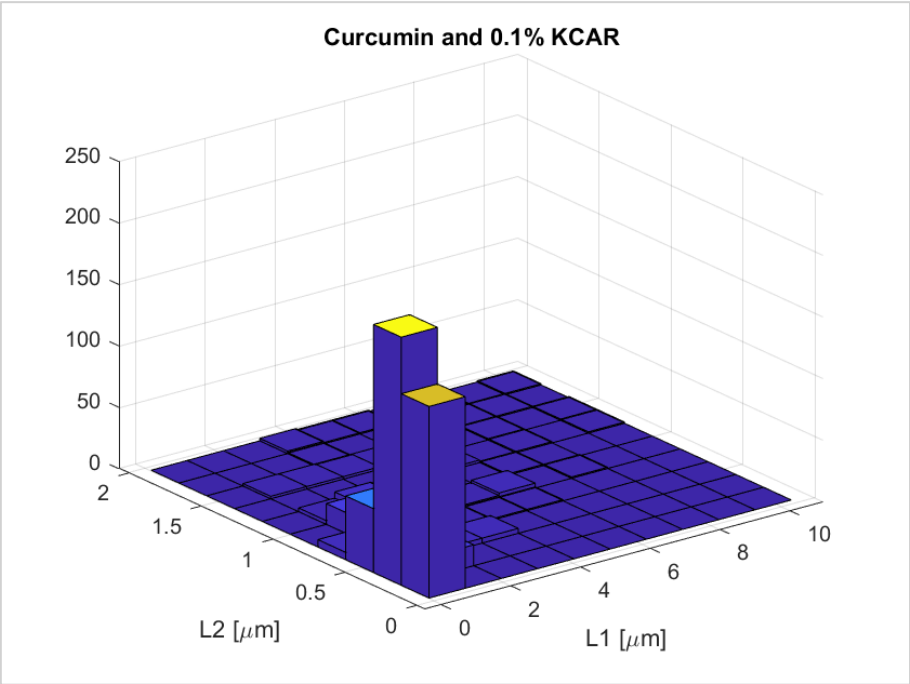

Figure A.22: Three-dimensional distribution of dimensions considering major side (L1) and minor side (L2) of Form III obtained by antisolvent with 0.1% KCAR (experiment ANTISOLV_01KCAR)

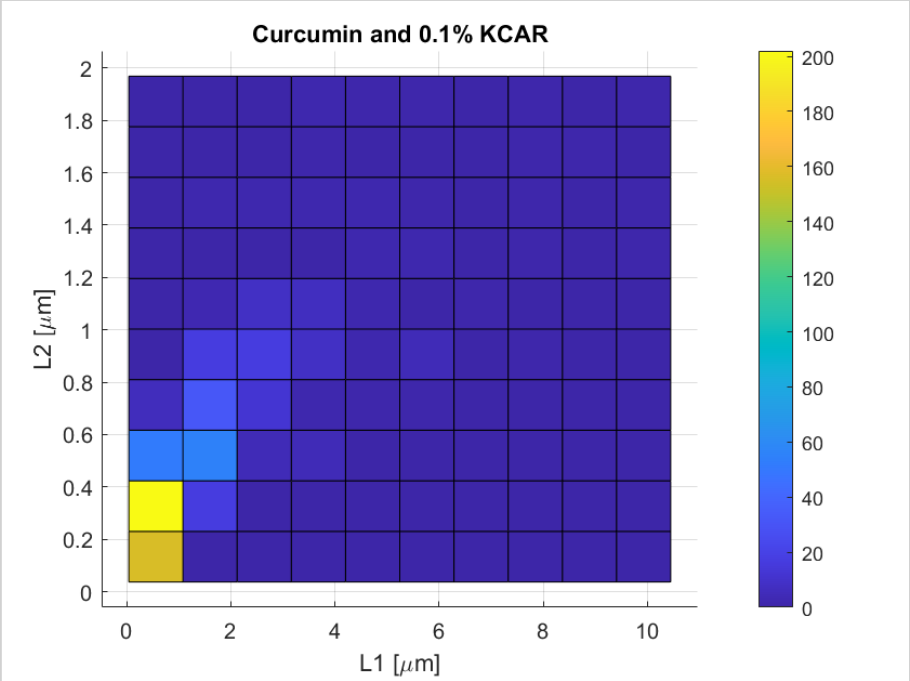

Figure A.23: Bidimensional distribution of dimensions considering major side (L1) and minor side (L2) of Form III obtained by antisolvent with 0.1% KCAR (experiment ANTISOLV_01KCAR)

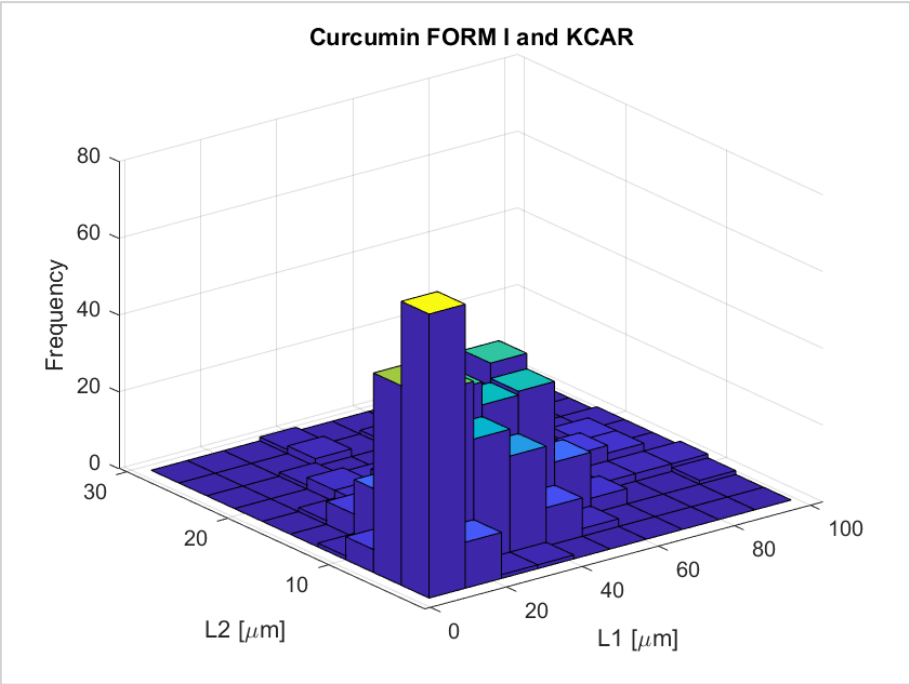

Figure A.24: Three-dimensional distribution of dimensions considering major side (L1) and minor side (L2) of Form I obtained by cooling with KCAR (experiment COOL_KCAR)

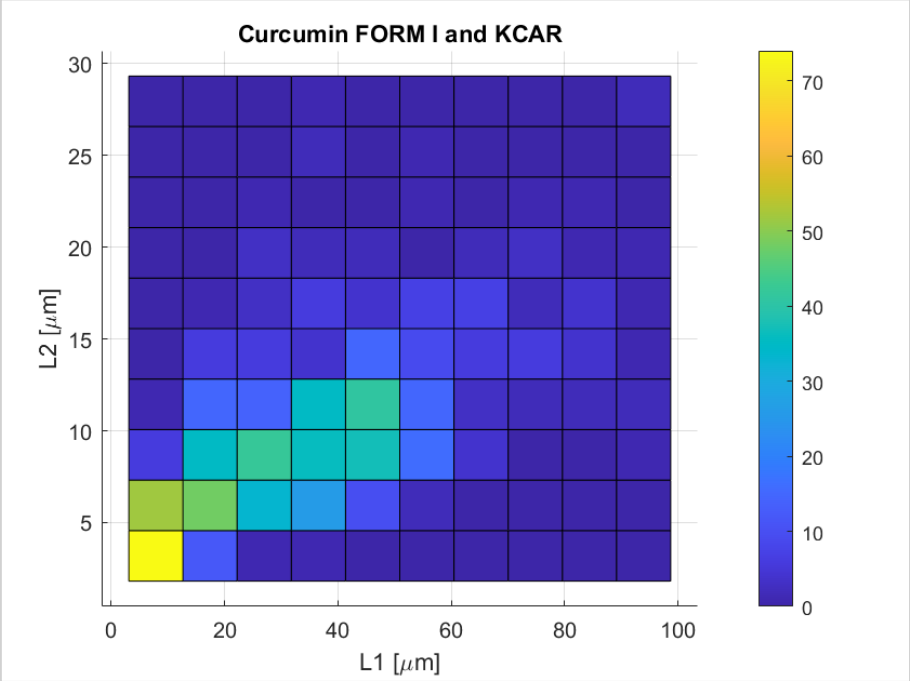

Figure A.25: Bidimensional distribution of dimensions considering major side (L1) and minor side (L2) of Form III obtained by antisolvent with KCAR (experiment COOL_KCAR)

References

[1] M. Destribats, M. Rouvet, C. Gehin-Delval, C. Schmitt, B.P. Binks, Emulsions stabilised by whey protein microgel particles: Towards food-grade Pickering emulsions, Soft Matter. 10 (36) (2014) 6941–6954, https://doi.org/10.1039/C4SM00179F

[2] Bo Pang, Huan Liu, Kai Zhang, Recent progress on Pickering emulsions stabilized by polysaccharides-based micro/nanoparticles, Advances in Colloid and Interface Science, Vol. 296, 2021, 102522, ISSN 0001-8686, https://doi.org/10.1016/j.cis.2021.102522

[3] Liangshan Ming, Hailian Wu, Ao Liu, Abid Naeem, Zishu Dong, Qimeng Fan, Gaochuan Zhang, Hongning Liu, Zhe Li, Evolution and critical roles of particle properties in Pickering emulsion: A review, Journal of Molecular Liquids, Volume 388, 2023, 122775, ISSN 0167-7322, https://doi.org/10.1016/j.molliq.2023.122775

[4] Sharifi-Rad J, Rayess YE, Rizk AA, Sadaka C, Zgheib R, Zam W, Sestito S, Rapposelli S, Neffe-Skocińska K, Zielińska D, Salehi B, Setzer WN, Dosoky NS, Taheri Y, El Beyrouthy M, Martorell M, Ostrander EA, Suleria HAR, Cho WC, Maroyi A, Martins N. Turmeric and Its Major Compound Curcumin on Health: Bioactive Effects and Safety Profiles for Food, Pharmaceutical, Biotechnological and Medicinal Applications. Front Pharmacol. 2020 Sep 15;11:01021. doi: 10.3389/fphar.2020.01021. PMID: 33041781; PMCID: PMC7522354

[5] Zembyla M.; Murray B.S.; Sarkar A.; Water-In-Oil Pickering Emulsions Stabilized by Water Insoluble Polyphenol Crystals; 2018; Langmuir 2018, 34, 34, 10001–10011; DOI: 10.1021/acs.langmuir.8b01438

[6] Sanphui P. and Bolla G.; Curcumin, a Biological Wonder Molecule: A Crystal Engineering Point of View; Cryst. Growth Des. 2018, 18, 5690-5711; DOI: 10.1021/acs.cgd.8b0064

[7] Themed issue: Polymorphism and crystal forms, New J.Chem., 2008, 32, 1657-1658, doi:10.1039/B814474P (Editorial)

[8] Gelardi M, Presidente dell'Accademia Italiana di Rinologia, Policlinico Universitario, Bari, Il danno mucosale nel reflusso laringo faringeo (RLF), MedTOPICS, Periodico Quindicinale, n.14/2017 (https://www.medtopics.it/periodici/articolo.14.2017/index.html)

[9] C.L.G. Harman, M.A. Patel, S. Guldin e G. Davies. «Recent developments in Pickering emulsions for biomedical applications». In: Current opinion in colloid interface science 39 (2019), pp. 173–189 (cit. alle pp. 11, 13–15).

[10] Y. Ming, Y. Xia e G. Ma. «Aggregating particles on the O/W interface: Tuning Pickering emulsion for the enhanced drug delivery systems». In: Aggregate (Hoboken) 3 (2) (2022), n/a (cit. pp. 14, 15)

[11] Giulia Del Duca, Emmanuele Parisi, Fiora Artusio, Eleonora Calì, Silvia Fraterrigo Garofalo, Chiara Rosso, Valentina Cauda, Michele R. Chierotti, Elena Simone, A crystal engineering approach for rational design of curcumin crystals for Pickering stabilization of emulsions, Food Research International, Vol. 194, 2024,114871, ISSN 0963-9969, https://doi.org/10.1016/j.foodres.2024.114871

[12] Giulietti M, Bernardo A, Crystallization by Antisolvent Addition and Cooling, Chemical Engineering Department Federal University of São Carlos UFS Car Brasil, 2012, https://cdn.intechopen.com/pdfs/39142/InTechCrystallization_by_antisolvent_addition_and_cooling.pdf

[13] D. J. McClements. Food Emulsions: Principles, Practices, and Techniques.CRC Press, 2015 (cit. a p. 4).

[14] T. F. Tadros. Emulsions: Formation, Stability, Industrial Applications. De Gruyter, 2016 (cit. a p. 4).

[15] J Bibette and F Leal Calderon and P Poulin, Emulsions: basic principles, Journal: Reports on Progress in Physics, Vol.62, n.6, pag.969, June 1999, doi:10.1088/0034-4885/62/6/203

[16] D. J. McClements. *Food Emulsions: Principles, Practices, and Techniques*. CRC Press, 2015 (cit. a p. 4).

[17] David MNV, Akhondi H. Emulsions. [Updated 2023 Jul 30]. In: StatPearls [Internet]. Treasure Island (FL): StatPearls Publishing; 2024 Jan-. Available from: https://www.ncbi.nlm.nih.gov/books/NBK559084/

[18] F.B. Carvalho-Guimarães, K.L. Correa, T.P. de Souza, J.R. Rodríguez Amado, R.M. Ribeiro-Costa e J.O.C. Silva-Júnior. «A Review of Pickering Emulsions: Perspectives and Applications». In: Pharmaceuticals (Basel, Switzerland) 15 (11) (2022) doi: 10.3390/ph15111413

[19] Deng W., Ybin L., Li W., Shouhui C., Pickering emulsions stabilized by polysaccharides particles and their applications: a review. Food Science and Technology, 42, 10.1590/fst.24722

[20] Zhang, M.; Li, X.; Zhou, L.; Chen, W.; Marchioni, E. Protein-Based High Internal Phase Pickering Emulsions: A Review of Their Fabrication, Composition and Future Perspectives in the Food Industry. *Foods* 2023, *12*, 482. https://doi.org/10.3390/foods12030482

[21] Y. Chevalier e M.A. Bolzinger. «Emulsions Stabilized with Solid Nanoparticles:Pickering Emulsions». In: Colloids and surfaces. A, Physicochemical and engineering aspects 439 (2013), pp. 23–34 (cit. alle pp. 7, 8, 11).

[22] P. Trucillo. «Drug Carriers: A Review on the Most Used Mathematical Models for Drug Release». In: Processes 10.6 (2022), pp. 1094– (cit. alle pp. 2, 11, 16–21).

[23] Yang Y.; Fang Z.; Chen X.; Zhanng W.; Xie Y.; Chen Y.; Liu Z,; Yuan W.; An overview of Pickering Emulsions: Solid-Particles Materials, Classification, Morphology and Applications; 2017; Frontiers in Pharmacology, Volume 8, Article 287; doi: 10.3389/fphar.2017.00287

[24] Fujii, S., Okada, M. e Furuzono, T. (2007). Nanoparticelle di idrossiapatite come emulsionanti particellari sensibili allo stimolo e blocchi di costruzione per materiali porosi. J. Colloid Interface Sci. 315, 287–296. doi: 10.1016/j.jcis.2007.06.071.

[25] Fujii, S., Okada, M., Sawa, H., Furuzono, T. e Nakamura, Y. (2009). Nanoparticelle di idrossiapatite come emulsionante particellare: fabbricazione di microsfere biodegradabili rivestite di idrossiapatite. Langmuir 25, 9759–9766. doi: 10.1021/la901100z

[26] Anand P, Kunnumakkara AB, Newman RA, Aggarwal BB. Bioavailability of curcumin: problems and promises. Mol Pharm. 2007 Nov-Dec;4(6):807-18. doi: 10.1021/mp700113r. Epub 2007 Nov 14. PMID: 17999464.

[27] Staff, Farmaci Naturali, Curcumina (curcuma): proprietà farmacologiche e nutrizionali, FondazioneARTOI,2019https://www.artoi.it/curcuma/#:~:text=La%20curcumina%20%C3%A8%20un%20potente,di%20proteine%20ad%20azione%20antiossidante.

[28] Noorafshan A. and Soheil Ashkani-Esfahani S.; A Review of Therapeutic Effects of Curcumin; Current Pharmaceutical Design, 2013, 19, 2032-2046

[29] Nelson K.M.; Dahlin J.L.; Bisson J.; Graham J.; Pauli G.F.; Walters M.A.; The Essential Medicinal Chemistry of Curcumin. J Med Chem. 2017 Mar 9;60(5):1620-1637. doi: 10.1021/acs.jmedchem.6b00975. Epub 2017 Jan 11. PMID: 28074653; PMCID: PMC5346970.

[30] Portincasa P., Lembo A., De Bari O., Di Palo D., Maggio A., Cataldo I., Calamita G., The Role of Dietary Approach in Irritable Bowel Syndrome, Vol. 24, Journal: Current Medicinal Chemistry, April 2017, p.11, doi: 10.2174/0929867324666170428102451.

[31] A.S. Myerson. Handbook of Industrial Crystallization. Butterworth-Heinemann, 2002 (cit. alle pp. 6, 8, 10, 11, 18)

[32] Komal Upendra Pandey, Sameer Vishvanath Dalvi, Understanding stability relationships among three curcumin polymorphs, Advanced Powder Technology, Volume 30, Issue 2, 2019, Pages 266-276, ISSN 0921-8831, https://doi.org/10.1016/j.apt.2018.11.002.

[33] Chroni A, Mavromoustakos T, Pispas S. Curcumin-Loaded PnBA-*b*-POEGA Nanoformulations: A Study of Drug-Polymer Interactions and Release Behavior. *International Journal of Molecular Sciences*. 2023; 24(5):4621. https://doi.org/10.3390/ijms24054621

[34] J. Pan, J. Chen, X. Wang, Y. Wang e J. Fan. «Pickering emulsion: From controllable fabrication to biomedical application». In: Interdisciplinary Medicine 1-3 (2023), n/a (cit. alle pp. 6, 7).

[35] D. Gonzalez Ortiz, C. Pochat-Bohatier, J. Cambedouzou, M. Bechelany e P. Miele. «Current Trends in Pickering Emulsions: Particle Morphology and Applications». In: Engineering (Beijing, China) 6 (4) (2020), pp. 468–482 (cit. alle pp. 7, 8).

[36] Lauren S, Biolin Scientific, What is Pickering emulsion, 2023, https://www.biolinscientific.com/blog/what-is-pickering-emulsion

[37] B. P. Binks, S. O. Lumsdon, Langmuir 2000, 16, 8622] [J. Giermanska-Kahn, V. Schmitt, B. P. Binks, F. Leal-Calderon, Langmuir 2002, 18, 2515.] [B. P. Binks, J. H. Clint, Langmuir 2002, 18, 1270

[38] Dalvi, Sameer V. and Dave, Rajesh N., Controlling Particle Size of a Poorly Water-Soluble Drug Using Ultrasound and Stabilizers in Antisolvent Precipitation, Industrial \& Engineering Chemistry Research, Vol. 48, n. 16, pp 7581-7593, 2009, doi:10.1021/ie900248f

[39] Rahman, MS; Hasan, MS; Nitai, AS; Nam, S.; Karmakar, AK; Ahsan, MS; Shiddiky, MJA; Ahmed, MB Sviluppi recenti della carbossimetilcellulosa. Polimeri **2021**, 13, 1345. https://doi.org/10.3390/polym13081345

[40] Kukrety A., Singh R., Singh P. and Ray S., Comprehension on the synthesis of Carboxymethylcellulose (CMC) Utilizing Various Cellulose Rich Waste Biomass Resources, Sept.2018, Vol.9, pp. 1-9, Journal: Waste and Biomass Valorization, doi: 10.1007/s12649-017-9903-3.

[41] Dul M., Paluch K., Kelly H., Healy A., Sasse A., Tajber L., Self-assembled carrageenan/protamine polyelectrolyte nanoplexes-Investigation of critical parameters governing their formation and characteristics, Vol. 123, Journal: Carbohydrate Polymers, Feb. 2015, doi: 10.1016/j.carbpol.2015.01.066

[42] Prashant Dahal, Srinivas Janaswamy, Hydrocolloid-based nutraceutical delivery systems: Potential of κ-carrageenan hydrogel beads for sustained release of curcumin, Food Research International, Volume 183,2024, 114223, ISSN 0963-9969, https://doi.org/10.1016/j.foodres.2024.114223.

[43] Stephany Cunha de Rezende, Olga Ferreira, Arantzazu Santamaria-Echart, Madalena Maria Dias, Maria Filomena Barreiro, Evaluating the potential of natural polymers for water-dispersible curcumin-based solid dispersion colourant systems for food applications, Journal of Food Engineering, Volume 371, 2024, 111986, ISSN 0260-8774, https://doi.org/10.1016/j.jfoodeng.2024.111986

[44] H. Tung, E. L. Paul, M. Midler e J. A. McCauley. *Crystallization of Organic Compounds: An Industrial Perspective*. John Wiley Sons, 2008 (cit. alle pp. 5, 13)

[45] Dai, H., Lu, X., Peng, Y., Yang, Z., & Zhu, H. (2017). Characteristics of metastable zone in the crystallization process: A case study of sparingly soluble hydroxyapatite. *Desalination and Water Treatment*, *62*. https://doi.org/10.5004/dwt.2017.1647

[46] Kocks, C.; Krekel, C.M.; Gausmann, M.; Jupke, A. Determination of the Metastable Zone Width and Nucleation Parameters of Succinic Acid for Electrochemically Induced Crystallization. *Crystals* **2021**, *11*, 1090. https://doi.org/10.3390/cryst11091090

[47] D. Friso. Ingegneria dell'industria agroalimentare. Teoria, applicazioni e dimensionamento delle macchine e impianti per le operazioni unitarie. CLEUP, 2017 (cit. a p. 14)

[48] Desiraju, Gautam R, Crystal Engineering: From Molecule to Crystal, Journal of the American Chemical Society, Vol. 135, n.27, pp 9952-9967, 2013, doi:10.1021/ja403264c

[49] Desiraju, Gautam R, Crystal engineering: A brief overview. Journal of Chemical Sciences, 2010, 122(5), 667–675. https://doi.org/10.1007/s12039-010-0055-2.

[50] J. H. Harker, J. R. Backhurst e J.F. Richardson. Chemical Engineering. Elsevier Science Technology, 2002 (cit. a p. 7)

[51] K.L. Choong, R. Smith,Optimization of batch cooling crystallization,Chemical Engineering Science, Vol. 59, Issue 2, pp. 313-327, ISSN 00092509, https://doi.org/10.1016/j.ces.2003.09.025

[52] Lynch, Michael and Weiner, Ed, HPLC: high performance liquid chromatography, Environmental Science \& Technology, Vol.13, n.6, pp 666-671, 1979, doi:10.1021/es60154a007

[53] Valentini V., CNR Istituto di Struttura della Materia, Area di ricerca di Tor Vergata, Monterotondo - Roma, Spettrometro Raman Dilor XY, https://www.ism.cnr.it/it/tempism/analisi/spettroscopia/laboratoridispettroscopia/spettroscopia-raman-e-micro-raman/raman-dilor-xy-rm.html

[54] Scarani A, Åström M, IGR – Italian Geomological Review, Spettroscopia Raman:tecnica e applicazioni gemmologiche, n.2, Sett. 2017, https://www.rivistaitalianadigemmologia.com/2021/01/20/spettroscopia-raman-tecnica-e-applicazioni-gemmologiche/#comments

[55] Guide to Raman Spectroscopy | Bruker. (n.d.). Retrieved July 25, 2024, from https://www.bruker.com/en/products-and-solutions/infrared-and-raman/ramanspectrometers/what-is-raman-spectroscopy.html

[56] H. Zhao, Y. Yang, Y. Chen, J. Li, L. Wang e C. Li. «A review of multiple Pickering emulsions: Solid stabilization, preparation, particle effect, and application». In: Chemical engineering science 248 (2022), p. 117085 (cit. alle pp. 5, 6).

[57] Gill P, Moghadam TT, Ranjbar B. Differential scanning calorimetry techniques: applications in biology and nanoscience. J Biomol Tech. 2010 Dec;21(4):167-93. PMID: 21119929; PMCID: PMC2977967.

[58] Jillavenkatesa, A., Lum, L. e Dapkunas, S. (2001), NIST Recommended Practice Guide: Particle Size Characterization, Pubblicazione speciale (NIST SP), National Institute of Standards and Technology, Gaithersburg, MD, [online], https://doi.org/10.6028/NBS.SP.960-1 (consultato il 14 ottobre 2024)

[59] D. Wang, L.-S. Fan, 2 - Particle characterization and behavior relevant to fluidized bed combustion and gasification systems, Editor(s): Fabrizio Scala, In Woodhead Publishing Series in Energy, Fluidized Bed Technologies for Near-Zero Emission Combustion and Gasification, Woodhead Publishing, 2013, Pages 42-76, ISBN 9780857095411, https://doi.org/10.1533/9780857098801.1.42.

[60] Nikon's Microscopy U, Polarized Light Microscopy, 2014, url: https ://www.microscopyu.com/techniques/polarized-light/polarized-lightmicroscopy (cit. a p. 31).

[61] K. Akhtar, S.A. Khan, S.B. Khan e A.M. Asiri. «Scanning Electron Microscopy: Principle and Applications in Nanomaterials Characterization». In: Handbook of Materials Characterization. Springer, Cham, 2018 (cit. a p. 26).

[62] Abdullah Alghunaim, Suchata Kirdponpattara, Bi-min Zhang Newby, Techniques for determining contact angle and wettability of powders, Powder Technology, Volume 287, 2016, Pages 201-215, ISSN 0032-5910, https://doi.org/10.1016/j.powtec.2015.10.002.

[63] Mukherjee N., "Solids' wettability: a short note", 11 june 2022

[64] Fucheng Guo, Jianzhong Pei, Jiupeng Zhang, Bin Xue, Guoqing Sun, Rui Li, Study on the adhesion property between asphalt binder and aggregate: A state-of-the-art review, Construction and Building Materials, Vol. 256, 2020, 119474, ISSN 0950-0618, https://doi.org/10.1016/j.conbuildmat.2020.119474

[65] Peram, M. R., Jalalpure, S. S., Joshi, S. A., Palkar, M. B., & Diwan, P. V. (2017). Single robust RP-HPLC analytical method for quantification of curcuminoids in commercial turmeric products, Ayurvedic medicines, and nano vesicular systems. Journal of Liquid Chromatography & Related Technologies, 40(10), 487–498. https://doi.org/ 10.1080/10826076.2017.1329742

[66] Horosanskaia, E.; Yuan, L.; Seidel-Morgenstern, A.; Lorenz, H. Purification of Curcumin from Ternary Extract-Similar Mixtures of Curcuminoids in a Single Crystallization Step. Crystals **2020**, 10, 206. https://doi.org/10.3390/cryst10030206

[67] Van Nong et al., Fabrication and vibration characterization of curcumin extracted from turmeric (Curcuma longa) rhizomes of the northem Vietnam, SpringerPlus (2016) 5:1147

[68] He Y, Liu H, Bian W, Liu Y, Liu X, Ma S, Zheng X, Du Z, Zhang K, Ouyang D. Molecular Interactions for the Curcumin-Polymer Complex with Enhanced Anti-Inflammatory Effects. Pharmaceutics. 2019 Sep 1;11(9):442. doi: 10.3390/pharmaceutics11090442. PMID: 31480578; PMCID: PMC6781554.

[69] Holder, Cameron F. and Schaak, Raymond E., Tutorial on Powder X-ray Diffraction for Characterizing Nanoscale Materials, ACS Nano, vol.13, n.7, pp. 7359-7365, 2019, doi: 10.1021/acsnano.9b05157, PMID: 31336433, https://doi.org/10.1021/acsnano.9b05157

[70] Ganshang Si, Jiaxiang Liu, Zhengang Li, Zhiqiang Ning, Yonghua Fang, Quartz Tube Enhanced Raman Scattering Spectroscopy, 2022, Frontiers in Physics, 10.930007.10.3389/fphy.2022.930007